Damage Modelling and Detection in Beams and Plates by Analytical and Numerical Methods.

Akshay Satpute

Thesis submitted to Cardiff University for the award of PhD

December 2024

Acknowledgement

I would like to express my heartfelt gratitude to my supervisors, Prof. David Kennedy, Prof. Carol Featherston, and Dr. Abhishek Kundu, for their invaluable guidance, encouragement, and unwavering support throughout the past three years. I wish to express my deepest thanks to my late parents, whose values and sacrifices continue to inspire me every day. I am profoundly grateful to my partner, who has been my family and an unfailing source of strength, patience, and encouragement throughout this journey.

I also gratefully acknowledge the financial support provided by the Government of India (Ministry of Social Justice & Empowerment) for funding my doctoral research.

Abstract

This PhD thesis focuses on developing advanced damage detection methods for beam and plate structures to prevent catastrophic failures, with a particular emphasis on plate structures. The research is grounded in vibrational analysis, specifically leveraging changes in natural frequency as a diagnostic tool.

In the initial phase, a rotational spring is used to model a crack in isotropic beam structures. The reduced stiffness of the beam at the location of the crack is incorporated into the dynamic stiffness matrix. The natural frequencies are extracted using the Newton-Raphson method and Wittrick-William algorithm. The obtained results are validated against previous research studies. Additionally, the results are compared with an analytical solution based on a strain energy approach, which is developed as part of this work. To achieve computational efficiency, the strain energy approach is employed for crack location and characterization in beams, using both noise-free and noise-contaminated natural frequencies. For noise-free simulations, vector analysis and gradient-based optimization are utilized to obtain crack parameters, while interval arithmetic methods are applied for crack localization in noise-contaminated simulations. The developed analytical solution for beam structures is further used as a framework to solve the inverse problem. Its use enhances computational efficiency during parameter optimization.

Building on the insights gained from the beam studies, a novel method for isotropic plate structures is developed to calculate the degradation in natural frequencies due to the presence of cracks. This method considers changes in rotation and bending moments to calculate the total change in the strain energy of the plate. Using the law of conservation of energy, a formulation is developed to calculate the difference between the intact and cracked plate by integrating changes in strain energy over the crack length. This methodology is validated against prior research for simple crack cases parallel to plate edges. The analytical formulation is further expanded to model arbitrarily oriented cracks, incorporating the twisting effect on the change in strain energy of the cracked plate. To validate this expanded work, a corresponding model is developed using the finite element software ABAQUS.

The developed analytical solution based on the strain energy approach is further employed as a framework to solve an inverse problem for determining crack parameters. This involves identifying the location and characterization of damage using the first six natural frequencies of the cracked plate. The inverse problem is formulated using the least-squares difference method and solved using gradient-based optimization.

The methods presented in this thesis provide promising results in terms of accuracy and computational efficiency. For future work, improvements are highlighted to expand the research for complex geometries, environmental conditions, sensor inaccuracies, and human errors.

Contents

List of Figures

List of Tables

Notations

C	Compliance used for beams.
$C(d/h)$	Non-dimensional compliance.
D	Flexural rigidity of the plate.
d	Depth of crack.
E	Young's Modulus.
h	Thickness.
I	Moment of inertia.
k^*	Rotational spring used in beam.
l	Length of the crack.
l_e	Length of the element used in ABAQUS to model the intact as well as cracked plate.
μ	Weight density.
T_0	Kinetic energy of intact structure.
T_c	Kinetic energy of cracked structure.
U_0	Strain energy of intact structure.
U_c	Strain energy of cracked structure.
U_d	Incremental strain energy associated with the discontinuous rotation θ.
x_0, y_0	Midpoint of the crack.
x_1, y_1	Starting point of the crack.
x_2, y_2	End point of the crack.

Greek Symbols

$\bar{\delta}_n(x)$	Normalised change between squares in the natural frequencies of intact and damaged beams (δ_n).
$\bar{\delta}_m(x)$	Normalised change between squares in the natural frequencies of intact and damaged beams based on measured or synthetic data.
$\bar{\delta}^L{}_{(n=1,2\ldots i)r}$	Normalized lower limits of the relative changes in the natural frequencies.
$\bar{\delta}^u{}_{(n=1,2\ldots i)r}$	Normalized upper limits of the relative changes in the natural frequencies.
δ_n	Difference between squares in the natural frequencies of intact and damaged beams for n^{th} mode of vibration.

δ_i^m	Difference between squares in the natural frequencies of intact and damaged beam structure for 'n' mode of vibration obtained using experiments or simulations
δ_i^s	Scaling factor for to set up an inverse problem (error function) for beam structures.
δ_{mn}	Difference between squares in the natural frequencies of intact and damaged plate structure for 'm' and 'n' mode of vibration.
$\delta^r{}_{(m,n)}$	Relative change in the natural frequencies of cracked plate with respect to intact plate.
$\delta_{nr}(x/l)$	Relative change in natural frequency for beam, with length l, and location of crack (x).
$\delta^{\mathrm{M}}{}_{\mathrm{mn}}$	Difference between squares in the natural frequencies of intact and damaged plate structure for 'm' and 'n' mode of vibration obtained using experiments or simulations.
$\delta^{\mathrm{MS}}{}_{\mathrm{mn}}$	Scaling factor for to set up an inverse problem (error function) for plate structures.
$\omega^L{}_{nc}$	Lower limit for natural frequencies of cracked beam.
$\delta^u{}_{nr}$	Upper limits of the relative changes in the natural frequencies.
φ	Orientation of crack in a plate with respect to X - axis.
ω_0	Natural frequency if intact structure.
ω_c	Natural frequency of cracked structure.
ω_{mn0}	Natural frequencies of intact plate.
$\delta\theta$	Change in rotation across the crack.
λ	Non-dimensional frequency parameter for beam structure.
λ^*	Non-dimensional local compliance.

1 Chapter 1: Introduction

1.1 Motivation

Beams and plates are essential structural elements commonly found in civil and mechanical systems, including buildings, bridges, as well as aerospace and automotive structures. Beams and plates are designed to efficiently carry and transfer a range of loads and can be designed in various sizes, shapes and materials as per the requirement. Depending upon the serviceability of the structure, they may be susceptible to static and dynamic loads, including dead loads, live loads, wind loads, earthquake loads, and fatigue loads.

During their service life, structural components may experience corrosion or erosion due to environmental effects or a loss of mass and stiffness in their structural members due to excessive and repetitive loading conditions. Due to such factors, damages may occur in the structures. There is also a high probability of growth in the damage that has already occurred. Ultimately, this condition can cause a catastrophic failure of the structure and may lead to a significant loss of life and economic loss.

To avoid such calamities, regular inspections and maintenance are required for structures which are continuously subject to dynamic loads. Continuous monitoring of structural health can provide valuable insight to enable decision making concerning the reuse, repair or replacement of damaged structural components. The regular inspection, continuous monitoring, and maintenance of a structure can reduce the frequency of catastrophic failures causing loss of life and economic loss.

In the next section, an overview related to the current non-destructive damage detection techniques and methods adopted for continuous health monitoring of the structures is provided.

1.2 Damage Detection Methods in Industry

Structures or structural components can be either inspected periodically or monitored continuously. Thus, structural health inspections can be differentiated into non-destructive testing (NDT) and structural health monitoring (SHM). These different strategies comprise the main ways of inspecting structures without causing damage.

A wide range of NDT techniques is available in the industry, allowing for detailed periodic assessments of structural integrity. On the other hand, SHM represents a more advanced approach that involves continuous or periodic monitoring of structural components using sensors and data analysis. SHM methods include strain measurement, vibration analysis, acoustic emission monitoring, and other sensor-based techniques.

1.2.1 Methods of non-destructive testing

There are a variety of NDT techniques available in industry. Local NDT includes Visual Testing (VT), Magnetic Particle Testing (MT), Radiographic Testing (RT), Ultrasonic Testing (UT), Eddy Current Testing (ECT), Acoustic Emission Testing (AE), Thermal Infrared Testing (IRT).

1.2.1.1 Local NDT Methods

Magnetic Testing (MT) [1] is one of the oldest methods in NDT. It was first used in 1929 for industrial applications. When a crack or defect is present, the magnetic flux is disrupted, creating a leakage field at the location of the discontinuity. As a result, the magnetic particles accumulate near these regions, making the defects visible, as illustrated in Figure 1.1.

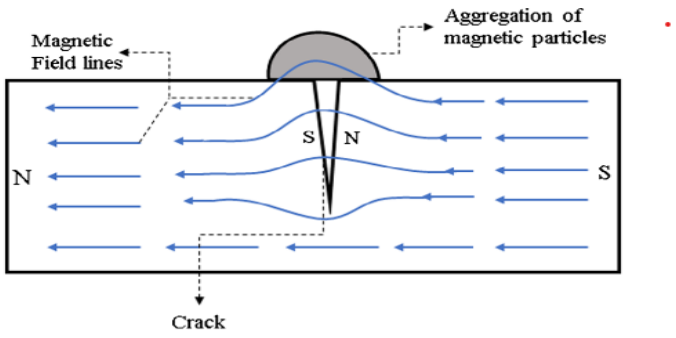

Figure 1.1 – Magnetic particle Non-destructive testing. [1]

Ultrasonic Testing (UT) is one of the most widely used methods in non-destructive testing (NDT). This technique uses high-frequency sound waves, typically in the range of 0.5 to 15 MHz, to detect flaws in materials, components, and structures. A pulse generated by a piezoelectric material transmits the sound waves into the specimen.

Changes in the velocity or path of the pulse indicate the presence of discontinuities within the material.

Sound waves are reflected when they encounter a boundary between two materials with different acoustic impedances, such as a crack, void, or inclusion within the specimen. These reflected waves are captured by the transducers and converted into electrical signals, which are then displayed as visual representations (e.g., waveforms or images) on a screen for analysis.[2].

The Eddy Current Test (ECT) employs the magnetic field generated by an alternating current flowing through a primary coil positioned near the specimen. This magnetic field induces eddy currents within the conductive material of the specimen. The eddy currents flow in a swirling pattern and create their own magnetic field, which interacts with the primary coil. The resulting changes in the magnetic field are detected by a secondary coil. Discontinuities or flaws in the metal can be identified at locations where there are changes in impedance, which are reflected in the readings from the secondary coil [3].

Deformation of a structure due to external loading, causes the material to release energy in the form of elastic waves. These waves are called acoustic emissions. They travel to the surface of the material. The amount of energy released is high at damage locations compared to intact parts. The waves can be captured by the transducers and amplified to generate a signal for interrogation. Using this mechanism the source of the elastic waves can be identified, which corresponds to the damage location in the material.

The selection of an appropriate non-destructive testing (NDT) method depending on the type and location of the damage. However, the implementation of local NDT techniques may not be possible for inaccessible areas within the structure. To overcome this difficulty, global NDT techniques may be required.

1.2.1.2 Global NDT Methods

Two commonly used global non-destructive testing (NDT) methods are the Damage Index Method (DIM) and Vibration-based Damage Identification (VDI). The Damage Index Method includes techniques such as Frequency Response Function (FRFs), Wavelet Analysis (WA), Artificial Neural Networks (ANN), Fast Fourier Transform (FFT) Analysis, Autocorrelation Function (AF), and Cepstrum Analysis (CA). Alternatively the Vibration-based Damage Identification techniques include the Strain

Energy Method (SEM), Natural Frequency Based Method (NFM), Modal Damping based Method (MDM), Mode Shape Method (MSM), and Modal Curvature based Method (MCM).

The Damage Index Method (DIM) is a comprehensive approach that utilizes various analytical techniques to detect and assess structural damage. One of the most effective techniques within DIM is Wavelet Analysis (WA). Wavelet Analysis is particularly well-suited for handling nonstationary signals that are commonly encountered in structural health monitoring.

Introduced through developments in applied mathematics during the 1980s, wavelet analysis has become a highly effective method for examining signals that vary with time, such as those produced by structural vibrations. Unlike Fourier analysis, which represents signals as a combination of sine waves, wavelet analysis employs wavelets that are confined in both time and frequency. This dual localization enables the method to identify short-lived events and subtle changes within a signal, making it particularly well-suited for damage detection in structures.

The applications of Wavelet Analysis in the context of the Damage Index Method are diverse and have demonstrated significant potential. Researchers have employed techniques such as using Gaussian wavelets for modal parameter identification [4].The relationship between the Lamb wave and the amplitude coefficients is utilised to identify the damage [5]. The use of spectral plate elements was considered by Krawczuk *et.al.*[6] to model the damaged part of a plate based on the split in two signals when the wave passes through a damaged part. Chang and Chen [7] used spatial wavelet transform analysis to detect damage in a rectangular plate, identifying damage through peak coefficients observed during the analysis. However, when applied to a clamped plate with edge cracks, the method produced inaccurate results. Improvements in this model have been made with the help of two-dimensional continuous wavelet transforms for rectangular steel plate clamped at all edges [8].

The versatility and effectiveness of Wavelet Analysis in structural health monitoring have made it a valuable tool within the Damage Index Method. By leveraging its ability to identify subtle changes and localize damage, Wavelet Analysis has proven to be a powerful approach for detecting and assessing structural integrity, particularly in the

presence of nonstationary signals that are challenging to analyse using traditional methods.

Use of Artificial Neural Networks (ANN) is another significant method in the DIM. The concept of ANN is based on the mathematical model developed by McCulloch and Pitts [9]. The aim of this developed algorithm was to replicate the functioning of the brain's neural network using a computational framework. ANNs can learn from input data, adjust weights to minimize errors, and associate patterns with structural damage. They excel at recognizing anomalies in complex data, improving in accuracy as more data is fed into the model. The combination of learning, association, and pattern recognition makes ANNs well-suited for detecting the presence of defects in structures.

In the 1980s, this approach was adopted for detecting damage in structures. Artificial Neural Networks (ANN) can be trained using the backpropagation method, which relies on gradient-based optimization. Research has been conducted using this method to analyse post-earthquake structures and the results have been compared with traditional techniques [10]. For both single and multiple spring systems, Non-Destructive Testing (NDT) has been performed using ANN, utilizing changes in eigenvalues and residual stress data for training purposes [11].

1.2.1.3 Vibration Characteristics

Vibration-based damage identification (VDI) methods are very helpful in detecting damages like cracks, corrosions, and fatigue damages that occurs in accessible and inaccessible areas of structures. Based on the use of VDI, the number of inspections can be reduced. In addition, it offers lower operating costs.

The measurements used to implement this technique can be classified into two parts. Measurement of static deflections can be considered as the first part. The relationship between the deflection and the stored strain energy can be defined for an intact structure. Damaged structures can show unpredictable patterns in the deflection for the same load due to the loss in stiffness caused by damage, corrosion, and cracks. Measurement of static deflection is quite useful in the inspection of the wings and fuselage structures in aircraft, as well as bridges and building structures. Measurement of static deflection at inaccessible areas, along with nonlinear behaviour and environmental factors, can be considered as challenges in the application of this method.

In the second part, natural frequencies, mode shapes, and modal damping can be considered for the VDI. The Strain Energy Method is a widely used vibration-based non-destructive testing (NDT) technique for identifying structural damage. This method detects changes in the strain energy by comparing mode shapes from the undamaged and damaged states of a structure. An advanced algorithm developed by Cornwell *et al.*[12] can accurately locate damage using only a few modes, even with a small stiffness reduction. The Differential Quadrature Method (DQM) is used to compute strain energy from modal analysis, allowing for the creation of a damage index that can identify surface cracks through peak locations, although irregularities in mode shapes can sometimes produce false peaks in undamaged areas [13].

A Modal Strain Energy Damage Index (MSE-DI) algorithm has been used to detect and locate delamination in composite stiffeners, particularly in aircraft structures [14]. More recently, time-domain methods using dynamic response data and time series analysis have gained attention for structural damage identification. These include state-space analysis to extract damage-sensitive parameters, as well as nonlinear time series analysis techniques like examining state-space distributions and Poincare maps of dynamic responses. A space-time autoregressive moving average (STARMA) model has also been developed to identify damage in specific regions of vibrating plates [15].

However, time-domain methods can be sensitive to noise, which can compromise the accuracy of their damage detection algorithms and lead to potential failures in identifying damage.

Overall, VDI is an attractive method to employ for global NDT which can be performed without prior knowledge of the damage locations including inaccessible areas. Doebling *et al,*[16]. Wang and Chan [17] and Fan and Qiao [18] have presented comprehensive review papers on damage modelling and detection, highlighting various techniques and approaches used in the field.

1.2.1.4 Significance of Natural Frequencies

Cracks or damage, caused by corrosion or fatigue in structural elements impact the vibrational characteristics of structures, including static deflection, mode shape, natural frequencies, and modal damping. Measuring static displacements and mode shapes can be challenging in areas of the structure that are difficult to access. However, natural frequencies can be measured at accessible points on the structure, allowing for

experimentation. Even for cracks located in hard-to-reach areas, shifts in natural frequencies can be detected from any accessible point, simplifying the experimental analysis.

Previous studies have successfully demonstrated the use of natural frequencies as a parameter for detecting damage in aluminium plates [19]. The sensitivity of natural frequencies to damage, combined with the cost-effectiveness of these methods makes them attractive as a damage detection technique. However, factors such as temperature, humidity, additional mass, and boundary conditions can affect their efficiency. Furthermore, local changes in stiffness caused by a small crack do not significantly affect the overall structural stiffness, which is why the resulting changes in natural frequencies are generally small in magnitude.

Considering the vital need to maintain the safety and integrity of plates with cracks or other forms of damage, it is essential for engineers to comprehend the static, dynamic, buckling, and post-buckling behaviour of these plates. Conventional local non-destructive testing (NDT) techniques need prior knowledge of where damage may occur and physical access to the structure, which can obstruct their effectiveness. As a result, a global quantitative NDT approach that relies on variations in natural frequencies is especially beneficial for examining large, complex plate-like structures.

In this thesis, an analytical solution has been created using the Rayleigh quotient for a cracked isotropic beam and plate structure, where the crack is modelled as a rotational spring. This solution establishes a connection between the degradation of natural frequencies in the beam and plate structures. The results have been validated using finite element analysis. Damage quantification for beam structures has been shown through vector algebra, interval arithmetic, and gradient-based optimization. Gradient-based optimization method has been employed for the damage quantification in a plate structure. An overview of the thesis is given in following sections.

The studies conducted in this thesis have not considered damping, which assumes of ideal, undamped free vibration. This simplification provides a clearer understanding of the system's fundamental dynamic behaviour and natural frequencies without the complications introduced by energy dissipation mechanisms. However, it is important to note that damping, whether structural or viscous, is being omitted in this preliminary analysis and fundamental study. While this simplification aids in understanding the

system's response, it is essential to recognize that damping can significantly impact performance in real-world engineering applications.

Structural damping arises from the material properties and geometry of a system, often represented through hysteretic mechanisms or complex stiffness. In contrast, viscous damping is typically associated with external or environmental interactions and is modelled as a force that is proportional to velocity. Both types of damping lead to a decrease in amplitude over time and can also cause shifts in natural frequencies. In lightly damped systems, these frequency shifts are often small enough to be considered negligible for certain analyses. However, in heavily damped systems, more complex interactions can occur, including mode coupling and more pronounced frequency shifts, which can significantly affect the system's dynamic behaviour.

Excluding damping is reasonable in initial theoretical models or in cases where it is negligible, such as during preliminary design phases. However, in practical applications, even minimal damping can influence resonance amplitude and dynamic stability. Future research may incorporate damping effects to investigate these influences, particularly in evaluating modal damping ratios and enhancing predictions of resonance behaviour and energy dissipation.

1.3 Thesis aims and objectives

The development of a mathematical model to calculate the degradation in the natural frequencies of beam and plate structures due to the presence of cracks can be considered a direct problem. Conversely, predicting the crack location and severity using the degradation observed in the natural frequencies of beam and plate structures relative to their intact state can be described as an inverse problem.

The aim of this thesis is to solve both the direct and inverse problems for isotropic beam and plate structures. In the first part (direct problem), the focus is on the development of analytical methods to estimate the degradation in natural frequencies caused by damage (cracks). In the second part, the focus shifts to precisely solving the inverse problem, which involves predicting the location and characterizing the crack using the framework developed to calculate the degradation in natural frequencies from the direct problem.

The objectives of the thesis are defined as follows:

1) Development of a mathematical model to calculate the degradation in the natural frequencies of isotropic beam and plate structures.
2) Solving the inverse problem for beam and plate structures to predict the location and characterization of cracks.

The thesis is divided into two parts. In Chapters 3 and 4, the objectives are achieved for beam structures. In Chapters 5 and 6, inspired by the outcomes of Chapters 3 and 4, the same objectives are extended to plate structures.

In the next section, an overview of the thesis is presented, summarizing each chapter.

1.4 Thesis Overview

This thesis provides a comprehensive exploration of damage modelling and detection in isotropic beam and plate structures based on natural frequencies. Following this introduction Chapter 2 presents a detailed literature review, subdivided into two key parts. The first part focuses on research related to crack modelling and detection in beam structures, while the second part deals with crack modelling and detection methods in plate structures.

Chapter 3 concentrates on the free vibration analysis of a cracked beam. The effect of crack is modelled using rotational spring within the beam structure, and the dynamic stiffness matrix is formulated using this model. The Newton-Raphson method is employed to compute eigenvalues, and an analytical solution based on the strain energy approach is developed to quantify the degradation in the beam's natural frequencies due to the presence of a crack.

In Chapter 4, the thesis examines the detection of single cracks in beam structures with a focus on computational efficiency. An analytical solution based on the strain energy approach is utilized as the foundation for crack localization and quantification. Additionally, three methods:1) Vector Algebra, 2) Interval Arithmetic, and 3) Gradient-Based Optimization, are implemented for crack identification, with the latter leveraging the MATLAB FMINCON toolbox.

Chapter 5 shifts attention to the free vibration analysis of a simply supported isotropic plate structure. This chapter is divided into two parts: the first models a crack parallel

to the plate edge using a rotational spring and validates the observed degradation in natural frequencies with prior studies and advanced finite element analysis [20]. The second explores the effects of arbitrarily oriented cracks, considering twisting effects, and conducts comparative studies using the finite element software ABAQUS [21].

Chapter 6 addresses damage quantification in plate structures. Building on the numerical methodologies from Chapter 4, gradient-based optimization emerges as a suitable technique for crack quantification in beam structures. Inspired by these results, the same approach is applied to plate structures. An error function is formulated using the least squares method, and with an optimization process focussing on minimising this error to determine the crack parameters is executed through the MATLAB FMINCON toolbox. This chapter demonstrates the robustness and effectiveness of the proposed technique through numerical examples and comparative studies.

Finally, Chapter 7 provides a comprehensive conclusion summarizing all the research studies conducted in this thesis. It highlights the efficiencies of the proposed methods, discusses the remaining research gaps, and outlines potential future directions for extending this work.

1.5 Publication List

One journal paper has been prepared based on the analytical solution developed to calculate the degradation in the natural frequencies in an isotropic plate structure and implemented damage detection techniques, described in Chapter 3 and 4.

1. **A. Satpute**, D. Kennedy, and C. Featherston, A. Kundu, 2025 Crack modelling and detection in an isotropic plate structure based on strain energy approach. In preparation. For submission to Computers and Structures.

Moreover, five conference papers have been presented which have arisen from Chapters 3, 5 and 6.

1. **A. Satpute**, D. Kennedy, and C. Featherston, "Damage modelling and detection in beams by Newton Raphson method," presented at the 15th World Congress on Computational Mechanics & 8th Asian Pacific Congress on Computational Mechanics, Yokohama, Japan. 2021.
2. F. Masoudian, **A. Satpute**, D. Kennedy, C. A. Featherston, and S. Ilanko, "Natural frequencies of cracked rectangular plates: An energy approach," presented at the 13th International Symposium on Vibrations of Continuous Systems (ISVCS13), Pomeroy, Kananaskis Mountain Lodge, Alberta, Canada,2023.
3. **A. Satpute**, D. Kennedy, and C. Featherston, "Crack modelling and detection in a plate structure," presented at the UNIfied Conference 2023, Huddersfield, UK, 2023.
4. **A. Satpute**, D. Kennedy, and C. Featherston, A. Kundu "Vibration-based crack detection in plates based on natural frequency degradation," presented at the XIVth International Conference on Recent Advances in Structural Dynamics, Southampton, UK. 2024. doi:10.1088/1742-6596/2909/1/012017
5. **A. A. Satpute**, D. Kennedy, C. A. Featherston, and A. Kundu, "Detecting cracks in plates using vibration analysis and natural frequency degradation," presented at the UNIfied International Conference on Emerging Technologies in Cyber-Physical Systems and Industrial AI, Malaviya National Institute of Technology, Jaipur, India, 2024.

2 Chapter 2: Literature Review:

2.1 Introduction

Environmental changes and unexpected loading can cause defects in materials and damage to structures. An efficient design and adequate maintenance of structures can be helpful to improve the lifespan of and avoid catastrophic failures. Regular assessment of structures can reduce the risk of economic loss and, in the worst scenario, loss of life.

The damage can be observed in the form of cracks, delamination or deterioration of the material over the service life of the structure. Preliminary and detailed analysis regarding the damage location within beams, frames and plate structures made of isotropic or anisotropic material can be considered using changes that occur in the dynamic response of the structures.

Quantification of changes that occurred in the dynamic parameters of the structures i.e. mode shapes, amplitude, natural frequencies, damping for a predetermined damage location and severity can be considered as a direct problem to create a baseline. With the combination of the generated baseline model and dynamic response from the damaged structure, the damage location and severity can be obtained. This can be considered as an inverse problem.

A wide range of research work along with their limitations has been studied in this chapter for beam and plate structures using the concept of direct and inverse problems. The chapter explores the research areas for beams and plate structures regarding damage modelling and detection based on the changes observed in the dynamic parameters i.e. natural frequencies, mode shapes, and amplitudes. Along with that, literature with various optimization techniques was studied for the damage quantification. (i.e. Bayesian approach, neural network, machine learning.)

2.2 Direct Problem: Beam and Framed Structures

Obtaining the dynamic parameters of the beam structures with the predefined crack location and severity has been covered in this section.

Christides and Barr [22] utilised a local function which assumes an exponential decay from the distance of the crack. The solution was considered for two symmetric cracks at one location using displacement and stress-strain fields in the Euler-Bernoulli beam with the Rayleigh-Ritz method. The natural frequencies were calculated incorporating the local function and further validated using experimental results.

This theory was extended to beams which consist of double-sided cracks, occurring in the case of cyclic loading and single-sided cracks, occurring in fluctuating loading by Ostachowicz and Krawczuk [23]. The authors determined the inherent frequencies of a cantilever beam subject to damage, specifically considering cases where the beam contained two single-edge or double-edge cracks using an analytical solution based on the change in strain energy. The opening mode of the crack during vibration analysis is considered.

Hu and Liang *et al*.[24] employed an integrated approach for damage modelling using massless, infinitesimal spring to represent the individual cracks with the continuum damage concept. The theoretical relationship between the changes in the eigenfrequencies and the location and severity of the cracks was developed using Castigliano's theorem. The continuum model was developed by associating the stress concept with Hamilton's principle. The integrated function can be developed with those two described models. The method was applied for a simply supported beam with two individual cracks.

Hearn and Testa [25] used the correlations between the changes in natural frequencies and mode shapes concerning changes in stiffness to model cracks in a frame structure. For damage localization, the ratio of the changes in natural frequencies for different modes led to the elimination of the severity of the crack. The experiments were conducted on welded steel frames and wires. The changes in the natural frequencies were considerable for the steel frames. On the other hand, very little change in natural frequencies was observed for the damaged wires. In case of wires, the change in damping was significant than the axial stiffness.

Teughels *et al*. [26] employed the finite element approach to model change in the bending stiffness matrix for a cracked reinforced concrete beam. Using the residual force vector obtained from the equation of motion, effect of damage in the beam, frame, and plate was deduced using a model based on finite element analysis by Ge and Lui

[27]. Chatzi *et al.* [28] implemented an extended finite element method (XFEM) to model the complex flaws like cracks and holes. The developed simulation could identify shifts in the strain fields for the damaged structure, which was considered a baseline model.

Escobar *et al.* [29] considered changes in the element stiffness matrix for damage modelling in the case of three-dimensional structures. The matrix transformation method was used to update the stiffness matrix of the structure based on dynamic parameters (mode shape and natural frequencies) for damage identification.

Rizos *et al.* [30] developed closed-form solutions to incorporate damage. Beam structures were divided by a hinge modelled using a rotational spring and the equations of motion were solved to obtain the eigenfrequencies of the damaged beam. Wittrick and Williams [31] developed an algorithm by utilising the finite strip method for a linearly elastic, undamped system modelled using a finite or infinite degree of freedom system. The developed algorithm provides the number of natural frequencies below a trial value. Caddemi and Calio [32], based on their earlier research [33], formulated a closed-form expression for the dynamic stiffness matrix for a Euler–Bernoulli beam containing multiple cracks. These were modelled using the Dirac's delta generalized function in the flexural stiffness. These expressions were further employed to model damage in frame structures. Utilizing the Wittrick–Williams algorithm, the authors obtained the natural frequencies and mode shapes of both intact and damaged frames [34]. Labib *et al.* [35] explored the direct problem for a cracked beam and frame structure using the Wittrick-Williams algorithm and utilising the bisection method. Khiem and Tran [36] developed a simplified closed-form solution using the location and magnitude of the damage and relating these to changes in the eigenvalues. In other studies, Khiem and Toan [37] considered the nonlinearity relating to the severity of a crack. Jazi *et al.* [38] developed a closed-form expression for the transverse displacement of uneven beams with multiple cracks.

Most of the research studies have shown progress in calculating the dynamic parameters for an open crack, occurring due to a high static load, especially in reinforced concrete structures. The assumption for the open crack is valid in most of the cases. For a breathing crack, studies introduce non-linearity resulting in bilinear dynamic parameters. Chati *et al.* [39] incorporated such non-linearity using finite element

analysis. A similar approach was used by Chandros *et al.*[40] who modelled cracks as continuous flexibility based on the displacement field in the region of the crack.

Morassi [41] developed a relationship between changes in the square of the natural frequencies concerning the square of the displacement at the location of the crack in a damaged beam using pretribulation method. The crack is represented as a rotational spring. In this method, the mode shape is assumed to be the same for damaged and undamaged structures.

Among the methods discussed, the development of closed-form solutions for columns, beams, and frames offers a computationally efficient approach for determining the natural frequencies of cracked beams and frames [33], [34], [42]. Additionally, the use of a rotational spring to model a crack within the dynamic stiffness matrix allows for accurate incorporation of displacements and rotations near the crack, enabling precise determination of natural frequencies in cracked beam and frame structures. This has been addressed using the Wittrick-Williams algorithm [35]. In this thesis, both numerical and analytical methods have been implemented using the rotational spring model in beams, and the results have been compared.

2.3 Inverse Problem: Beam and Framed Structure.

Analytical or numerical models, based on the known parameters of the damage can be considered as the baseline for the development of damage detection methods. The developed mathematical relationships between the change in the dynamic response and the damage parameters can be used in closed-form solutions. Iterative methods and optimization algorithms can then be employed to minimise the difference between the baseline model and the actual response of the structure to obtain the unknown parameters of the damage.

Rizos *et al*. [30] used a rotational spring to model a crack in a cantilever beam. The relationship between the crack location and magnitude was defined. After experimental results were obtained for a cracked beam member in terms of changes in amplitude for the first three vibration modes, a set of non-linear equations was prepared and solved to obtain the crack location and severity. This method was shown to be effective when the crack depth exceeded 10 % of the beam's depth. A massless rotational spring was further employed with the intersection of frequency contour lines, which provided the damage location and severity by Hu and Lang [24]. The method mentioned in [24] was

based on symbolic computation. Further, it was efficiently defined by Maiti and Patil [43] without using symbolic computations. The eigenvalue problem was solved using a numerical method that could be applied to different boundary conditions and geometries of beam structure using differential equations.

Nandwana and Maiti [44] modelled a crack using a rotational spring for a stepped isotropic cantilever beam. The response for each uniform section was obtained by solving the equation of motion equation. Chaudhari and Maiti [45] obtained the mode shape of the cracked beam using the Frobenius technique. The damage location in both cases was obtained using the plots between the non-dimensional stiffness and locations for the first three vibration modes. The intersection of the curve gives the location of the damage. The analytical modelling is required to perform the damage detection procedures for [44] and [41]. To avoid the repetition of the analytical model, Chinchalkar [46] deduced a numerical method, based on finite element analysis, to solve the direct problem. The inverse problem was solved using rank-one modification of an eigenvalue problem.

Jinhee [47] modelled a crack in a beam using finite element analysis. In this work, the Jacobian matrix was updated using the Newton-Raphson method. The crack was defined in terms of location and severity parameters. The natural frequencies of the beam were calculated for multiple cracks. However, the number of cracks needs to be known before using this method which is a limitation.

Ghadami *et al.* [48] developed an algorithm to find the severity and locations of multiple cracks using the Rayleigh-Ritz method. The differences in the natural frequencies were presented in terms of the change in Young's modulus. The algorithm works more efficiently if the number of cracks is known. Maghsoodi *et al*.[49] employed a similar approach to solve forward and inverse problems for stepped beams. Along with that Nandkumar and Shankar [50] and Rubio *et al.* [51] have introduced a similar method based on the assumption of the number of cracks. These methods were extended by Cademi and Calio [42] to overcome the limitations based on the assumption of a number of cracks using explicit expression.

Finite element analysis has been observed in numerous studies for damage modelling and detection in isotropic beams. Kam and Lee [52] utilized mode shapes to locate damage. Hasssiotis *et al.* [53] employed the localized reduction in stiffness causing

changes in the first four natural frequencies to update the stiffness matrix. Bicanic and Chen [54] utilized an iterative procedure based on the characteristic equations of damaged and undamaged structures. Nikolakopoulos *et.al.*[55] developed a computational-graphical method. The contours of the eigenvalues of the cracked structure are plotted. The eigenvalues are then calculated using the finite element method. The intersection of the contours and the dimensionless change in the natural frequencies are then employed for damage localization and severity detection. The intersection of the curves based on the first three natural frequencies for the damaged beam, which locates the damage, also seems features in the studies conducted by Patil and Maity [43]. Pau *et al.* [56] modelled the damage in two-hinge parabolic arches using finite element analysis. Damage parameters were obtained by minimizing the objective function, which is the total of the squared variances between the numerical and experimental values of the frequency variations.

Lee and Chung [57] applied Armon's rank ordering method to approximate damage localization and used this approximation to update the structure's stiffness. The model updating technique was employed by Teughels *et al.* [26] using mode shapes of undamaged and damaged beam structures for damage detection. Escobar *et al.* [29] implemented the transfer matrix method, an iterative method for localizing damage in a 10-storey building.

Greco and Pau [58] utilized the Wittrick-Williams algorithm to model a crack in an Euler-Bernoulli beam using a rotational spring. To solve the inverse problem, the least squares difference between the uncracked natural frequencies and the cracked natural frequencies with respect to the original natural frequencies of the structure is used as an optimization criterion. This optimization determines the severity of the crack, followed by the crack location. The effect of noise is studied using Monte Carlo simulation. Labib *et.al* [59] employed interval arithmetic to evaluate the range of potential damage in frames. With the help of probability distribution, the severity and the location were evaluated.

Friswell *et al.* [60] employed a finite element model to establish a baseline representation of an intact beam. Using synthetic data generated from a cracked beam, they updated the model through a genetic algorithm (GA)-based optimization approach.

Bakir *et al.* [61] employed an alternative approach - 'Coupled Local Minimizers'(CLM) for model updating.

The use of Frequency Response Functions (FRF) has been widely explored in the field of damage detection for bridges. Liu *et al*.[62] utilized FRF by employing the gapped smoothing technique (GSM). The displacement curvature is calculated using FRF. The damage is located where a deviation is observed in the smoothed curvature. A smooth continuous cubic polynomial is obtained using GSM. Damage assessment relies on the precision of estimating the displacement curvature through neighbouring points. Points with lower accuracy indicate the damage location. In the case of an undamaged structure, irregularities can be seen in the obtained curvature due to external factors like ageing or environmental conditions, as the undamaged part is assumed to be smooth, which is a drawback of the GSM. Sampaio *et al.* [63] improved on this by employing the Frequency Response Curvature Method (FRCM). In this method, the displacement curvature is calculated using FRF for the undamaged structure to establish a baseline. Deviation and irregularities in the displacement curvature can be observed for the undamaged structure to define a damage index. This method overcomes the limitations encountered with the GSM. A disadvantage of this technique is that frequency range selection can impact the results. Selecting narrow frequency ranges near the structure's natural frequencies can provide information regarding small damages in the structure. Conversely, selecting a broader range of frequencies can cause displacement curvatures to be influenced by other structural characteristics, potentially leading to the oversight of damage indices produced by small cracks.

Based on the advantages of GSM and FRCM, Limongelli [64] employed the interpolation damage detection method (IDDM) using a cubic spline interpolation function. This has been applied to a multistorey frame structure to determine the location of the floor with reduced stiffness.

The operational deflection shape (ODS) of a structure is commonly described as the structural displacement occurring at a specific frequency. Zhang *et al.* [65] utilized the ODS curvature to detect damage in beam and plate-like structures. To eliminate the need for a baseline, the approximation of an undamaged structure's ODS curvature is considered a smooth line. This method can be used for the structure, before and after damage, and for damage identification. Transmissibility can be used as a substitute for

the FRF. This can be defined as the correlation of the responses at two separate locations regardless of the input. Maia *et al.* [66] employed the correlation of acceleration response transmissibility for damage identification due to its increased sensitivity compared to FRF.

In damage detection, the primary challenges revolve around addressing the complexities inherent in real-world structures and the presence of noise in measurements [67], [68]. Traditional procedure-based methods often struggle to achieve the desired accuracy under these conditions. To overcome this limitation, numerous probabilistic approaches have been developed [69]. Among these, Bayesian inference has been considered since the 1990s, offering a means to derive posterior distributions based on observations and prior knowledge [70], [71].

Figueiredo *et al*. [72] applied Bayesian inference, employing a Markov chain Monte Carlo (MCMC) method, to quantify damage in bridge structures. Similarly, Arangio and Bontempi [73] utilized Bayesian methodology in conjunction with neural networks to identify bridge damage using vibrational response data. Subsequently, Arangio and Bontempi extended this approach to detect damage in cable-stayed bridges, focusing on identifying damage in columns and external span portions [74]. In. In the case of machine learning (Supervised), Sparse Bayesian Learning (SBL) has attracted attention for damage quantification.

Genetic algorithms [74],[75], are also extensively employed for damage detection in structures. Based on simulated and experimental results, they provide a robust tool for finding the global minima related to the objective error function. The literature also shows the implementation of neural networks [62],[76] and the Bees algorithm [77].

In this section, various methodologies for damage detection in beam structures are explored. It has been observed that different approaches have been developed. One common method involves the development of a baseline model using numerical or analytical techniques, which is then used as a framework to minimize the discrepancy between experimental data and model predictions to estimate damage parameters. On the other hand, methodologies such as Frequency Response Function (FRF) analysis using Operating Deflection Shapes (ODS) do not require baseline models. For efficient and cost-effective damage detection in beam structures, tracking changes in natural frequencies can be a promising approach. These methodologies can incorporate noise

modelling to better match experimental results. Furthermore, techniques such as gradient-based optimization, Markov Chain Monte Carlo (MCMC), Sparse Bayesian Learning (SBL), or Genetic Algorithms (GA) can be employed to solve the inverse problem with improved accuracy.

2.4 Direct problem: Plate Structure

The impact of a crack on a plate structure has been studied over the last six decades for different loading and boundary conditions. The length, orientation, and depth of the crack can cause a significant shift in the dynamic parameters. The first investigation of the changes in the vibrational characteristics was observed by Lynn and Kumbasar [78]. They presented the homogeneous Fredholm integral equation using Green's function approach.

Solecki [79] used the Green-Gauss theorem to handle the rigid support to model the crack in an isotropic, simply supported plate structure. The finite Fourier transform was coupled with the Green-Gauss theorem to obtain the vibrational response. These studies showed good agreement with other similar studies based on analytical methods [80] for cracks parallel to the edges of the plate. Hirano and Okazaki [81] used the weighted residual method to obtain a solution for an isotropic plate with three different boundary conditions for cracks parallel to the edges of the plate. Further, Solecki [82] incorporated the finite Fourier expansion to model the singularity near the crack tip.

Qian *et al.* [83] modelled a crack in a simply supported and cantilevered plate with the help of finite element analysis. The authors utilized the changes in the strain energy due to the crack to integrate the stress intensity factor, characterising the stress singularities at the crack tip under bending, shear, and twisting. The results show good agreement with the studies conducted by Solecki [82]. Krawczuk *et.al.* [6] modelled a crack in a rectangular plate using a closed-form solution for the applied stresses. The stiffness matrix for the elements near the crack was considered along with the additional compliance due to the crack. The changes in the eigenvalues were expressed based on the location and the length of the crack. Similar studies were conducted for a static internal crack based on forced vibration analysis to provide the relationship between the changes in the amplitude and the crack parameters [55]. These studies investigated the effect of the plastic zone near the crack tips on the flexibility of the plate, and the response was compared to that of structures with purely elastic behaviour. The study

concluded that the plastic zone near the crack tip had a relatively small effect on the global flexibility as compared to the pure elastic behaviour. Fujimoto *et.al* [84] utilized a hybrid approach to model a centrally located crack in a plate structure. The Finite element method and body force method were used to model the stress singularity near the crack. Saito *et al.* [85] studied the linear and nonlinear vibrations of a cantilever plate with a crack using the veering phenomenon. In addition, an estimation of the nonlinear resonant frequencies was obtained using a bilinear frequency approximation. However, the method provided good results for a relatively large crack length ratio. Bachene *et al.* [86] used an extended finite element approach to model an all-through-the depth, centrally located crack using Mindlin's plate theory. Both shear and the twisting effects were considered while solving the eigenvalue problem. The subspace iteration method was adopted to obtain the eigenvalue for square and rectangular plates with different boundary conditions.

To overcome the computational inefficiency in the numerical method provided by Lynn and Kumbasar [78], Keer and Sve [87] provided a dual series equation to represent the stress near the crack tip. Stahl and Keer [80] utilised a Fredholm integral equation of the second kind to obtain the eigenfrequencies of an isotropic plate with external and internal cracks running parallel to the edges of the plate.

An internal crack in an annular plate was studied by Lee [88] using the Rayleigh-Ritz method. Initial studies were conducted on the plate with simply supported and clamped inside and outside edges. Lee and Lim [89] used the Rayleigh-Ritz method with domain decomposition for isotropic and orthotropic plates. The authors incorporated the shear deformation effect using Reissner theory. Liew *et al.* [90] explored a similar technique based on the Rayleigh-Ritz method with domain decomposition. However, the solution exhibited discontinuity in the slope and displacement near the boundaries of the domain. The reason for this phenomenon was the inadequate stiffness of the spring used to represent the crack, which resulted into an inaccurate calculation of the natural frequencies for the cracked plate. Khadem and Rezaee [91] used the modified comparison function to obtain the natural frequencies of a cracked plate with different boundary conditions. The method was based on the Rayleigh-Ritz method. The accuracy of the modified comparison function was improved on the assumption of a change in the mode shape near the cracked region.

Later, Wu and Shih [92] expanded Shen and Pierre's [93] Galerkin based method for analysing beam-like structures. by incorporating von Karman plate theory to study the dynamic instability and nonlinear response of simply supported cracked plates under periodic in-plane loads. They used the incremental harmonic balance method to solve the cracked plate model and discovered that stability behaviour and vibration response were influenced by factors such as crack location, aspect ratio, vibration amplitude, and loading conditions. Xiao *et al.* [94] explored the variation in the dynamic parameters for a moderately thick plate on an elastic foundation. The authors employed the Galerkin method along with the harmonic balance method to solve nonlinear vibration equations derived from Reissner plate theory and the Hamilton variational principle. Israr *et al.*[95] employed the Galerkin method to represent the governing equation of a cracked plate. Nonlinearities were introduced using the stress-strain field with the help of Berger's approach. The problem was studied for an isotropic plate with a crack parallel to the edge of the plate. Huang and Leissa [96] utilized a corner function to represent the stress singularity near the crack tip using the Rayleigh-Ritz method. The authors expanded the studies for a thick plate for both simply supported and fixed boundary conditions.

The existing literature indicates that the effects of cracks oriented in arbitrary directions have been explored to a lesser extent compared to those of centrally located cracks and cracks that are parallel to the edges of the plates. Maruyama and Ichinomiya [97] conducted an experimental analysis of clamped rectangular plates with slits at various locations and arbitrary orientations using Time-Averaged Holographic Interferometry. The shift in the natural frequencies was studied for the various slit lengths, positions, and angles of inclination. Wu and Law [98] developed an enhanced stiffness model based on the theory presented by Lee [88] for anisotropic plate structures. They further extended this theory to thick anisotropic plates, demonstrating good agreement with the experimental analyses conducted [99]. Additionally, the authors expanded the developed model to accommodate complex structures with various boundary conditions and loading scenarios [100].

Many of the studies that have been conducted have related to cracked beam and plate structures with the crack modelled using the line spring method (LSM). The LSM can be considered to provide an approximate solution for analytical problems. Rice and Levy [101] used the LSM to model part-through-thickness cracks using the

assumptions of Kirchoff's plate theory. Stress intensity factors were calculated based on the forces and moments acting on the cracked section, with the solution expressed as an Airy stress function. While this method offers a reasonable approximation for the impact of a crack that extends through the thickness of a part, it comes with considerable computational expense. To address this issue, newer techniques utilizing the LSM have been introduced including studies to incorporate the shear effect into LSM by Delale and Erdogan [102]. The model holds better agreement up to a 0.8 crack-depth ratio. King [103] utilised virtual ligament springs to model the behaviour of a crack in a component. The effect of the ligament spring was centralised for simplification in the stress strain measurements to approximate the crack impact. The studies explored characteristics like the J-integral and crack opening displacements (COD). Yang [104] updated the LSM to incorporate nonlinearities like thermal and residual stresses. Their updated model shows a good match with finite element analysis for semi elliptical, part-circular, and triangular crack shapes. Miyazaki [105] integrated the static LSM to a dynamic finite element program to perform transient analyses. Joseph and Erdogan [106] utilized the LSM to calculate the stress intensity factor for a cracked plate with forced vibration analysis and the combination of different modes. Israr *et al*. [95] used the Duffing equation to model a crack running parallel to the edge of a plate to provide the relationship between the tensile and bending stresses at the crack location. A similar approach was considered by Jain and Joshi [107] to analyse the frequency response of a plate with an internal crack. Gupta *et. al.* explored the same approach for functionally graded plate structures [108], [109].

The simplified line spring model was effectively used to model a crack in beam and plate structures. Researchers such as Caddemi, Calio [42], and Labib *et al.* [32] employed the rotational spring approach to model cracks in beam-like structures. Luo *et al.*[20] further utilized the analogous rotational spring model to determine the natural frequencies of an isotropic plate with a crack parallel to the edge.

Ranjbaran and Seifi [110] have modelled surface and internal crack using LSM. The effect of crack has been incorporated using compliance in the governing equation of plate. natural frequencies of the plate have been determined using least square quadrature method. Heo *et al*. [111] applied peridynamics to investigate free vibrations in cracked Mindlin plates, validating their hybrid PD-FEM ANSYS model against experimental and numerical benchmarks. Their study revealed that natural frequencies

depend critically on plate thickness, crack length, and orientation, with tapered geometries inducing asymmetric mode shapes. Ma *et al.*[112] developed an analytical wave propagation method to study the forced vibration of rectangular plates with part-through surface cracks. By modelling the crack either within the governing equations or as a spring interface between two intact plates, they derived wave modes to accurately compute vibration responses under various boundary conditions. Their results show high agreement with FEM.

The research studies discussed in this section provide an overview of crack modelling in isotropic plate structures using both analytical and numerical methodologies for internal and surface cracks. Several methods exist for introducing nonlinearity and modelling damage, including the Galerkin method, Green-Gauss theorem, and Berger's approach, each offering unique advantages depending on the problem context. The Line Spring Model (LSM), however, is particularly advantageous for crack modeling as it simplifies the representation of cracks by concentrating the effects into a line of springs, effectively capturing the stress field variations near the crack. This makes LSM especially useful in problems involving localized damage, where it can be integrated into both numerical and analytical frameworks with relative ease. Furthermore, in inverse problem formulations, LSM facilitates efficient optimization of parameters such as the crack-depth ratio due to its reduced computational complexity and strong physical interpretability.

This thesis focuses on developing an analytical solution using the strain energy approach to achieve a computationally efficient method for determining shifts in natural frequencies caused by the presence of cracks in isotropic plates. To model the crack, a rotational spring analogy, like the approach proposed by Bilello [113] and validated by Caddemi and Calio [42], is employed for a simply supported configuration. This method offers a streamlined yet accurate framework for analysing the structural impact of cracks on vibration behaviour.

2.5 Inverse Problem: Plate Structures

It can be observed that many of the damage detection techniques developed for beam-like structures have been further extended to plate-like structures. In the case of beam-like structures, the inverse problem involves the identification of first the location and then the severity of the damage. However, in the case of plate-like structures, the inverse

problem becomes more complicated due to the greater number of damage parameters and different geometric conditions as compared to beam-like structures.

In past decades, numerous research studies have been published concerning damage quantification based on vibration analysis in beam and plate structures. According to Kirkegaard and Rytter [114] damage detection methods can be considered at four distinct levels.

Level 1: Identifying that damage is present in the structure.

Level 2: In addition to Level 1, determining the geometric location of the damage.

Level 3: Building on Level 2, quantifying the severity of the damage.

Level 4: Further extending Level 3, predicting the remaining service life of the structure.

Damage detection methods based on vibration response can be categorized in two main types, models-based methods and response-based methods. In case of model-based methods, an analytical or numerical model needs to be prepared and the response from the damaged structure can be used to update such model. On other hand, in the case of response-based method the model is not required. From the response obtained through experiments on real structures, the singularity can be captured.

In addition, on the basis of domain-based methods, the detection of damage can be further classified in three specific parts [115].

1. Modal domain: Modal domain methods based on natural frequencies, mode shapes, change in the curvature, damping, and strain energy.
2. Spatial Model Domain: This domain concerns changes in the mass, stiffness and damping matrices.
3. Response Domain: This domain focuses on the spatio-temporal or spatio-spectral domains, which include frequency response functions (FRF), operational deflection shapes (ODS), and transmissibility functions.

The use of natural frequencies has been considered by numerous researchers to develop analytical and numerical models, combined with experimental data, for the purpose of damage identification and quantification. Natural frequencies are preferred over mode shapes because they do not require the installation of additional sensors, making the

approach cost-effective. Additionally, shifts in the natural frequencies can help to understand the global effects. With just a few initial modes of vibration, the damage can be quantified.

In previous studies, researchers have employed various algorithms to obtain damage parameters through optimization. The methods chosen for damage detection in plate-like structures are explored in this section.

Cawley and Adams [19] utilized the ratio of changes in the natural frequencies across various vibration modes to identify the location of damage within aluminium and composite plate structures. Theoretical results derived from finite element analysis were compared against experimental measurements to determine the precise damage location. Stubbs *et al*. [116] developed a method to calculate the damage index based on fractional strain energy for sub regions of 1D structures. Corwell *et. al* [12] extended a similar approach for 2D plate structures with experimental validation. Zhang *et al*. [117] derived a new vibrational characteristic called Frequency the Surface Shift (FSS) using an auxiliary spring mass system for plate structures. FSS is equivalent to the square of the mode shapes. The local changes that occurred in the mode shape of the structure due to local damage were hence classified with this approach.

Dome and Morz [118] demonstrated damage detection in beam and plate structures based the shift in the natural frequencies. They employed rigid support in beam and plate structures to model the damage and obtain the shifts in the eigenvalues. Using optimization, the minimum distance between the theoretical and experimental values corresponding to the shifts in the natural frequencies was obtained. Li *et al.*[119] proposed a damage index with the help of strain modes using Rayleigh's Ritz method. The employed technique was validated using numerical and experimental analysis. Yam *et al.* [120] studied the out-of-plane deflection of a plate structure to define the slope, curvature of the damaged plate in terms of damage index to narrow down the possible damage locations. Lee and Shin [121] introduce a new structural damage identification method (SDIM) for plate structures. This approach utilizes frequency response function (FRF) data from damaged states, rather than modal data. The method iteratively refines the damage localization through a reduced-domain approach and performs well even with noisy data. Numerical simulations demonstrate the feasibility of this technique, showing improved accuracy compared to traditional methods. Lu *et al*. [122] employed

an artificial neural network (ANN) approach to solve the inverse problem for aluminium plates. The training data was generated based on damage parameters obtained by modelling the interaction of Lamb waves with finite element simulations of the damaged plates. Khatir and Wahab [123] utilized the strain fields of damaged plates to optimize the damage parameters using the Jaya algorithm. The data was obtained using proper orthogonal decomposition and radial basis function combined with the Jaya algorithm.

Williams *et al.* [124] introduced the Damage Location Assurance Criterion (DLAC), derived from the modal assurance criterion in modal analysis. This approach can also be applied to identify multiple damage locations. Hosseini-Hashemi *et.al.* [125] developed a closed form solution to extract the natural frequencies for a functionally graded plate structure using Midland theory. With similar forward problem, Yang *et al.* [126] solved the inverse problem utilising intersection of frequency contour line to investigate for damage quantification. Jiang et *al.* [127] utilized the concept of singular value decomposition to identify singularities in the mode shapes of a damaged aluminium plate. A wavelet finite element model of the damaged plate was developed based on the results provided by the singular value decomposition analysis, and ant colony optimization was employed for the purpose of damage quantification. Pan et *al.* [128] introduced a novel noise response rate (NNR) concept to select vibration modes less affected by noise for damage detection using natural frequency shifts. The NNR approach was applied to a curved plate and found to outperform conventional methods. The work presented a promising technique to improve the reliability of vibration-based damage identification.

Krawczuk *et al.* [129] developed a finite spectral plate element model to analyse wave propagation in cracked plates. In their approach, they treated cracks with variable stiffnesses as line springs. The method allowed for efficient prediction of damage parameters based on vibration response, to enhance structural health monitoring. Friswell *et al.*[130], [131]. used a genetic algorithm to locate damage in beam and plate structures, with the help of eigen sensitivity. Horibe and Watanabe [132] also employed a genetic algorithm to identify crack locations in plate structures. However, there work was limited to the identification of cracks aligned parallel to the plate edges.

Yin *et al.* [133] utilised a Bayesian method to studying thin plates, using only a few measured points to understand their dynamic response. Moore *et al.* [134] developed a Bayesian method for analysing cracked plates that vibrate freely, using data from an earlier model by Solecki [135]**.** They used a simulated time series for estimating the required parameters. Li *et al.* [119] employed the ultrasonic scattering field of a damaged plate to assess damage. The measured scattered field was compared with simulated scattering fields generated using finite element analysis. The Markov chain Monte Carlo algorithm was then utilized to accurately determine the location and severity of the damage.

Singh *et al*. [136] used Lamb waves to determine the reflection and transmission coefficients near a damage site. Through experiments, these coefficients were derived using Shkerdin's orthogonality relation, which was then applied in simulations based on finite element analysis to identify the damage parameters. Chatzi *et al.* [137] utilized the extended finite element method (X-FEM) in conjunction with a genetic algorithm (GA) to detect voids and cracks in an elliptical shape**.** Xiang and Liang [138] conducted damage detection on a plate structure in two phases. In the first phase, they identified the damage location using a wavelet finite element model, which was able to reveal singularities in the mode shape. In the second phase, particle swarm optimization was applied to assess the severity of the damage. Mohan *et al.*[139] employed a frequency response function (FRF) in combination with genetic algorithms (GA) and particle swarm optimization (PSO) to detect damage in beam and framed structures. The authors concluded that PSO is more efficient than GA due to its rapid convergence and superior local search capabilities. Dinh-Cong *et al.* [140] employed a finite element model and a Modified Differential Evolution (MDE) algorithm for the purpose of detecting damage in plate structures. The updated finite element model used in the optimization process considered the elimination of non-damaged elements, leadings to the improved computational efficiency of the method.

In this thesis, cracks in beam and plate structures are modelled using a rotational spring approach. The rotational spring model for the beam is inspired by the methods presented in references [35] and [20] . This advancement introduces a computationally efficient analytical framework for preliminary analysis of isotropic plate structures with surface cracks that are partially through the thickness and arbitrarily oriented. Analytical modelling of arbitrarily oriented cracks has been explored to a limited extent

in previous research, primarily due to the complexity involved. The present work addresses this gap by offering an efficient and adaptable solution that enhances early-stage damage assessment capabilities. The degradation in the natural frequencies can be calculated by providing material properties, geometrical properties, and crack parameters. In contrast, traditional methods require different simulations for each case, which could take comparatively more time.

This thesis also presents a solution to the inverse problem for beam and plate structures. The degradation in the natural frequencies of a cracked plate has been utilized to determine the crack parameters. An inverse problem has been formulated using the degradations in the natural frequencies of actual and simulated data through the least square difference method. The developed error function is further optimized using gradient-based optimization efficiently.

The advancements made in this work provide promising results in the field of damage detection, particularly in terms of accuracy and computational efficiency, and match the standards mentioned in the literature studies. The work demonstrates significant development over existing methods in damage modelling and provides insights into incorporating more complexity in the inverse problem. Furthermore, the inverse problem offers very promising results and creates opportunities to expand the research by incorporating additional complexities.

3 Chapter 3: Free vibration analysis of intact and cracked beams

3.1 Introduction

A structure's natural frequencies can be calculated using eigenvalue analysis based on Newton's second law of motion. In the case of single-degree and multiple-degree freedom systems, eigenvectors can be estimated using the stiffness and mass matrices associated with the eigenvalues. Beam and plate structures are considered continuous systems. In the case of a continuous system, eigenvalues also can be estimated by solving equations based on Newton's second law of motion employing analytical and numerical methods based on the boundary conditions of that structure.

The present study employs the Euler-Bernoulli beam theory to analyse the free vibration characteristics of cracked beam structures. This theory assumes that plane cross-sections remain flat and perpendicular to the neutral axis during bending, effectively neglecting the influence of transverse shear deformation. Such an assumption is valid for slender beams, particularly when the length-to-depth ratio exceeds 10-15. The beam configurations considered in this research fall within this slenderness range, where the effects of shear deformation are minimal. As a result, the Euler-Bernoulli model provides sufficiently accurate predictions for the natural frequencies of the beams under consideration.

Moreover, the analysis in this study is focused on the lower vibration modes, where the influence of shear deformation and rotary inertia is relatively insignificant. The use of Euler-Bernoulli theory also simplifies the mathematical formulation, which is particularly beneficial when modelling the additional complexity introduced by the presence of cracks. Given the geometric proportions of the beams, the vibration range of interest, and the need for analytical clarity, the application of Euler-Bernoulli beam theory is well-justified and appropriate for the scope of this investigation.

In this chapter, the free vibration analysis of an isotropic beam is examined. Initially, the vibration analysis of an intact beam is considered. The dynamic stiffness matrix for the beam from the reference [31], [35], is used. Using Newton Raphson method, the determinant of the dynamic stiffness matrix is calculated to obtain the natural frequency parameters.

A similar procedure is adapted to find the natural frequency parameters for the cracked beam. The loss in axial stiffness due to a crack in a beam is often neglected because

cracks significantly impact bending stiffness more than axial stiffness. Bending effects dominate the structural behaviour of beams, making the rotational spring model focusing on flexural rigidity reductions sufficient for practical analysis. This simplification avoids unnecessary complexity without compromising accuracy for most engineering applications [32], [35].

An analytical solution based on Rayleigh's quotient is used to validate the results obtained. The analytical formulation based on Rayleigh's quotient is further considered for damage detection. The applied methods ignore the structure's damping and non-linear behaviour.

3.2 Natural Frequencies of an Intact Beam.

Consider a beam with length *'L'*, breadth *'b'* and depth *'h'*, fixed at both ends, shown in Figure 3.1.

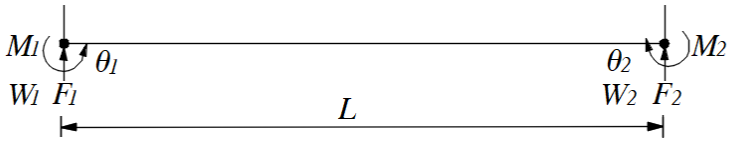

Figure 3.1: Beam fixed at both ends.

where θ_1 and θ_2 are rotations associated with the bending moments. M_1 and M_2. w_1 and w_2 are the vertical displacements associated with the forces F_1 and F_2.

The dynamic stiffness matrix can be expressed as [35]:

$$\begin{Bmatrix} F_1 \\ M_1 \\ F_2 \\ M_2 \end{Bmatrix} = \begin{bmatrix} a_n & b_n & -d_n & e_n \\ b_n & c_n & -g_n & f_n \\ -d_n & -g_n & \alpha_n & -h_n \\ e_n & f_n & -h_n & \gamma_n \end{bmatrix} \begin{Bmatrix} w_1 \\ \theta_1 \\ w_2 \\ \theta_2 \end{Bmatrix} \tag{3.2.1}$$

Here, 'n' denotes the members or substructure number. For a single beam, n =1. The elements in the stiffness matrix can be expressed:

$$\left.\begin{aligned} a_n = \alpha_n = \frac{EI\lambda^3(S_nC_n' + C_nS_n')}{\sigma_n}, \quad & b_n = h_n = \frac{EI\lambda^2(S_nS_n')}{\sigma_n}, \\ c_n = \gamma_n = \frac{EI\lambda(S_nC_n' - C_nS_n')}{\sigma_n}, \quad & e_n = g_n = \frac{EI\lambda^2(C_n' - C_n)}{\sigma_n}, \\ d_n = \frac{EI\lambda^3(S_n + S_n')}{\sigma_n}, \quad & f_n = \frac{EI\lambda^3(S_n - S_n')}{\sigma_n}, \end{aligned}\right\} \tag{3.2.2}$$

in which

$$\left.\begin{aligned} S_n = \sin\lambda L_n, \quad & C_n = \cos\lambda L_n \\ S_n' = \sinh\lambda L_n, \quad & C_n' = \cosh\lambda L_n \\ \lambda = \sqrt[4]{\frac{\mu\omega^2}{EI}}, \quad & \sigma_n = 1 - C_nC_n' \end{aligned}\right\} \tag{3.2.3}$$

where, E is Young's Modulus, I is moment of inertia, and μ is the mass per unit length of the beam.

From Figure 3.2 it can be seen that, when the beam is fixed at both ends, the rotations and deflections at these ends are restricted. To simplify the problem, a node is considered at the midpoint of the beam. The dynamic stiffness matrix is expressed in Eq. (3.2.4)

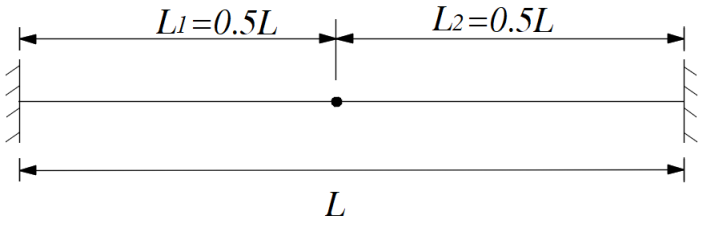

Figure 3.2 - Beam fixed at both ends (Node at midspan).

$$\begin{Bmatrix} F_1 \\ M_1 \\ F_2 \\ M_2 \\ F_3 \\ M_3 \end{Bmatrix} = \begin{bmatrix} a_1 & b_1 & -d_1 & e_1 & 0 & 0 \\ b_1 & c_1 & -g_1 & f_1 & 0 & 0 \\ -d_1 & -g_1 & a_2+\alpha_1 & b_2-h_1 & -d_2 & e_2 \\ e_1 & f_1 & b_2-h_1 & c_2+\gamma_1 & -g_2 & f_2 \\ 0 & 0 & -d_2 & -g_2 & \alpha_2 & -h_2 \\ 0 & 0 & e_2 & f_2 & -h_2 & \gamma_2 \end{bmatrix} \begin{Bmatrix} w_1 \\ \theta_1 \\ w_2 \\ \theta_2 \\ w_3 \\ \theta_3 \end{Bmatrix} \tag{3.2.4}$$

Based on the boundary conditions, the dynamic stiffness matrix can be updated from Eq. (3.2.4) to Eq. (3.2.5)

$$\begin{Bmatrix} F_1 \\ M_1 \\ F_2 \\ M_2 \\ F_3 \\ M_3 \end{Bmatrix} = \begin{bmatrix} a_1 & b_1 & -d_1 & e_1 & 0 & 0 \\ b_1 & c_1 & -g_1 & f_1 & 0 & 0 \\ -d_1 & -g_1 & a_2+\alpha_1 & b_2-h_1 & -d_2 & e_2 \\ e_1 & f_1 & b_2-h_1 & c_2+\gamma_1 & -g_2 & f_2 \\ 0 & 0 & -d_2 & -g_2 & \alpha_2 & -h_2 \\ 0 & 0 & e_2 & f_2 & -h_2 & \gamma_2 \end{bmatrix} \begin{Bmatrix} 0 \\ 0 \\ w_2 \\ \theta_2 \\ 0 \\ 0 \end{Bmatrix} \tag{3.2.5}$$

Eq. (3.2.5) can be further simplified

$$\begin{Bmatrix} F_2 \\ M_2 \end{Bmatrix} = \begin{bmatrix} a_2 + \alpha_1 & b_2 - h_1 \\ b_2 - h_1 & c_2 + \gamma_1 \end{bmatrix} \begin{Bmatrix} w_2 \\ \theta_2 \end{Bmatrix} \tag{3.2.6}$$

The determinant of the dynamic stiffness matrix can then be expressed as:

$$|k| = (a_2 + \alpha_1)(c_2 + \gamma_1) - (b_2 - h_1)^2 \tag{3.2.7}$$

For the midpoint node, $a_2 = \alpha_1$, $c_2 = \gamma_1$ and $b_2 = h_1$, which results in:

$$|k| = (2\alpha_1)(2\gamma_1) = 4\alpha_1\gamma_1 \tag{3.2.8}$$

To find the natural frequencies of the beam, we need to solve the equation for $|\mathrm{k}| = 0$.

$$4\alpha_1\gamma_1 = 0 \tag{3.2.9}$$

Eq. (3.2.9) can be satisfied when $\alpha_1 = 0$ or $\gamma_1 = 0$.

If $\alpha_1 = 0$ then

$$S_1C_1' + C_1S_1' = 0$$

$$\tan(\lambda/2) = -\tanh(\lambda/2)$$

which occurs when $(\lambda/2)$ is close to $\big(i - (1/4)\big)\pi$ where $i = 1,2,3, \ldots$

If $\gamma_1 = 0$ then

$$S_1C_1' - C_1S_1' = 0$$

$$\tan(\lambda/2) = \tanh(\lambda/2)$$

which occurs when $(\lambda/2)$ is close to $\big(i + (1/4)\big)\pi$ where $i = 1,2,3, \ldots$

A numerical procedure is required to find these zeros accurately. The Wittrick-Williams algorithm [31] has been considered by Labib *et al.* [35], with the bisection method to calibrate the natural frequencies of the cracked beam after the introduction of the crack as a rotational spring.

In the Section 3.3, a crack is introduced represented by a rotational spring. To improve the efficiency and accuracy of the results, Newton-Raphson method is employed along with the symbolic computation toolbox available in MATLAB.

3.3 Natural Frequencies of a Cracked Beam: Crack Modelling Based on a Rotational Spring.

As discussed in the literature review, various methods have been used to model damage in beam and frame-like structures. including finite element analysis (FE) and extended finite element analysis (XFEM). Modelling a crack based on the consequent loss of stiffness is the mostly frequency used method. Researchers have carried out a number of studies regarding open and breathing crack and the employment of linear or non-linear rotational springs with or without consideration of axial stiffness and damping.

Cademmi and Calio [32], [34] provided a formulation for the stiffness of a rotational spring, employed to model a concentrated crack in a Euler Bernoulli beam based on the depth of the crack. Formulation for the stiffness of a rotational spring is expressed in Eq. (3.3.1). Figure 3.3 shows a simply supported cracked beam.

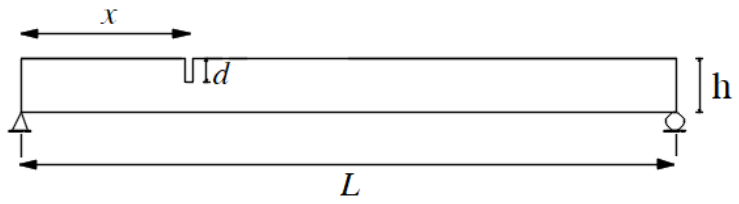

(a)

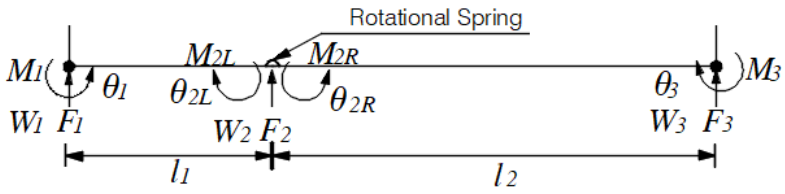

(b)

Figure 3.3 - Beam with a crack a) beam with crack depth '*d*'. b) Rotational spring model with resulting forces.

$$k^* = \frac{EI}{L}\frac{1}{\lambda^*} \tag{3.3.1}$$

Here, λ^* is the non-dimensional local compliance, which can be further expressed by the formulation given in Eq. (3.3.2)

$$\lambda^* = \frac{h}{L} C(d/h) \tag{3.3.2}$$

$C(d/h)$ is a nondimensional term, which is given by:

$$C(d/h) = a_0 \sum_{n=1}^{10} a_n \left(\frac{d}{h}\right)^n \tag{3.3.3}$$

Cademmi and Calio [32] developed the formulation for this dimensionless parameter expressed in Eq. (3.3.4)

$$C(d/h) = \frac{(d/h)[2 - (d/h)]}{0.9[1 - (d/h)]^2} \tag{3.3.4}$$

Labib *et al.* [35] provided a comparison of this non-dimensional parameter with previous literature and concluded on the accuracy of the formulation used in Eq. (3.3.4), setting the upper limit of the crack depth ratio to 0.4.

To conduct studies regarding the damage modelling and the detection in this thesis, this parameter Eq. (3.3.4) will be utilized to evaluate the non-dimensional compliance and stiffness associated with the rotational spring. The derivation of the dynamic stiffness matrix for beam which are fixed at both ends with a concentrated crack at their midpoint is explained in section 3.4.

3.4 Derivation of The Dynamic Stiffness Matrix for a Cracked Beam.

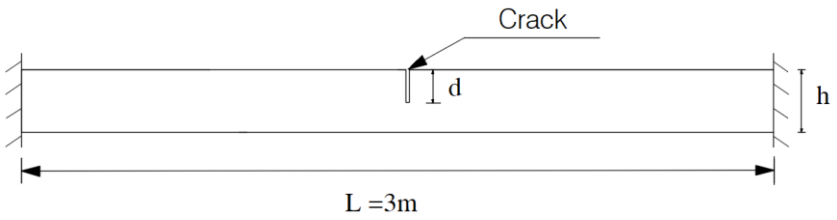

(a)

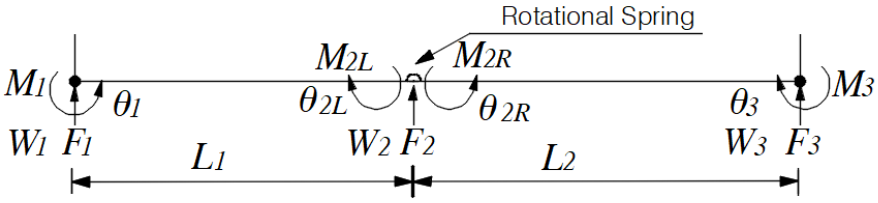

(b)

Figure 3.4 - Beam with fixed ends: a) with crack b) Free body diagram with rotational spring model.

The crack can now be introduced into the dynamic stiffness matrix for the beam. Based on a rotational spring with stiffness k^* with three degrees of freedom, the node corresponding to the spring is associated with a vertical displacement and rotations at the left-and right-hand sides of the crack as shown in Figure 3.4 The stiffness matrix associated with the rotations of the crack is expressed in Eq. (3.4.1)

$$\begin{Bmatrix} M_L \\ M_R \end{Bmatrix} = \begin{bmatrix} k^* & -k^* \\ -k^* & k^* \end{bmatrix} \begin{Bmatrix} \theta_L \\ \theta_R \end{Bmatrix} \tag{3.4.1}$$

The dynamic stiffness matrix can be developed based on reference [35], as follows:

$$\begin{bmatrix} F_1 \\ M_1 \\ F_2 \\ M_{2L} \\ M_{2R} \\ F_3 \\ M_3 \end{bmatrix} = \begin{bmatrix} a_1 & b_1 & -d_1 & e_1 & 0 & 0 & 0 \\ b_1 & c_1 & -g_1 & f_1 & 0 & 0 & 0 \\ -d_1 & -g_1 & a_2+\alpha_1 & -h_1 & -b_2 & d_2 & e_2 \\ e_1 & f_1 & -h_1 & k^*+\gamma_1 & -k^* & 0 & 0 \\ 0 & 0 & -b_2 & -k^* & k^*+c_2 & -h_2 & f_2 \\ 0 & 0 & -d_2 & 0 & -g_2 & a_2 & -h_2 \\ 0 & 0 & c_2 & 0 & f_2 & -h_2 & \gamma_2 \end{bmatrix} \begin{bmatrix} w_1 \\ \theta_1 \\ w_2 \\ \theta_{2L} \\ \theta_{2R} \\ w_3 \\ \theta_3 \end{bmatrix} \quad (3.4.2)$$

where the elements of the stiffness matrix from Eq. (3.4.2) can be expressed as

$$\left.\begin{aligned} a_1 = \alpha_1 = \frac{EI\lambda^3(S_1C_1' + C_1S_1')}{\sigma_1}, \quad b_1 = h_n = \frac{EI\lambda^2(S_1C_1' + C_1S_1')}{\sigma_n}, \\ C_1 = \gamma_1 = \frac{EI\lambda(S_1C_1' - C_1S_1')}{\sigma_1}, \quad e_1 = g_1 = \frac{EI\lambda^2(C_1' - C_1)}{\sigma_n}, \\ d_1 = \frac{EI\lambda^3(S_1 + S_1')}{\sigma_1}, \quad f_n = \frac{EI\lambda^3(S_1 + S_1')}{\sigma_1}, \end{aligned}\right| \quad (3.4.3)$$

$$\left.\begin{aligned} S_1 = \sin\lambda L_1, \quad C_1 = \cos\lambda L_1 \\ S_1' = \sinh\lambda_1, \quad C'_1 = \cosh\lambda L_1 \\ \lambda = \sqrt[4]{\frac{\mu\omega^2}{EI}}, \quad \sigma_1 = 1 - C_1C'_1 \end{aligned}\right| \quad (3.4.4)$$

$$\left.\begin{aligned} a_2 = \alpha_2 = \frac{EI\lambda^3(S_2C_2' + C_2S_2')}{\sigma_1}, \quad b_2 = h_2 = \frac{EI\lambda^2(S_2C_2' + C_2S_2')}{\sigma_n}, \\ C_2 = \gamma_2 = \frac{EI\lambda(S_2C_2' - C_2S_2')}{\sigma_1}, \quad e_2 = g_2 = \frac{EI\lambda^2(C_2' - C_2)}{\sigma_n}, \\ d_2 = \frac{EI\lambda^3(S_2 + S_2')}{\sigma_2}, \quad f_n = \frac{EI\lambda^3(S_2 + S_2')}{\sigma_2}, \end{aligned}\right| \quad (3.4.5)$$

$$\left.\begin{aligned} S_2 = \sin\lambda L_2, C_2 = \cos\lambda L_2 \\ S_2' = \sinh\lambda_2, C'_2 = \cosh\lambda L_2 \\ \lambda = \sqrt[4]{\frac{\mu\omega^2}{EI}}, \quad \sigma_2 = 1 - C_2C'_2 \end{aligned}\right| \quad (3.4.6)$$

Here, k^* can be expressed based on the crack depth (d) from Eq. (3.3.1). After applying boundary conditions, the dynamic stiffness matrix can then be updated:

The determinant of the dynamic stiffness matrix is expressed in Eq. (3.4.7), as a function of the non-dimensional frequency parameter (λ).

$$f(\lambda) = (a_2 + \alpha_1)[(k + \gamma_1)(k + c_2) - k^2] + h_1[(k + c_2)(-h_1) - b_2 k] - b_2[h_1 k + b_2(k + \gamma_1)] \tag{3.4.7}$$

Eq. (3.4.8) is the differential of Eq. (3.4.7) with respect to the non-dimensional frequency parameter (λ) which allows us to apply the Newton-Raphson method for the determination of the non-dimensional frequency parameters associated with the natural frequencies. Appendix (B) provides the MATLAB codes for formation of Eq. (3.4.8).

$$f'(\lambda) = \frac{df(\lambda)}{d\lambda} \tag{3.4.8}$$

3.5 Application of Newton-Raphson Method.

The Newton-Raphson method can be defined as an iterative method for approximating the roots of real-valued functions through successive refinements of initial trial values or estimates. Its iterative formula leverages function evaluations and derivatives to swiftly converge towards solutions, rendering it particularly effective for sufficiently smooth functions.

However, the limitations associated with this method are in relation to singularities and discontinuities of the function, which require the accurate selection of initial guesses and convergence criteria. Despite these limitations, its widespread adoption across scientific and engineering disciplines underscores its computational prowess and utility in tackling complex numerical challenges.

The Newton-Raphson iteration formulation is a key component of this root-finding method. The formulation is expressed in the Eq. (3.5.1)

$$x_{n+1} = x_n - \frac{f(x_n)}{f'(x_n)} \tag{3.5.1}$$

It provides a recursive process to update an initial guess x_n to obtain a better approximation x_{n+1} of the root of a function $f(x)$. Mathematically, the formula states that the next approximation x_{n+1} is equal to the current approximation x_n minus the ratio of the function value $f(x_n)$ to its derivative $f'(x_n)$ at that point. In essence, it adjusts the current estimate based on the function's slope (derivative) at that point, aiming to approach the root by iteratively refining the approximation. This process continues until a satisfactory level of precision or convergence is achieved.

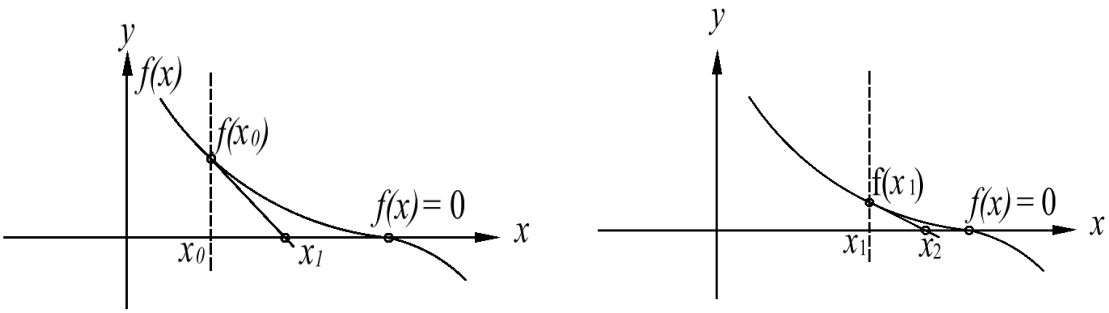

(a) (b)

Figure 3.5 - Graphical representation of Newton-Raphson method a) Initial Guess (x_0) with obtained root (x_1) b) Using ' x_1' as a trial value for next iteration to obtain (x_2).

Figure 3.5 illustrates the graphical interpretation of the Newton Raphson method for finding the root of a function $f(x)$. In Figure 3.5(a), an initial guess x_0 is chosen, from which a tangent is drawn to the curve at the point (x_0, $f(x_0)$). The intersection of this tangent with the x-axis gives the next approximation x_1 , which is expected to be closer to the actual root.

This new estimate x_1 is then used as a refined initial guess, as shown in Figure 3.5 (b). Repeating this process iteratively leads to successive approximations x_2, x_3..... that converge to the actual root of the function.

Newton Raphson method is applied using the MATLAB symbolic computational tools. From Eq. (3.4.7) and Eq. (3.4.8), the non-dimensional frequency parameter can be updated based on Eq. (3.5.2).

$$\lambda_{n+1} = \lambda_n - \frac{f(\lambda_n)}{f'(\lambda_n)} \tag{3.5.2}$$

The non-dimensional parameter is updated with each iteration, and the iteration stops when it satisfies the expected tolerance, which depends on the difference between the function's final value and the last two updated parameters.

$$Tolerance < |f(\lambda_{n+1}) - f(\lambda_n)|$$

The initial trial guess used in this method is obtained from the original natural frequencies of the structure. The significance behind this choice is that the damaged natural frequencies will be close to the original natural frequencies due to a single crack in the beam. A numerical example is considered in the next section 3.5.1 to obtain the results for the degradation in the natural frequencies of the beam because of the presence of a single crack. The results are validated with the method based on the Wittrick-Williams algorithm mentioned in [35].

In this thesis, the Newton-Raphson method has been used to determine the non-dimensional frequency parameters for cracked beams by solving the determinant of the dynamic stiffness matrix. Furthermore, for both beam and plate structures, analytical solutions have been developed to obtain the natural frequencies of cracked configurations. The Newton-Raphson method is fundamentally designed to solve equations involving a single variable. In the case of the inverse problem for a beam, two parameters (crack location and severity) must be identified, whereas for plate structures, a total of five parameters are to be determined. Therefore, direct implementation of the Newton-Raphson method was not feasible. Instead, an inbuilt toolbox available in MATLAB, FMINCON, which employs the interior-point algorithm and internally utilizes a Newton-Raphson-based approach for multivariable functions, has been used to solve the inverse problem for both beam and plate structures.

3.5.1 Numerical Example.

Figure 3.6 illustrates an isotropic beam fixed at both ends, has a Young's modulus of 2.06 x 10^{11} N m^{-2} and a mass per unit length of 185.40 kg m^{-1}. It has a length L = 3 m, with a breadth (b) and depth (h) of 198 mm and 122 mm respectively, and a 10 mm deep crack.

A single crack is modelled at two different locations in the beam presented in Figure 3.6.

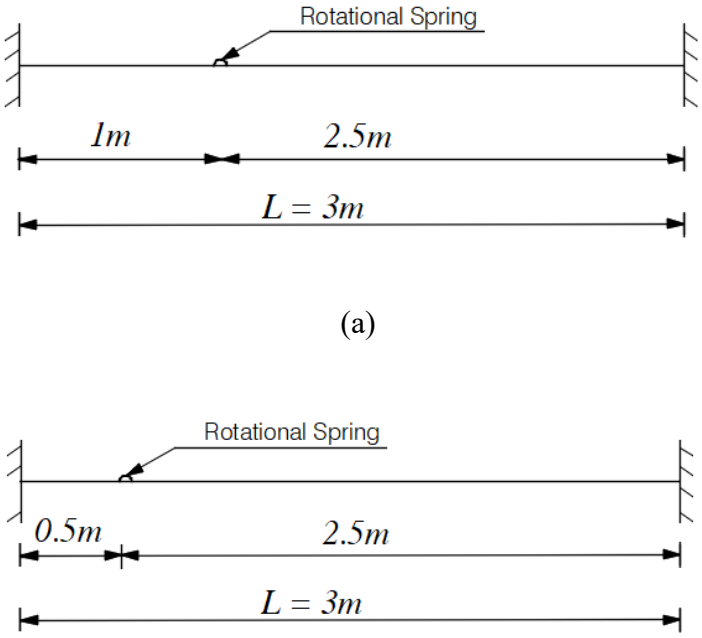

Figure 3.6 - Beam with fixed end supports with a crack at, (a) 1m, (b) 0.5 m from left hand support.

Table 3.1- Natural frequencies of a cracked beam using W-W algorithm and N-R method shown in Figure 3.6 (a).

Mode	(a)	(b)	(c)	(d)	(e)	(r)
1	448.129	438.871	438.871	9.257	9.269	0.998
2	1235.286	1164.962	1164.959	70.33	70.2	1.00043
3	2421.654	2412.327	2412.326	9.327	9.324	1.00033
4	4003.118	3864.854	3864.848	138.2	138.28932	0.99982

Table 3.2 - Natural frequencies of a cracked beam using W-W algorithm and N-R method shown in Figure 3.6 (b).

Mode	(a)	(b)	(c)	(d)	(e)	(r)
1	448.129	444.53	444.51	3.59	3.6307	0.99136
2	1235.280	1226.72	1226.7	8.553	8.5532	1.00005
3	2421.65	2325.327	2325.4	96.324	96.25132	1.00076
4	4003.11	3792.16	3792.1	210.95	211.0379	0.99958

Table 3.3 – Reference for Table 3.1 and Table 3.2

(a)	Uncracked natural frequencies (rad/sec)
(b)	Cracked natural frequencies calculated using the Wittrick-Williams algorithm (rad/sec) [35].
(c)	Cracked natural frequencies calculated using the Newton-Raphson method (rad/sec)
(d)	Error for uncracked natural frequencies. (a) - (b) rad/sec
(e)	Error for uncracked natural frequencies. (a) - (c) rad/sec
(r)	Ratio. (d)/(e)
Tolerance	10^{-4}

From Table 3.1 and Table 3.2 , it can be observed that the results obtained using the Newton-Raphson method closely match the results from [35] which are based on the

Wittrick-Williams algorithm and bisection method. The tolerance used for the iterations is 10^{-4} for accurate results.

The validation of the applied techniques is considered in section 3.6 based on the strain energy method explored by Morassi [41] for crack modelling and detection in a beam structure.

3.6 Strain Energy Approach.

The relationship of changes in the natural frequencies due to presence of crack, with respect to the stored strain energy of an intact cross section of the beam has been defined by Morassi [41].The formulation for the compliance and rotational spring was defined by Freund and Hermann [141] , based on energy release rate at the crack location due to bending moment. In this section, the relationship between the difference between the square of the natural frequencies between intact and cracked beam has been redeveloped using rotational spring and compliance provided by Biello and validated by Caddemi and Calio [34], and Labib *et al.* [35] . The formulation for the degradation in the natural frequency is derived for the simply supported beam with length (l), breadth (b) and depth (h) is shown in the Figure 3.7 below. The beam is made up of isotropic material with Young's modulus E. I is the moment of inertia and μ is the mass per unit length.

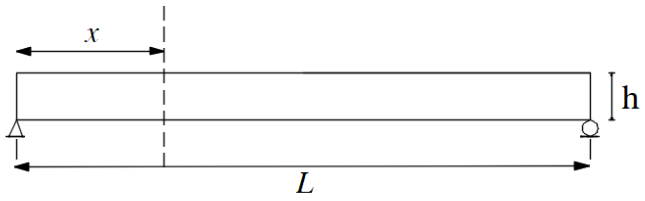

Figure 3.7 – Simply supported beam.

The vertical displacement at any point x in the n^{th} mode of vibration can be expressed as:

$$w(x) = a_n \cos(\zeta_n x) + b_n \sin(\zeta_n x) + c_n \cosh(\zeta_n x) + d_n \sinh(\zeta_n x) \qquad (3.6.1)$$

where (x) is the position along the length of the beam and $a_n, b_n, c_n,$ and d_n are parameters that depend upon boundary conditions and ζ_n can be expressed as:

$$\zeta_n = \frac{1}{\lambda_n}$$

λ_n is a non-dimensional frequency parameter, based on material properties and the vibration mode (n) from the Eq. (3.4.4).

The maximum strain energy U_0 and kinetic energy T_0 for the intact beam are expressed in Eq.(3.6.2) and Eq. (3.6.3) respectively, where $M(x)$ is the bending moment at location x and ω_0 is the natural frequency for the intact plate.

$$U_0 = \frac{1}{2EI}\int_0^l M(x)^2 dx \tag{3.6.2}$$

$$T_0 = \frac{1}{2}\mu\omega^2{}_0 \int_0^l \big(w(x)\big)^2 dx \tag{3.6.3}$$

After introducing a crack as a rotational spring shown in Figure 3.8 at the point x, there is a discontinuity of rotation ($\delta\theta$) across the crack.

The natural frequency is reduced to ω_c so that the new maximum kinetic energy is:

$$T_c = \frac{1}{2}\mu\omega^2{}_c \int_0^l \big(w(x)\big)^2 dx \tag{3.6.4}$$

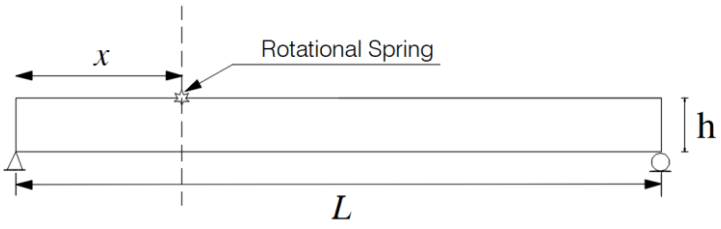

Figure 3.8 – A simply supported beam with a crack is represented by a rotational spring.

From the definition of compliance (C).

$$\delta\theta = C\big(M(x)\big)$$

And the incremental strain energy associated with the discontinuous rotation $\delta\theta$ in that portion is:

$$dU_d = \frac{1}{2}\delta\theta\big(M(x)\big) = \frac{1}{2}C\big(M(x)\big)^2$$

$$dU_d = \frac{1}{2}C\big(M(x)\big)^2 \tag{3.6.5}$$

From the law of conservation of energy, we can express that for an intact beam:

$$T_0 = U_0 \tag{3.6.6}$$

and for the damaged beam.

$$T_c = U_0 - dU_d \tag{3.6.7}$$

From Eq. (3.6.6), we can express:

$$T_0 - T_c = dU_d \tag{3.6.8}$$

which can be further simplified and expressed in terms of natural frequencies.

$$\frac{1}{2}\mu\,(\omega_0^2 - \omega_c^2)\int_0^l \big(w(x)\big)^2 dx = \frac{1}{2}C\big(M(x)\big)^2$$

$$(\omega_0^2 - \omega_c^2) = \frac{\big(M(x)\big)^2}{k_r{}^*\,\mu\,\int_0^l \big(w(x)\big)^2 dx} \tag{3.6.9}$$

where,

$$k_r{}^* = \frac{1}{C} \tag{3.6.10}$$

Now $M_n(x) = EIk_n(x)$ where $k_n(x)$ represents the curvature at the location x where the crack is considered.

$$\delta_n = (\omega_0^2 - \omega_c^2) = \frac{(EI)^2\big(k_n(x)\big)^2}{k^*{}_r\,\mu\,\int_0^l \big(w_n(x)\big)^2 dx} \tag{3.6.11}$$

δ_n can be expressed as a change between squares in the natural frequencies of intact and damaged beams.

The above expressions assume that the mode shape of the vibration does not change after the crack is introduced. Damping is also ignored. In the next section 3.6.1, the application of the strain energy approach is demonstrated for a crack present in a beam with fixed end supports.

3.6.1 Application of Strain Energy Approach for Beam Fixed at Both Ends.

A beam with a length of L, fixed at both ends is considered shown in Figure 3.9. A node at the midpoint divides the beam into two parts. On the left-hand side of the beam, a crack is modelled with the help of a rotational spring.

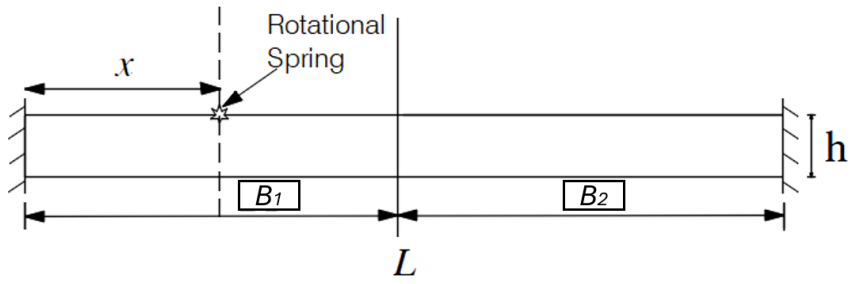

Figure 3.9 - A beam with concentrated crack at distance x from the left-hand fixed support.

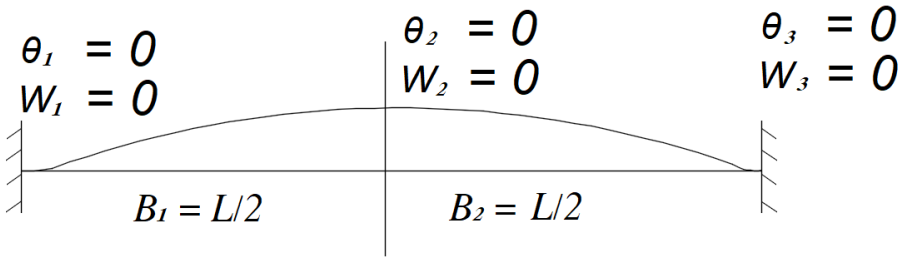

a) Symmetric modes of vibration. (Modes :1 and 3)

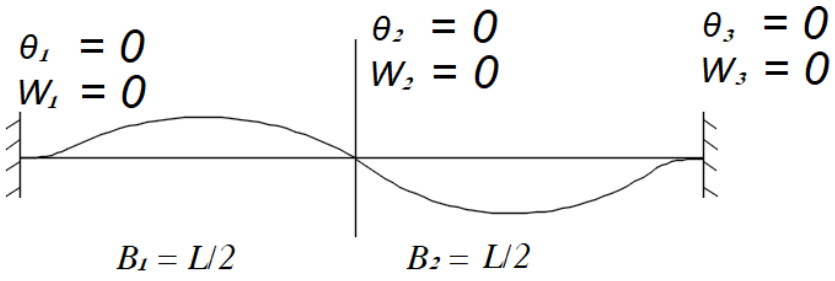

b) Antisymmetric mode of vibration. (Modes: 2 and 4)

Figure 3.10 - Modes of vibration. a) Symmetric and b) Anti-symmetric mode of vibrations

The symmetric and anti-symmetric modes of vibration are shown in Figure 3.10. For symmetric modes, the displacement becomes maximum at the midpoint node, and it is considered unity. Hence, rotation becomes zero. Vice versa for anti-symmetric modes, the rotation becomes maximum at the midpoint node, considered unity, and the displacement becomes zero. At the endpoints, because of the fixity, the values of the displacement and rotations are zero for all modes of vibration. Vertical displacement of the beam at a location (x) can be expressed in two parts: *B1* and *B2*

$$w_{nBi}(x) = a_{nBi}\cos(\zeta_n x) + b_{nBi}\sin(\zeta_n x) + c_{nBi}\cosh(\zeta_n x) + d_{nBi}\sinh(\zeta_n x) \tag{3.6.12}$$

where a, b, c and d denote the parameters for different modes of vibration and different beams. Also, 'i' denotes the part of beam i.e. *B1, B2* as shown in Figure 3.10. These parameters can be obtained by solving Eq. (3.6.12) with the appropriate boundary conditions.

For n = 1, for symmetric mode of vibration.

At $x = 0$,

$w_{nB1}(0) = 0, \theta_{nB1}(0) = 0.$

$$w_{nB1}(0) = a_{nB1} + c_{nB1} = 0 \tag{3.6.13}$$

$$\theta_{nB1}(0) = \zeta_n(b_{nB1} + d_{nB1}) = 0 \tag{3.6.14}$$

At $x = L/2, w_{nB1}(0) = 1, \theta_{nB1}(0) = 0$

$$w_{nB1}(L/2) = a_{n1B1}\cos(\zeta_n L/2) + b_{nB1}\sin(\zeta_n L/2) + c_{nB1}\cosh(\zeta_n L/2) + d_{nB1}\sinh(\zeta_n L/2) = 1 \tag{3.6.15}$$

$$\theta_{nB1}(L/2) = \zeta_n(-a_{n1B1}\sin(\zeta_n L/2) + \mathrm{bn_{B1}}\cos(\zeta_n L/2) + c_{nBi}\sinh(\zeta_n L/2) + d_{nB1}\cosh(\zeta_n L/2)) = 0 \tag{3.6.16}$$

Eqs. (3.6.13) to (3.6.16) can be expressed in the matrix form:

$$\begin{bmatrix} 1 & 0 & 1 & 0 \\ 0 & 1 & 0 & 1 \\ \cos(\zeta_n L/2) & \sin(\zeta_n L/2) & \cosh(\zeta_n L/2) & \sinh(\zeta_n x) \\ -\sin(\zeta_n L/2) & \cos(\zeta_n L/2) & \sinh(\zeta_n L/2) & \cosh(\zeta_n L/2) \end{bmatrix} \begin{Bmatrix} a_{n1} \\ b_{n1} \\ c_{n1} \\ d_{n1} \end{Bmatrix} = \begin{bmatrix} 0 \\ 0 \\ 1 \\ 0 \end{bmatrix} \tag{3.6.17}$$

After performing the matrix operations, the parameters $a_{11}, b_{11}, c_{11}, \text{and } d_{11}$ can be obtained for 1^{st} mode of vibration for the part B_1. Similarly, the parameters can be obtained for the n^{th} mode of vibration by considering displacements and rotations as per the symmetric or anti-symmetric mode of vibration.

An expression for the rotation can then be obtained from the first differential of the vertical displacement with respect to location (x).

$$\theta_{nBi}(x) = (\zeta_n)[-a_{nBi}\sin(\zeta_n x) + b_{nBi}\cos(\zeta_n x) + c_{nBi}\sinh(\zeta_n x) + d_{nBi}\cosh(\zeta_n x)] \quad (3.6.18)$$

Further differentiation of Eq. (3.6.18) provides an expression for the curvature.

$$k_{nBi}(x) = (\zeta_n)^2[-a_{nBi}\cos(\zeta_n x) - b_{nBi}\sin(\zeta_n x) + c_{nBi}\cosh(\zeta_n x) + d_{nBi}\sinh(\zeta_n x)] \quad (3.6.19)$$

Utilizing the parameters obtained from the matrix operations, the curvature for the n^{th} mode of vibration can be obtained. The degradation in the square of the natural frequencies of intact and cracked beams can be obtained using Eq. (3.6.11). The denominator of Eq. (3.6.11) can be obtained by integrating the square of the displacement function over the length of the beam.

$$J_{ni} = \int_0^l \big(w(x)\big)^2 dx \quad (3.6.20)$$

The integration operation in the Eq. (3.6.21) can be performed using the Symbolic computational toolbox available in MATLAB. However, to make the damage detection procedure more computationally efficient, this is not the preferred option. Integration is instead performed using conventional methods to increase computational efficiency. MATLAB codes for this section are provided in Appendix (C).

Eq. (3.6.20) can be evaluated based on trigonometric and hyperbolic identities as per Eq. (3.6.21)

Here, $\theta = (\zeta_n)\, x = x/\lambda_n$ and $d\theta = (\zeta_n)\, dx = dx/\lambda_n$

$$J_{ni} = \int_0^l \left(w(x)\right)^2 dx$$

$$\begin{aligned} = \lambda_n \Big[& (a_{nBi})^2 \left(\frac{\theta}{2} + \frac{\sin 2\theta}{4}\right) + (b_{nBi})^2 \left(\frac{\theta}{2} - \frac{\sin 2\theta}{4}\right) \\ & + (c_{nBi})^2 \left(\frac{\theta}{2} + \frac{\sin 2\theta}{4}\right) + (d_{nBi})^2 \left(-\frac{\theta}{2} + \frac{\sin 2\theta}{4}\right) \\ & + a_{nBi} b_{nBi} \left(\frac{\cos 2\theta}{2}\right) \\ & + c_{nBi} d_{nBi} \left(\frac{\cosh 2\theta}{2}\right) + (a_{nBi} c_{nBi})(\cos\theta \sinh\theta \\ & + \sin\theta \cosh\theta) + (a_{nBi} d_{nBi})(\cos\theta \cosh\theta \\ & + \sin\theta \cosh\theta) + (b_{nBi} c_{nBi})(-\cos\theta \cosh\theta \\ & + \sin\theta \sinh\theta) \\ & + (b_{nBi} d_{nBi})(-\cos\theta \sinh\theta + \sin\theta \cosh\theta) \Big]_0^{L\zeta_n} \end{aligned} \qquad (3.6.21)$$

The above expressions are a simplification of the strain energy approach. To determine the accuracy of the method with respect to the Newton-Raphson method, numerical examples and are considered in section 3.6.2.

3.6.2 Numerical Example and Validation.

An isotropic beam fixed at both ends has a Young's modulus of 2.06 x 10^{11} N m^{-2} and a mass per unit length of 185.40 kg m^{-1}. The beam has a length L = 3 m and breadth *(b)* and depth *(h)* of 198 mm and 122 mm, respectively. A single crack is modelled in this beam using Eq. (3.6.11). To ensure clarity, it is explicitly stated that only a single crack is considered in the analysis. This crack is individually placed at discrete intervals of 0.01 m along the beam length, up to 1.5 m. For each crack location, the normalized changes in the natural frequencies of the first four vibration modes are calculated using the Newton-Raphson method combined with the strain energy approach.

The results are plotted for crack depths of 0.01m and 0.05m in Fig. 3.11 and Fig.3.12 respectively. Due to the symmetry of the problem only half the beam is considered.

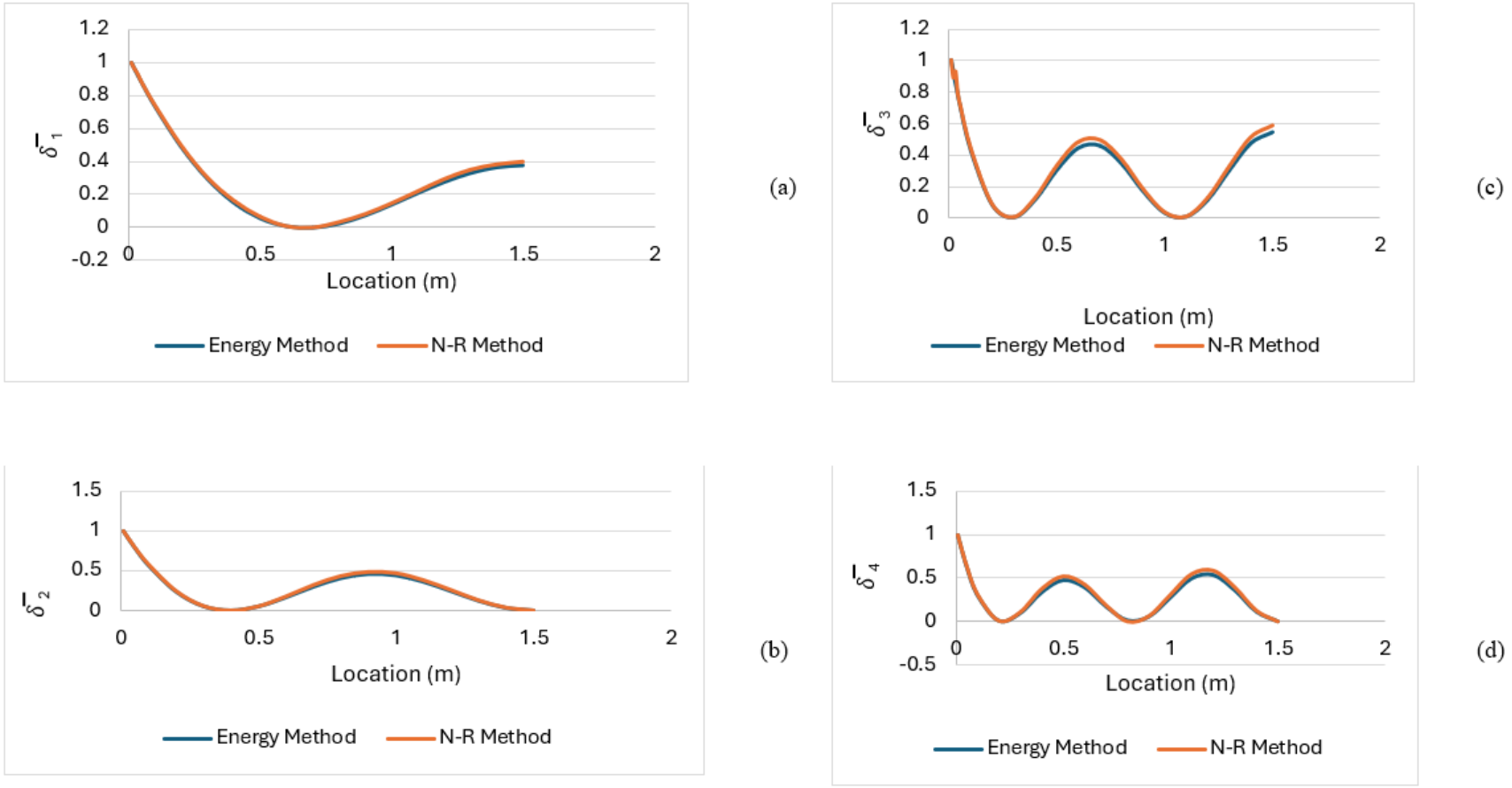

Figure 3.11 - Normalised natural frequencies vs location for d = 0.01m: a) n = 1, b) n =2, c) n = 3, d) n = 4.

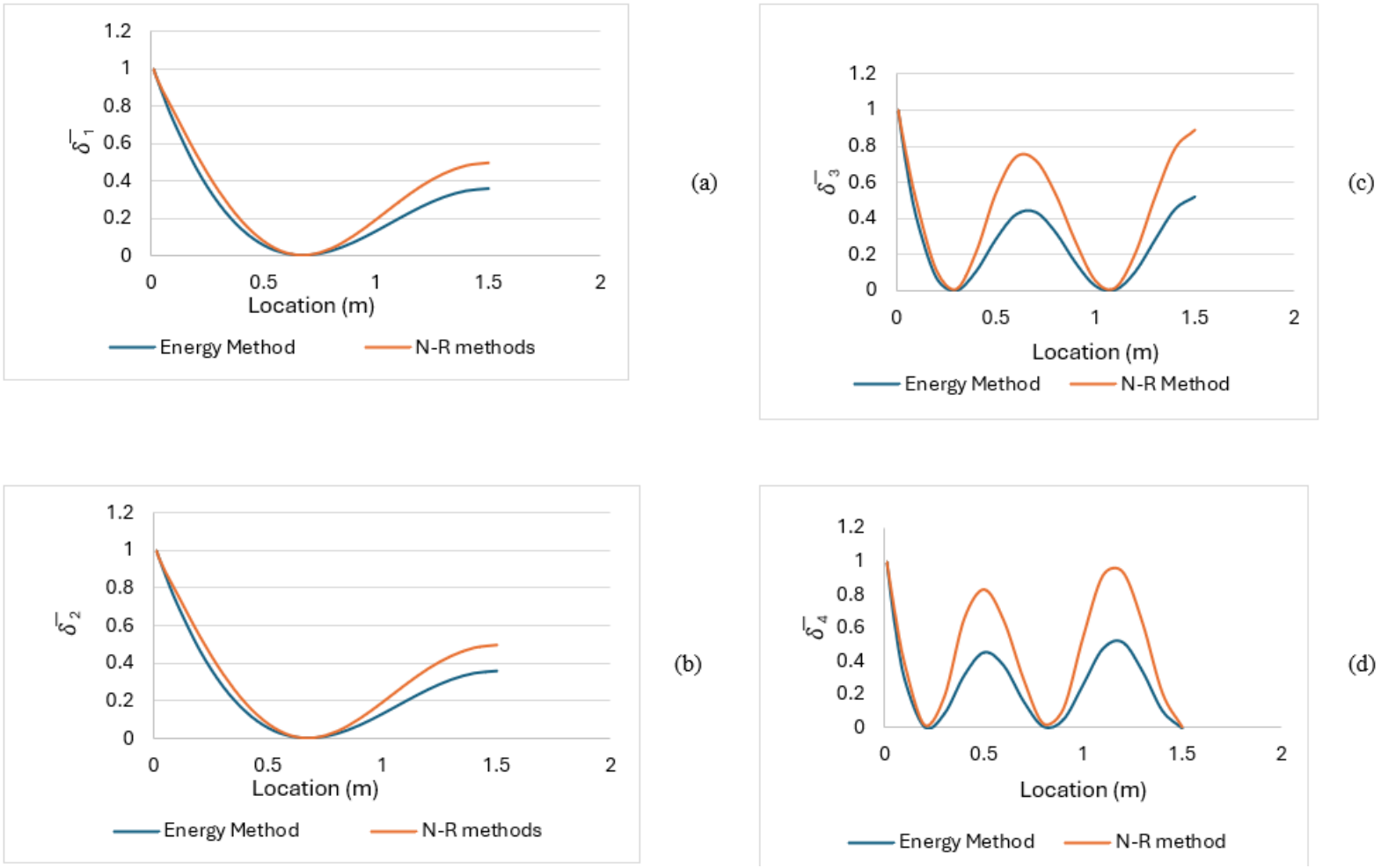

Figure 3.12-Normalised natural frequencies vs location for d = 0.05m: a) n = 1, b) n = 2, c) n = 3, d) n = 4.

Normalised absolute difference ($\bar{\delta}_{(i=1,2,,,n)}$) between the intact beam and the cracked beam has been determined and plotted on the y-axis, with the crack location along the x-axis in figure 3.11 and 3.12.

From Figure 3.11 it can be observed that the results with smaller cracks, for example 0.01 m depth, there is good agreement between the Newton-Raphson method and the strain energy approach. However, from Figure 3.12 it can be observed that when the crack becomes larger there is a more considerable difference of around 25 to 28 % in the between the two approaches.

When considering the Newton-Raphson method, the mode shapes of the damaged structure are not assumed to be the same as those of the intact structure with rotation across the rotational spring considered. In the case of the strain energy approach, the mode shapes are assumed to be the same for intact and damaged structures. For smaller cracks, this effect is negligible, resulting in better agreement between the strain energy approach and the Newton-Raphson method with 5% to 6% relative error.

3.7 Discussion.

This chapter examines the degradation in natural frequencies using a numerical method based on the Newton-Raphson method. A function based on the non-dimensional frequency parameter is obtained from the determinant of the dynamic stiffness parameters, in which the crack is modelled as a rotational spring.

Initially, the obtained results are validated against the Wittrick-Williams algorithm. Furthermore, the developed analytical solution based on the strain energy approach [35], in which a rotational spring has been used to represent the crack, is validated using the Newton-Raphson method.

It is observed that the results obtained using the Newton-Raphson Method provide a close match with the strain energy approach for the small cracks as compared to the deeper ones.

3.8 Conclusion.

The degradation in the natural frequencies of beams containing cracks has been observed using a numerical method, the Newton Raphson method, and an analytical

solution based on the strain energy approach. In each case, a rotational spring is employed to model the effect of the crack.

The Newton-Raphson method provides more accurate results for large cracks than the strain energy approach because it considers the changes in mode shape. However, the use of symbolic computation makes this method computationally inefficient for damage detection.

On the other hand, the strain energy approach matches the results based on the Newton-Raphson method for smaller cracks. The obtained analytical solution will not require any symbolic computation for damage detection method based on iterative or gradient-based methods to solve the indirect problem.

Chapter 4 explores damage quantification for a beam structure with a single crack. The strain energy method is considered for preparing the baseline model for quantifying single cracks in an isotropic beam to obtain computational efficiency.

4 Chapter 4: Single Crack Detection in Beams

4.1 Introduction.

This chapter is focused on finding the location and severity of a single crack in a beam. The formulations require a set of the first four to six natural frequencies of the cracked structure, which provides insight into crack quantification or inverse problem. The derived expression, based on strain energy and developed for solving the forward problem, is employed to address the inverse problem and calculate the pseudo-experimental values of degradation in the natural frequencies of the considered beam structure.

This chapter is divided into four sections. In section 4.2, the normalization of the degradations of a set of natural frequencies, to eliminate the crack severity parameters, is explained. In section 4.3, crack localization is achieved with the implementation of noise-free simulation of vector operations. In section 4.4, crack localization is obtained with noise-contaminated measurements. Upper and lower limits to the location coordinates are obtained by employing arithmetic intervals. In section 4.5, crack localization and severity are achieved simultaneously with the implementation of gradient-based optimization for noise-free pseudo experimental data using the FMINCON toolbox in MATLAB.

Formulations based on the strain energy approach derived in Chapter 3 (Eq. (3.6.11)) are used for producing the data required for the damage detection procedure described in sections 4.2 to 4.5.

4.2 Elimination of Crack Severity Parameter Through Normalization.

In Eq. (3.6.11), the part of the denominator regarding the integration of vertical displacement from zero to the overall length of the beam is denoted as J_n for the nth mode of vibration.

$$\delta_n(x) = \frac{(EI)^2\left(k_n(x)\right)^2}{k^*_r\,\mu\,(J_n)} = \frac{C(EI)^2\left(k_n(x)\right)^2}{\mu\,(J_n)} \tag{4.2.1}$$

After normalization of $\delta_n(x)$ for n = 1,2,3.... J, normalized degradation can be expressed as:

$$\bar{\delta}_n(x) = \frac{\delta_n(x)}{\sqrt{\sum_{n=1}^{j}(\delta_n(x))^2}} \tag{4.2.2}$$

As material properties and geometry i.e. Young's modulus ($\underline{E}$), moment of inertia (I) and mass per unit length (μ) are all constants, they can be eliminated during normalization along with crack compliance (C) which can be expressed as the reciprocal of the rotational spring (k^*_{r}).

In the denominator of Eq. (4.2.2), the summation can be extended over the total number of natural frequencies. The set of $\bar{\delta}_n$ can be regarded as a vector having maximum magnitude 1.0. For any mode of vibration, n = 1,2 ...J. $\bar{\delta}_n$ lies in the range $0 \leq \bar{\delta}_n \leq 1$.

In the crack detection procedures for noise-free procedures and noise-contaminated measurements, normalized degradations in the natural frequency can be calculated for a discrete number of points. These formulations have been obtained using MATLAB and are provided in the Appendix.

4.3 Localization of a Single Crack in a Beam: Using Noise-free Simulations.

Noise-free data related to degradation in natural frequencies can be utilized for damage localization by using normalized values, which will remove the dependence on crack severity.

A crack is modelled at a known location in the beam. Using Eq. (4.2.1) the degradation in the square of the natural frequencies of intact and damaged beams can then be evaluated. The set of normalized natural frequencies can be evaluated from Eq. (4.2.2). The data were obtained from these 'pseudo experiments' or 'synthetic data' is denoted $\bar{\delta}_m$ - a vector of the degradations in the natural frequencies.

For a beam, such vectors can be evaluated at discrete locations (x), denoted $\bar{\delta}_n(x)$. At this point, based on vector operations, the dot product of $\bar{\delta}_m$and $\bar{\delta}_n(x)$ yields its maximum value. The reason for this is that the dot product between two parallel unit vectors where the angle between them ($\emptyset$) tends to zero yields the maximum value of cosine.

In Eq. (4.3.1), $f(x)$ is the objective function used for crack localization.

$$\bar{\delta}_m . \bar{\delta}_n(x) = \left|\bar{\delta}_m\right| \left|\bar{\delta}_n(x)\right| \cos\emptyset$$

$$f(x) = \frac{\bar{\delta}_m . \bar{\delta}_n(x)}{|\bar{\delta}_m||\ \bar{\delta}_n(x)|} = cos\emptyset \tag{4.3.1}$$

4.3.1 Numerical Example.

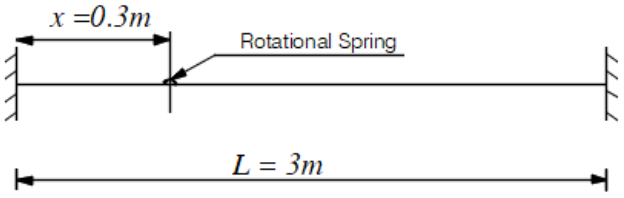

(a)

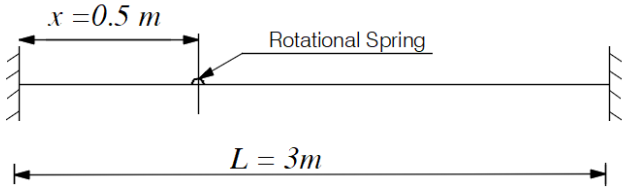

(b)

Figure 4.1: Beam with crack at (a) 0.3m, (b) 0.5m from the left-hand support.

A beam fixed at both ends is shown in Figure 4.1 with a single crack. The material properties of the beam and the physical properties are provided in Table 4.1.

Table 4.1 – Properties of beam fixed at both ends with the crack shown in Figure 4.1

Properties	
Young's modulus *(E)*	2.06 x 10^{11} N m^{-2}
Mass per unit length (μ)	185.40 kg m^{-1}
Breadth *(b)*	0.198 m
Depth *(h)*	0.122m
Crack depth *(d)*	0.05 m

For damage localization, natural frequencies of the damaged structures (ω_c) are required. These could be measured from a real structure. The natural frequencies of the damaged structure can be used to calculate the normalised degradation in the natural frequencies ($\bar{\delta}_m$) for first few modes of vibrations. For studies, $\bar{\delta}_m$ are calculated from simulations based on strain energy. This simulated data will be referred to as synthetic data.

Consider a single crack located 0.3 m or 0.5 m from the left support having a depth of 0.05 m. The degradations in the natural frequencies calculated using the strain energy approach are presented in Table 4.2 below.

Table 4.2 - Degradation in natural frequencies (δ_m) for crack locations 0.3 m and 0.5m for m = 1,2,3,4

Mode Number (m)	**1**	**2**	**3**	**4**
$\boldsymbol{\delta_m(x = 0.3)}$ **rad²/sec²**	17637.00	24023.08	4821.68	421616.00
$\boldsymbol{\delta_m(x = 0.5)}$ **rad²/sec²**	3493.37	22369.06	505795.60	2122849.75

These values can be normalized based on the Eq. (4.2.2) and then used for damage localization.

Table 4.3 – Normalised degradation ($\bar{\delta}_m$) in natural frequencies for crack locations 0.3 m and 0.5m for m = 1,2,3,4

Mode Number (m)	**1**	**2**	**3**	**4**
$(\overline{\boldsymbol{\delta}}_{\boldsymbol{m}}(\boldsymbol{x}=\mathbf{0.3})$	0.0423	0.1903	0.65402	0.7309
$(\overline{\boldsymbol{\delta}}_{\boldsymbol{m}}(\boldsymbol{x}=\mathbf{0.5})$	0.1089	0.0917	0.5400	0.8294

Using Eq. (4.3.1) the dot product of the vector $\bar{\delta}_m$ obtained from the measured natural frequencies and vectors $\bar{\delta}_n(x)$ calculated for trial values of x at intervals of 0.01m can be plotted.

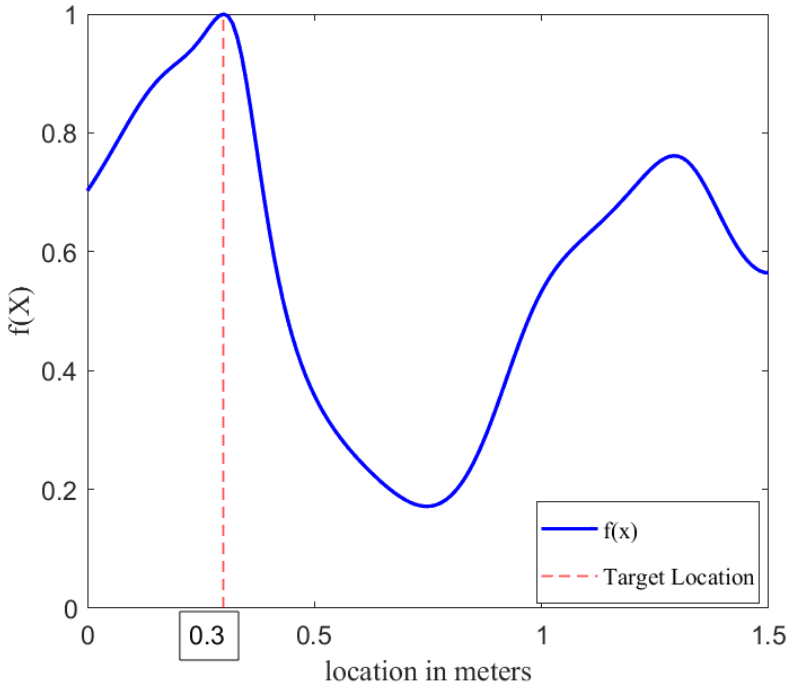

Figure 4.2 - Noise-free crack localization at location 0.3 m.

It can be observed Figure 4.2 that the function $f(x)$ yields a maximum value at 0.3m, which is the target crack location. A similar process based on a crack located at 0.5 m and shown in Figure 4.3 yields a maximum value for the objective function at 0.5 m, i.e. the target crack location. Appendix (D) presents the MATLAB codes developed for the calculations in this section.

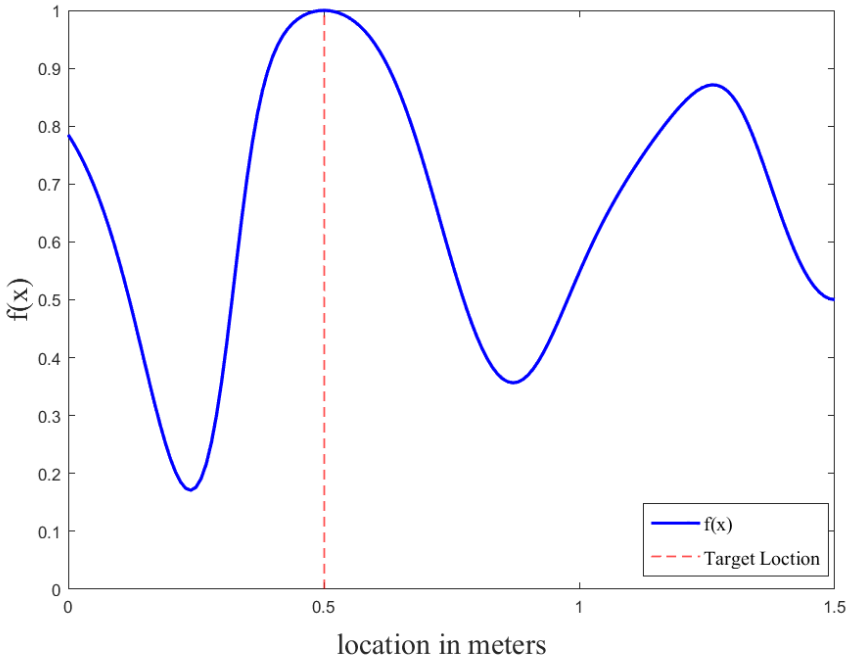

Figure 4.3 - Noise-free crack localization at location 0.5 m.

4.3.2 Discussion.

A method based on vector calculus is demonstrated for crack localization using noise-free data obtained through simulations based on the strain energy approach. Because of the normalization performed on the natural frequencies, the crack severity is eliminated, reducing the dependency of the outcome on the crack depth.

4.4 Localization of a Single Crack in the Beam: Interval Arithmetic and Noise Contamination.

4.4.1 Basic Operation of Interval Arithmetic:

To get the narrow intervals between the two real numbers Moore *et al.*[142] developed a technique using interval arithmetic. Consider two real positive numbers X and Y which can take a range of values between a lower limit (LL) and an upper limit (UL).

Here, X_{LL} and X_{UL} are the lower and upper limits of X, and similarly Y_{LL} and Y_{UL} are the lower and upper limits of Y:

$$X = [X_{LL}, X_{UL}],$$

$$Y = [Y_{LL}, Y_{UL}]$$

Mathematical operations between X and Y can be performed as:

$$[X + Y] = [\, X_{LL} + Y_{LL}, X_{UL} + Y_{UL}] \tag{4.4.1}$$

$$[Y - X] \;=\; [\, Y_{LL} - X_{UL}, Y_{UL} - X_{LL}] \tag{4.4.2}$$

$$\frac{1}{X} \;=\; \left[\frac{1}{X_{UL}}, \frac{1}{X_{LL}}\right] \tag{4.4.3}$$

$$\frac{Y}{X} \;=\; \left[\frac{Y_{LL}}{X_{UL}}, \frac{Y_{UL}}{X_{LL}}\right] \tag{4.4.4}$$

The above interval arithmetic operations provide the narrowest possible interval. This technique is considered to incorporate the effect of noise in the measurements to obtain the range of damage localization.

Consider Eq. (3.6.11), which expresses the difference between the squares of the natural frequencies between intact and cracked beams. For simplicity, we can consider the relative change in the natural frequencies and express it in the form of Eq. (4.4.5):

$$f(x) = \delta_{nr}(x/l) = 1 - \frac{\omega_{nc}}{\omega_{no}} \tag{4.4.5}$$

Here, ω_{no} and ω_{nc} are the natural frequencies of the intact and cracked beam respectively. Subscript *n* denotes a vibration mode, and *r* denotes a relative change in the natural frequency. x is the location of the crack. After the addition of noise (e),

$$\left.\begin{aligned} [\omega^{L}{}_{no}, \omega^{U}{}_{no}] &= [\omega_{no} - e, \omega_{no} + e] \\ [\omega^{L}{}_{nc}, \omega^{U}{}_{nc}] &= [\omega_{nc} - e, \omega_{nc} + e] \end{aligned}\right\} \tag{4.4.6}$$

ω_{no} and ω_{nc} lie in the range $[\omega^L{}_{no}, \omega^U{}_{no}]$ and $[\omega^L{}_{nc}, \omega^U{}_{nc}]$ respectively. Here, superscripts L and U denote lower and upper limits, respectively.

After applying interval arithmetic to Eq. (4.4.5), the upper and lower limits of the relative changes in the natural frequencies (δ_{nr}) Can be expressed as:

$$\delta^L{}_{nr} = 1 - \frac{\omega^U{}_{nc}}{\omega^L{}_{no}} \tag{4.4.7}$$

$$\delta^U{}_{nr} = 1 - \frac{\omega^L{}_{no}}{\omega^U{}_{nc}} \tag{4.4.8}$$

The interval arithmetic operations provide the range of intervals in which the relative change in natural frequency lie e.g. $\delta^L{}_{nr} \leq \delta_{nr} \leq \delta^U{}_{nr}$. In the case of closely spaced values of uncracked and cracked natural frequencies, it is possible that the numeric value of the lower limit of the original natural frequency can be less than the numeric value of the upper limit of the cracked natural frequency ($\omega^L{}_{no} < \omega^U{}_{nc}$). In this contex Eq. (4.4.7) may yield a negative value for the lower limit of the relative change in natural frequencies ($\delta^L{}_{nr}$). In such instances, the value of $\delta^L{}_{nr}$ can be considered zero when applying this technique for damage localization.

To eliminate crack severity, normalised values of δ_{nr} Eq. (4.2.2) can be used:

$$\bar{\delta}^L{}_{(n=i)r} = \frac{1}{\sqrt{1 + \frac{\sum_{i \neq j} \delta^U{}_{(n=j)r}}{\delta^L{}_{(n=i)r}}}} \tag{4.4.9}$$

$$\bar{\delta}^U{}_{(n=i)r} = \frac{1}{\sqrt{1 + \frac{\sum_{i \neq j} \delta^L{}_{(n=i)r}}{\delta^U{}_{(n=i)r}}}} \tag{4.4.10}$$

where subscripts *i* and *j* are the specified number of modes.

For the i^{th} normalized lower limit of the normalized relative change in natural frequency ($\bar{\delta}^L{}_{(n=i)r}$), the denominator of Eq. (4.4.9) uses the i^{th} mode of the lower limit of relative change in natural frequency along with a summation of the upper limits of the relative changes in natural frequencies . The upper limit relative change in natural frequency

for the i^{th} mode is excluded from this summation. These operations result in the narrowest possible range for damage localization.

A similar operation has been used for the calculation of upper limit of the normalized relative change in natural frequency ($\bar{\delta}^{U}{}_{(n=i)r}$) with the normalized upper limit of relative change in natural frequency expressed in Eq. (4.4.10).

These normalized upper and lower limit bounds for the selected mode can be plotted as horizontal lines along with $f(x)$ from Eq. (4.4.5) calculated at discrete points of the beam for selected natural frequencies. This is illustrated in Figure 4.4, with the intersections of $\bar{\delta}_{nr}(x/l)$ with the horizontal lines (upper and lower bounds), providing the possible range of crack locations.

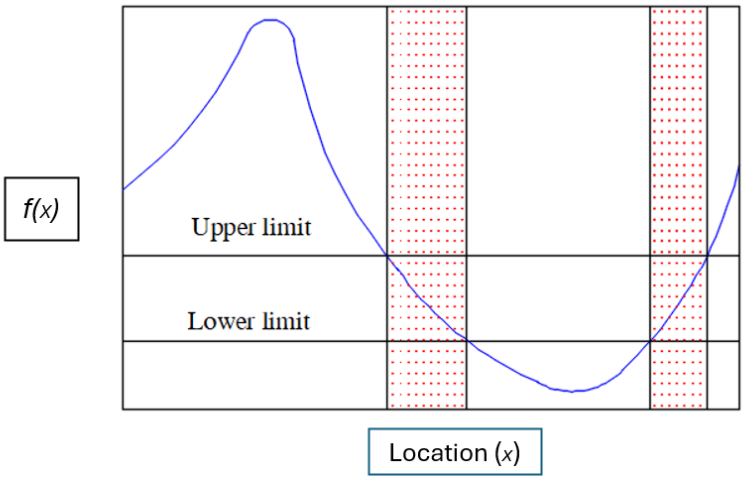

Figure 4.4 - Damage localization with help of interval arithmetic.

4.4.2 Numerical Example

A beam presented in the numerical example in Section 4.3.1(Figure 4.1 (b)) is reconsidered for crack localisation with noise incorporated. The depth of the crack is 0.05 m.

Table 4.4 - Cracked and uncracked natural frequencies for a beam with a crack located 0.5m from the left-hand support.

Mode (n)	1	2	3	4
Uncracked natural frequency $(\omega_{un})\ rad/s$	448.10	1235.30	2421.70	4003.10
cracked natural frequency $(\omega_{cn})\ rad/s$	444.10	1226.20	2314.90	3728.50

To obtain the upper $[\omega^{u}_{no}, \omega^{u}_{nc}]$ and lower limit $[\omega^{L}_{no}, \omega^{L}_{nc}]$ of the uncracked and cracked natural frequencies, a small amount of noise (e) was added to the data presented in Table 4.4.

After performing the mathematical operations expressed in Eq. (4.4.9) and Eq.(4.4.10), the upper $(\bar{\delta}^{U}{}_{nr})$ and lower limit ranges $(\bar{\delta}^{L}{}_{nr})$ of the normalized relative change in the natural frequencies were obtained for the randomly chosen noise.(e).

The results are presented in Figure 4.5,with ± 1 rad/s contaminated noise.

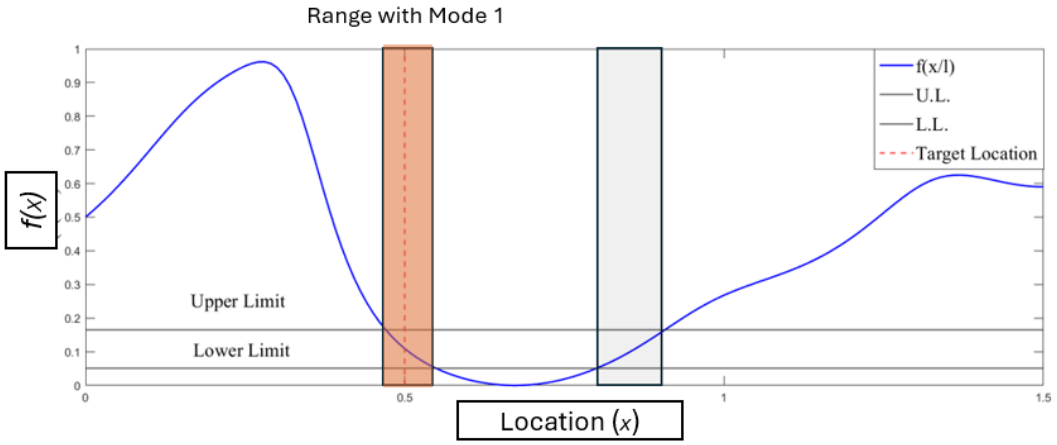

(a)

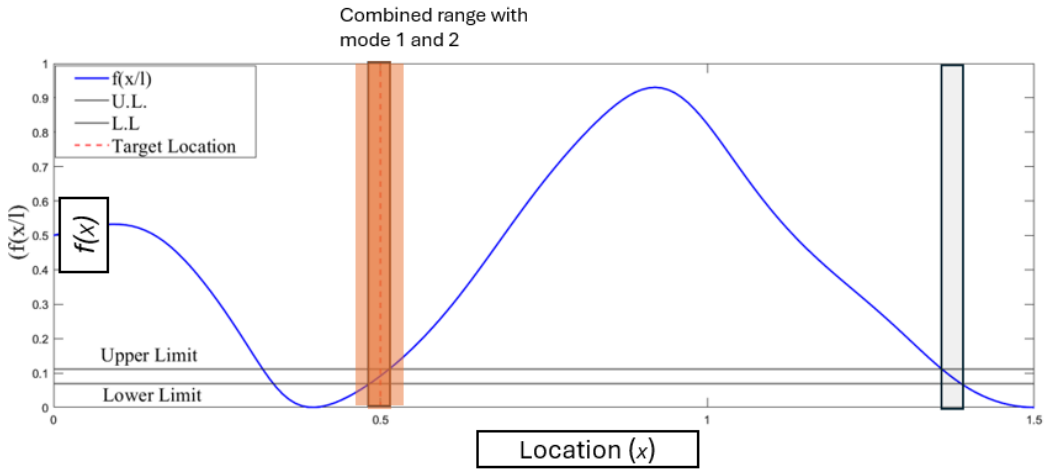
Combined range with
mode 1 and 2
f(x/l)
U.L.
L.L
Target Location
f(x)
(f(x/l)
Upper Limit
Lower Limit
Location (x)

(b)

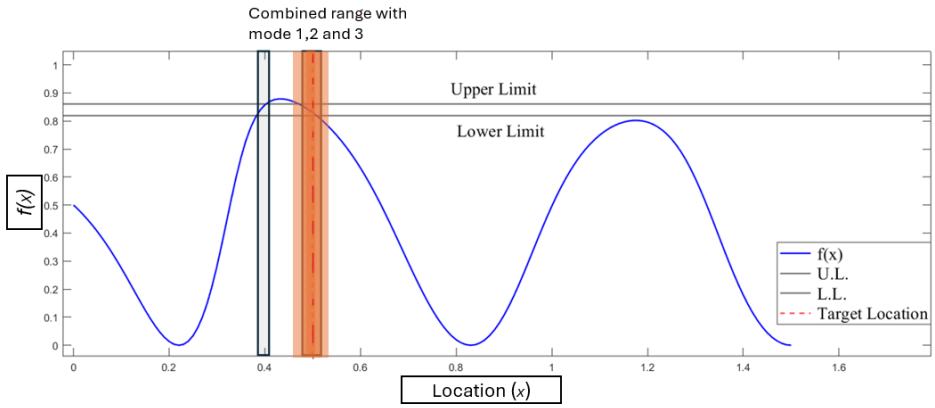
Combined range with
mode 1,2 and 3
Upper Limit
Lower Limit
f(x)
f(x)
U.L.
L.L.
Target Location
Location (x)

(c)

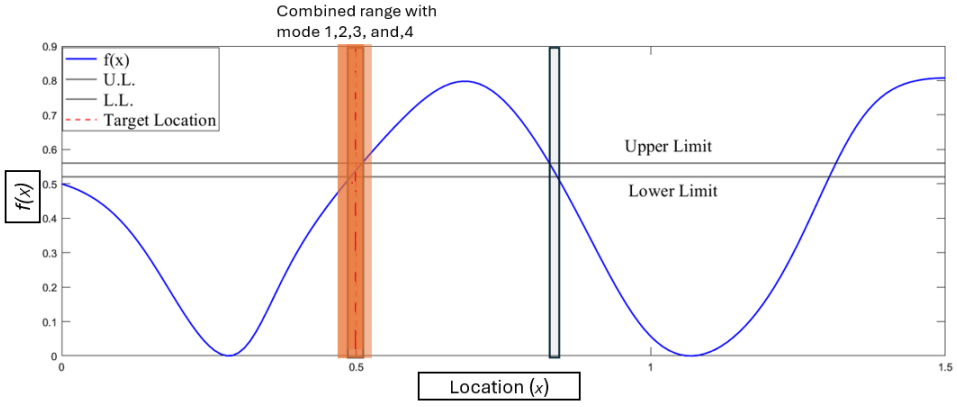

(d)

Figure 4.5 - Crack localization with noise ∓ 1 *rad/s* : a) mode (n) = 1, b) mode (n) = 2, c) mode (n) = 3, and d) mode (n) = 4.

In Figure 4.5 the crack locations can be identified from the intersection of the function of the normalized relative change in the natural frequencies $f(x)$ with the upper and lower limit bounds for the different natural frequencies. The target crack location at 0.5m from the left-hand side of the beam is represented by the dashed red line. The lightly shaded regions indicate the detected ranges for each frequency, whereas the superimposition can provide combined ranges for all frequencies utilized.

It can be observed that the intersection of the function with the upper and lower limit ranges for each mode of vibration determines the range within which the crack location is present. This range varies with respect to the mode of vibration and the level of noise. Table 4.5 presents the upper and lower limits, along with the associated errors, for the first four modes of vibration for the randomly selected noise in the simulations. In addition, Figure 4.6 represents the variation of error associated with the level of noise. The algebraic operations performed with the help of MATLAB. Appendix (E) presents the MATLAB codes for crack localisation using interval arithmetic method.

Table 4.5 - Upper and lower limit range for first four mode of vibrations.

Noise	Mode (i)	Lower Limit (LL)	Upper Limit (UL)	Error (UL-LL)
0.5 Hz	1	0.07882	0.1349	0.05608
	2	0.07895	0.10015	0.0212
	3	0.52854	0.5479	0.01936
	4	0.82651	0.8472	0.02069
1 Hz	1	0.05161	0.1645	0.11289
	2	0.0686	0.1111	0.0425
	3	0.5211	0.5603	0.0392
	4	0.8193	0.8612	0.0419
1.5 Hz	1	0.02456	0.1946	0.17004
	2	0.0584	0.1221	0.0637
	3	0.5134	0.5726	0.0592
	4	0.8117	0.875	0.0633
2 Hz	1	0	0.2254	0.2254
	2	0.0484	0.1332	0.0848
	3	0.5054	0.5847	0.0793
	4	0.8034	0.8883	0.0849

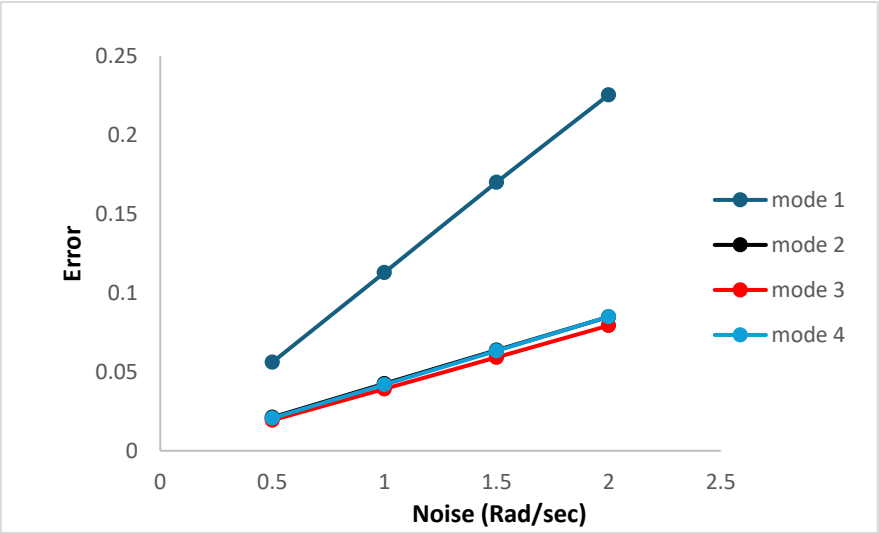

Figure 4.6 - Variation of error for first four modes of vibrations with respect to the added noise in the simulations.

4.4.3 Discussion

In this chapter, interval arithmetic with randomly assumed noise is used for the damage quantification of beams. This approach is applied to simulated measurements based on the strain energy method for damage localization.

With the noise-contaminated data for beams, an accurate range for damage localization has been shown. This range varies depending on the amount of contaminated noise. The range of possible damage location becomes larger with increase in noise. The crack severity is eliminated because of the normalization procedure, which simplifies the problem. The severity can also be obtained using a probability distribution with the ranges of the crack locations obtained [59]. This thesis does not focus on the severity calculation using probability distribution. A further section explores a gradient-based optimization technique to obtain both crack parameters (localization and severity) in the damage detection procedure.

4.5 Detection of the Single Crack using Gradient-based Optimization: MATLAB.

A single crack in a beam has been modelled using the strain energy method in Chapter 2. The developed expression for the corresponding changes in the natural frequency depends upon the crack location and severity. The severity of the crack can be expressed in terms of the ratio of the depth of the crack to the depth of the beam, the crack-depth ratio.

Based on Eq. (3.6.11) which provides the difference between the square of the natural frequencies of intact and damaged beams and the calculated or measured natural frequencies of the damaged beams, it is possible to develop an error function.

This developed error function can be solved using gradient-based optimization with the help of FMINCON which is an optimization toolbox available in MATLAB.

4.5.1 Methodology

In this section, an objective function is developed using least square fit technique for minimization. To develop the objective function, Eq. (3.6.11) is rewritten by substituting the stiffness of the rotational spring (k^*_r) with compliance (C) resulting in Eq. (4.5.1). This equation has two variables, the location of the crack (x) and the crack depth ratio (which is present in the formulation of the compliance (C)).

$$\delta_i(x, d/h) = \frac{C(EI)^2\left(k_n(x)\right)^2}{\mu \int_0^l \left(W_n(x)\right)^2 dx} \tag{4.5.1}$$

An objective function can then be defined in Eq.(4.5.2) to enable these two parameters (location and severity of crack) to be calculated through an optimization process (to minimise the error). Here, δ_i is the change in the square in the natural frequencies between the intact and damaged beam for a crack located at distance x from the end of the beam and having depth d for the mode of vibration. δ_i^m is the calculated change in the square in the natural frequencies for an unknown crack location and severity.

$\delta_i(x, d/h)$ represent the function to obtain the difference between the square of the natural frequencies of intact and cracked beam using the strain energy approach for the i^{th} mode of vibration (i = 1, 2,….n). δ_i^m are the set of difference between the square of the natural frequencies of intact and cracked beam. δ_i^m can be obtained by performing

experiments on real beam structures or from mathematical simulations. In the present study, values for δ_i^m are obtained using simulations based on Eq. (4.5.2)

δ_i^s is the set of changes in the squares of the natural frequencies of the beam for the known location and severity of the crack, which is used for normalization and scaling purposes.

$$f(x, d/h) = min \sum_{i=1}^{n} \left\{ \frac{\delta_i(x, d/h) - \delta_i^m}{\delta_i^s} \right\}^2 \rightarrow 0 \tag{4.5.2}$$

The search for crack locations is confined within the geometric boundaries of the beam. For a beam with length L along the x-axis and depth *d* along the y-axis, the potential crack positions are constrained such that the location along the x-axis satisfies $0 \leq x \leq L$ The crack depth is expressed in terms of a crack-depth ratio, defined as the ratio of the crack depth to the total depth of the beam. This ratio is limited to the range $0 \leq d/h \leq 0.9999$, as the proposed analytical model is not valid for a fully through-depth crack. These constraints establish a feasible search space for the crack detection process.

4.5.2 Background studies: Optimization toolbox FMINCON

The optimization process was carried out using the MATLAB optimization toolbox FMINCON. This toolbox can be used to find maximum and minimum values for established objective functions with optimized parameters. The flowchart in Figure 4.7 shows the workflow in FMINCON. The required input arguments are the objective function, equality and nonequality constraints, the search space, step size and tolerance. Some input arguments like equality and inequality constraints can be provided in terms of (expected values of optimized parameters) an upper and lower bound range. Based on the input arguments, a barrier function is created, and the gradient calculation is carried out by the solver using a customized step size. The gradient of the objective function can be provided in the input arguments to make the optimization process faster.

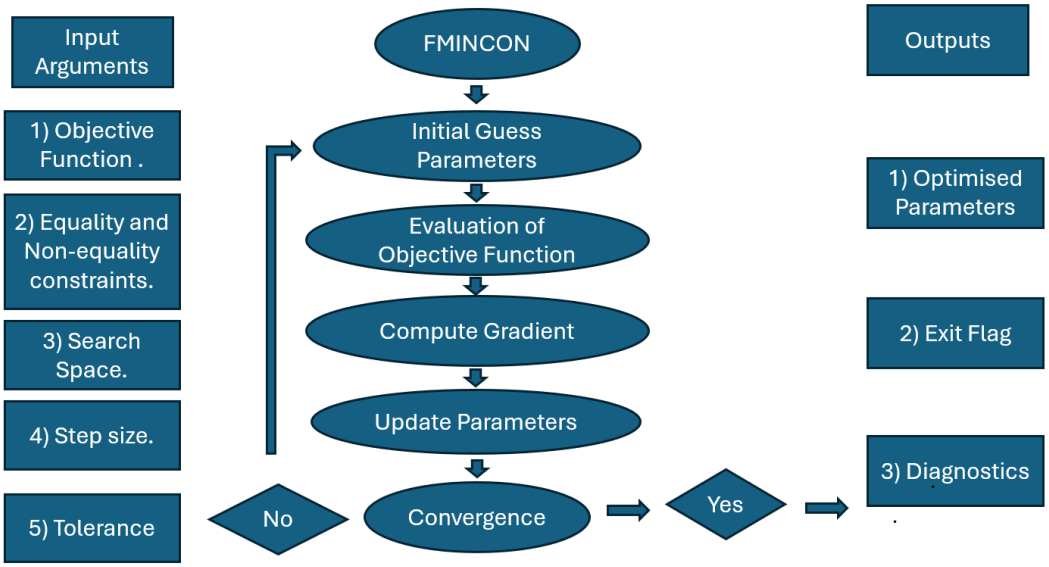

Figure 4.7 - Flowchart of optimization toolbox FMINCON.

The output provided by the solver consists of the history of iterations, optimized parameters, final values of the objective function for each trial value, and data in terms of exit-flag which represents satisfied and unsatisfied conditions as per optimality criteria applied in the input arguments.

4.5.3 Numerical Example and Results:

The beam considered in section 4.4.2 is considered here to demonstrate the crack quantification. As shown in Figure 4.8, The crack is located at 0.6 m from the left-hand support with the crack depth 0.05m.

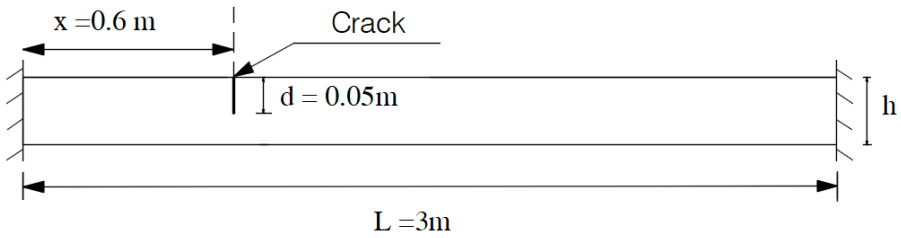

Figure 4.8 – Beam fixed at both ends, crack location 0.6 m from the left-hand support.

Eq. (4.5.2**)** represents the objective function where the target is the minimization of $f(x, d/h)$. A set of differences between the square of the intact and the damaged beams is shown in Table 4.6 and has been calculated using the strain energy approach (Eq. (4.5.1)). This data is referred to as synthetic data**.**

Table 4.6- Obtained synthetic data for (δ_i^m) and Figure 4.8 used for the optimization.

Modes (i)	**(1)**	**(2)**	**(3)**	**(4)**
$\bar{\delta}_i(rad^2s^{-2})$	583.89	73296.15	157584.40	114929.50

The data mentioned above is incorporated into Eq. (4.5.2) to create the objective function. This function is solved using a gradient-based optimization technique. To use the FMINCON solver, a set of feasible trial values for the parameters needs to be input. In the case of the numerical example mentioned in this section, the location of the crack and the crack-depth ratio are the main parameters. To ensure that these trial values do not exceed the physical boundaries of the beam, a range is required to be fixed., The range of trial values used is presented in Table 4.7. Using more than one set of trial values increases the likelihood of finding a global rather than local solution. In this case, ten random sets of trial values are used. The trial values in those sets were selected using Latin hypercube samples.

Table 4.7 - Range of trial values used to solve the inverse problem for a beam shown in Figure 4.8

Parameters	**Location (x)**	**Crack-depth ratio (C/d)**
Upper Limit (U_L)	1.5	0.9999
Lower Limit (L_L)	0	0

Once the synthetic data (mentioned in Table 4.6) are generated and the range for the trial values in the form of parameters of the crack (Table 4.7) in Eq. (4.5.2) are decided according to the geometry of the plate. An objective function can be developed for minimization using least square fit method. The random number of sets of trial values can be used as an input argument for the optimization. Each was converged to a particular value as per the convergence criteria. Tolerance of 10^{-6} is the criteria used for the convergence.

The results converged at global and local optima are present in Table 4.8.

Table 4.8 - Final values of crack parameters and error function for each of the 10 trial values.

Set	location (x)	d/h	$f(x, d/h)$
1	0.1	0.414	8.1920
2	0.6	0.409	1.28×10^{-6}
3	1.318	0.46	1.581
4	0.1	0.414	8.192
5	0.600	0.409	1.32×10^{-5}
6	0.600	0.409	5.44×10^{-6}
7	0.599	0.409	3.92×10^{-6}
8	0.600	0.409	2.01×10^{-6}
9	0.600	0.409	1.70×10^{-5}
10	0.1	0.414	8.1925

In Table 4.8 we can see that sets 2,5,6,7,8 and 9 converged as per the required tolerance as compared to sets 1,3,4 and 10.

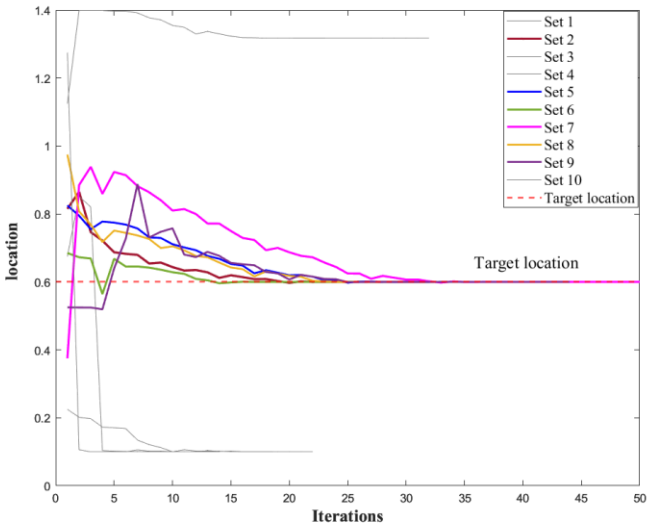

Figure 4.9 - Optimized location of crack for each of the 10 trial values

In Figure 4.9, it is evident that sets 2,5,6,7,8 and 9 have converged to the expected target location indicated by the dashed red line at 0.6 m. On the other hand, the final

values of the objective function for set numbers 1,3,4, and 10 are larger than the tolerance (10^{-6}).Using this phenomenon, the provided thickness of the lines for each set of iterations presented in Figure 4.9 is inversely proportional to the final value of objective function $f(x, d/h)$.This thickness variation indicates that the thicker lines converge with the expected value of the crack location. In addition, observed results in the solver indicate that the set numbers 2,5,6,7,8 and 9 converge with satisfying optimality criteria compared to the set numbers 1,3,4 and 10. Hence, those plots represent the likelihood of the actual damage location.

In Figure 4.10 convergence on the crack-depth ratios for each set of trial values can be seen. It can be observed that the same sets which converged to the target locations in the Figure 4.9 converge to the target crack-depth ratio. The target crack depth ratio is presented by a dashed red line in at 0.410. As shown in Figure 4.10 in the converge of the sets of trial values, which converge to the target crack-depth ratio, are shown in bold. The function files are attached in the Appendix (F).

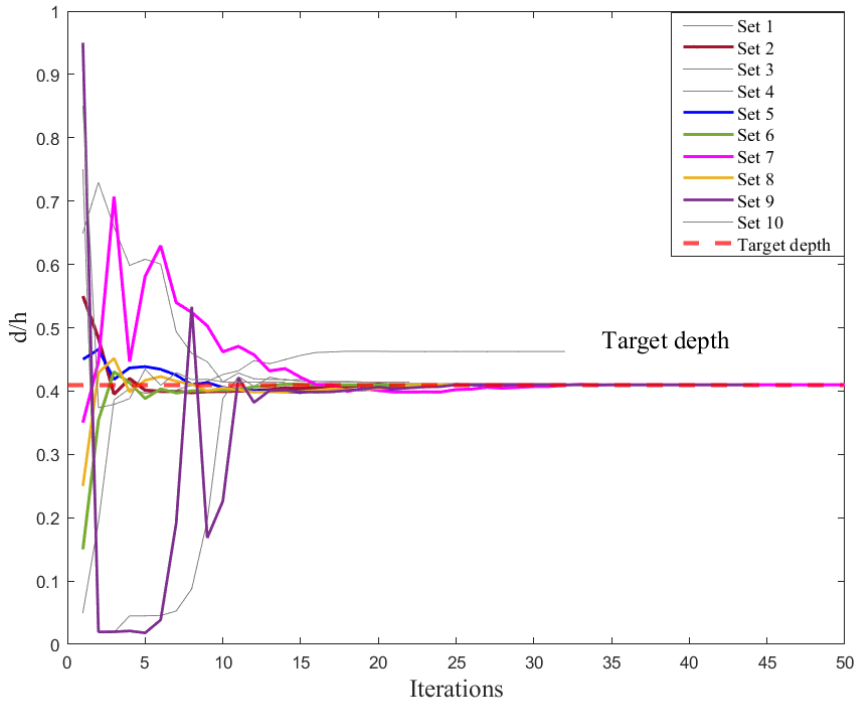

Figure 4.10 - Convergence of crack depth-ratio crack depth vs iterations for 10 sets of trial values.

4.5.4 Discussion

The gradient-based optimization used to obtain the crack parameters in the beam (location and severity) have been shown to provide accurate results. Using this technique, providing accurate input arguments (by selecting the trial values of the crack parameters without exceeding the geometrical boundaries of the plate) to the solver and defining key parameters, i.e., step size, tolerance, constraints, etc., can direct the outcome toward a global solution. This process can be made faster by providing the gradient of the objective function to the solver. In this piece of work, the gradient of the objective function is not provided due to simplicity of the problem.

4.5.5 Conclusion

In this chapter, the inverse problem is solved to determine the location and severity of a single crack in a beam. This is achieved in two stages, firstly localizing the crack and then assessing its severity. Two different approaches are used for the crack localization and the optimization is performed for the objective function created using least squares fit method to obtain the location and severity of the crack, followed by a numerical example.

The first stage is crack localization. Normalized natural frequencies are first used to eliminate the crack severity to make the problem one-dimensional. Crack localization is then achieved through two methods. In the first method, vector operations are performed with noise-free simulated data regarding the first four natural frequencies. In the second method, interval arithmetic operations are performed to obtain the range of crack locations based on the first four noise-contaminated natural frequencies.

The second part focuses on obtaining the crack location and severity in the beam (location and severity) using the gradient-based optimization techniques available in the solver FMINCON. The achieved results meet the defined targets for the damage detection procedure.

5 Chapter 5: Free Vibration Analysis of Intact and Damaged Plates.

5.1 Introduction.

Many studies related to the damage modelling of plates relate to the work on beams and have therefore already been discussed in literature review of Section 2.4. These studies are based on numerical, analytical, and experimental methods. Free vibration analysis of an isotropic plate structure with simply supported boundary conditions using the strain energy approach will be addressed in this chapter. Cracks will be modelled parallel to the edges of the plate and in arbitrary orientations. A novel approach to model a crack in the plate structure will be presented with parametric studies along with validation through comparison with finite element analysis.

5.2 Background Studies: Free Vibration Analysis of an Intact Plate.

In dynamic analyses, structures can be considered as single or multi-degree-of-freedom systems. However, plate structures are generally considered as continuous systems when obtaining their dynamic response. Using the Rayleigh-Ritz method or Galerkin method the expression for the natural frequencies of the plate can be obtained.

Consider a simply supported rectangular plate with length 'a', breadth 'b', and thickness 'h', made of isotropic material with a Young's modulus 'E', density 'ρ', and Poisson's ratio 'v', as shown in Figure 5.1. It vibrates at a natural frequency ω_{mn0}.

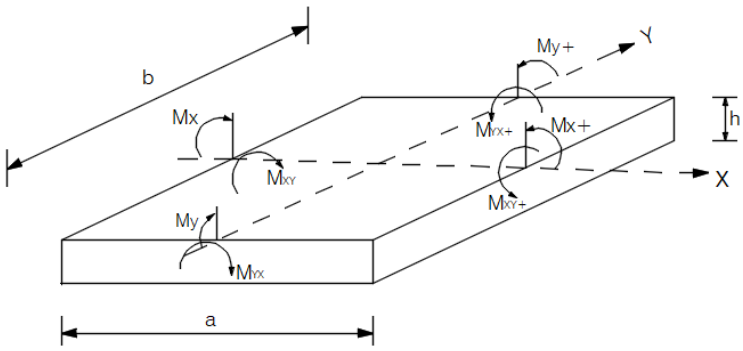

Figure 5.1 - Simply supported intact plate.

The expression for the displacement of the simply supported plate can be expressed by solving the equation of motion [143] where w_{mn} is the maximum amplitude of the plate. For simplicity this can be considered as unity.

$$w(x,y,t) = w_{mn}\, sin\left(\frac{m\pi x}{a}\right) sin\left(\frac{n\pi y}{b}\right) sin(\omega_{mn0}t) \tag{5.2.1}$$

Here, m and n are the number of half wavelengths in the x and y directions respectively. When $\omega t = n\pi$ the displacement is zero, the strain energy is zero and the kinetic energy takes its maximum value. The expression for the kinetic energy for an intact plate can be presented as:

$$T_0 = \frac{1}{2}\rho h \int_0^a \int_0^b \left(\frac{\partial w(x,y,t)}{\partial t}\right)^2 dy\, dx \tag{5.2.2}$$

$$T_0 = \frac{1}{2}\rho h \omega_{mn0}^2 w_{mn}^2\, cos(\omega_{mn0}t) \int_0^a \int_0^b sin^2\left(\frac{m\pi x}{a}\right) sin^2\left(\frac{n\pi y}{b}\right) dy\, dx \tag{5.2.3}$$

Under harmonic excitation, the maximum kinetic energy occurs when the cosine term reaches its peak value of one. Therefore, the expression for the maximum kinetic energy can be expressed as:

$$T_0 = \frac{1}{2}\rho h \omega_{mn0}^2 w_{mn}^2 \int_0^a \int_0^b sin^2\left(\frac{m\pi x}{a}\right) sin^2\left(\frac{n\pi y}{b}\right) dy\, dx \tag{5.2.4}$$

When $\omega t = \left(n + \frac{1}{2}\right)\pi$, the kinetic energy is zero and the strain energy takes its maximal value. The strain energy for the plate can be expressed as:

$$U_0 = \frac{D}{2}\int_0^a \int_0^b \left[\left(\frac{\partial^2 w}{\partial x^2} + \frac{\partial^2 w}{\partial y^2}\right)^2 - 2(1-v)\left\{\frac{\partial^2 w}{\partial x^2}\frac{\partial^2 w}{\partial y^2} - \left(\frac{\partial^2 w}{\partial x \partial y}\right)^2\right\}\right] dy\, dx \tag{5.2.5}$$

Here,

$$D = \frac{Eh^3}{12(1-v^2)} \tag{5.2.6}$$

For a simply supported plate, twisting effects can be ignored since the boundary conditions result in zero twisting moments and the twisting is minimal due to the

decoupled nature of the bending. The presented Eq. (5.2.5) for the strain energy can then be adopted as:

$$U_0 = \frac{D}{2}\int_0^a \int_0^b \left[\left(\frac{\partial^2 w}{\partial x^2} + \frac{\partial^2 w}{\partial y^2}\right)^2\right] dy\, dx \tag{5.2.7}$$

Here D is the flexural rigidity of the plate. Eq. (5.2.7) can be expanded employing the following terms

$$\left.\begin{aligned}\frac{\partial^2 w}{\partial x^2} &= -w_{mn}\left(\frac{m\pi}{a}\right)^2 \sin\left(\frac{m\pi x}{a}\right)\sin\left(\frac{n\pi y}{b}\right)\\ \frac{\partial^2 w}{\partial y^2} &= -w_{mn}\left(\frac{n\pi}{b}\right)^2 \sin\left(\frac{m\pi x}{a}\right)\sin\left(\frac{n\pi y}{b}\right)\end{aligned}\right\} \tag{5.2.8}$$

and the total strain energy for an intact plate can be expressed using Eq. (5.2.9).

$$\begin{aligned}U_0 = \frac{1}{2}Dw_{mn}^2\pi^4\left(\frac{m^2}{a^2}+\frac{n^2}{b^2}\right)^2\\ \int_0^a\int_0^b sin^2\left(\frac{m\pi x}{a}\right) sin^2\left(\frac{n\pi y}{b}\right) dy\, dx\end{aligned} \tag{5.2.9}$$

Conservation of energy requires that $T_0 = U_0$, which provides the equation for the natural frequencies of the simply supported plate modes of vibration corresponding to m and n half sine waves in the x and y directions.

$$\omega_{mn0} = \sqrt{\frac{D\pi^4}{\rho h}\left(\frac{m^2}{a^2}+\frac{n^2}{b^2}\right)^2} \tag{5.2.10}$$

5.3 Free Vibration Analysis of a Cracked Plate: Strain Energy Approach.

In this section an expression for the relative changes in the natural frequencies (RCNF) of the intact and the cracked plate is derived. Two cases are examined. The first is a crack parallel to the edge of the plate which is illustrated by a numerical example. The second is a crack in an arbitrary direction which is solved using an axis transformation and again illustrated by a numerical example.

5.3.1 Case I: Crack Parallel to Edge of the Plate

From the literature review it has been observed that the use of a line spring model helps to improve the computational efficiency of obtaining the natural frequencies of a cracked plate. In Section 3.3 a rotational spring for a beam structure was used for cases where the crack runs all-through-the-width of the beam. Caddemi and Calio [32] provided a formulation for the non-dimensional compliance of a rotational spring containing a crack. Labib *et al*.[35] utilized this expression for modelling damage in a beam structure.

For the beam shown in Figure 5.2 the expression for the compliance can be calculated from Eq. (3.3.1) to Eq. (3.3.4).

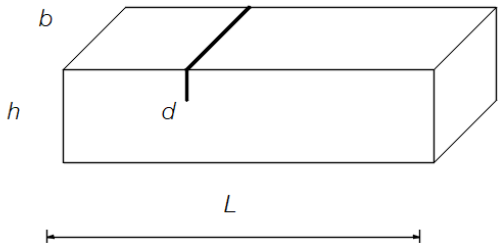

Figure 5.2 - Beam with the all-through-thickness crack.

Luo et al.[20] utilized a similar approach for plates, again using a rotational spring. In Figure 5.3 a crack running along the length of the plate can be considered analogous to a crack running all the way across a beam width.

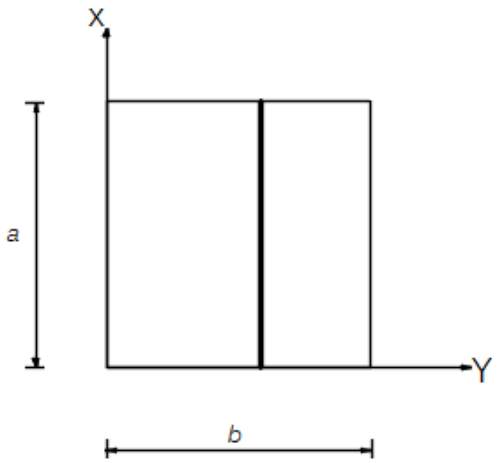

Figure 5.3 - Plate with all-through-length crack.

By analogy, the stiffness of a rotational spring representing a through-the-length crack in a plate is expressed in Eq. (5.3.1).

$$K_x = \frac{Da}{hC(d/h)} \tag{5.3.1}$$

A small portion of the crack with length dx running parallel to the x-axis is shown in Figure 5.4. The expression for the stiffness per unit length of the rotational spring is expressed in Eq. (5.3.2)

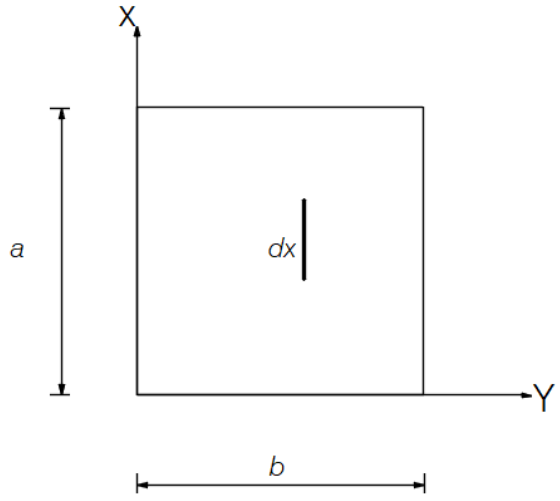

Figure 5.4 - Portion of crack parallel to the length.

$$K^*_x = \frac{D}{h}\ \frac{1}{C(d/h)} \tag{5.3.2}$$

Compliance (C_x) can be expressed as the reciprocal of the stiffness of the rotational spring (K^*_x).

$$C_x = \frac{h}{D}\ C(d/h) \tag{5.3.3}$$

The formulation provided for the compliance per unit length will be the same for cracks in any orientation. This quantity can be denoted as C_y for a crack along the y-axis. The notation C_n will be considered to represent the compliance per unit length for cracks in any arbitrary orientations in the subsequent sections.

5.3.1.1 Methodology

A plate is considered with a crack running from (x_1, y_1) to (x_2, y_2) with $y_1 = y_2$, i.e.in an orientation parallel to the edge of the plate (Figure 5.5).

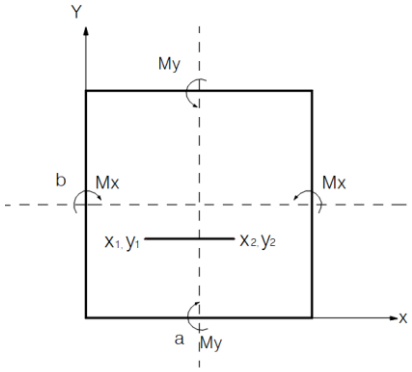

Figure 5.5 – Simply supported plate with a crack parallel to the x-axis.

The effect of the crack can be introduced using the compliance defined in Eq. (5.3.2). The length of the crack orientated parallel to the x-axis ($\varphi = 0^0$) of the crack can be given by,

$$l = x_2 - x_1 \tag{5.3.4}$$

Let a typical point (x, y) somewhere along the crack be identified by its position dx where $0 \leq dx \leq l$ given by :

$$x = x_1 + dx\ ,\ y = y_1 = y_2 \tag{5.3.5}$$

Consider a small portion of the crack of length dx, where the bending moment about the crack direction is M_x per unit length and the discontinuity of the rotation across the crack is

$$\delta\theta_y = (C_x/dx)\big(M_y dx\big) = C_x M_y \tag{5.3.6}$$

The incremental strain energy associated with the discontinuous rotation in that portion of the crack is

$$dU_d = \frac{1}{2}\delta\theta_y\big(M_y dx\big) = \frac{1}{2}C_x\big({M_y}^2 dx\big) \tag{5.3.7}$$

where M_x and M_y are the longitudinal and transverse bending moments per unit length, respectively, and M_{xy} is the twisting moment which gets nullified due to the longitudinal direction of the crack.

$$M_{xy} = -D(1-v)\left(\frac{\partial^2 w}{\partial x \partial y}\right) \tag{5.3.8}$$

$$M_x = -D\left(\frac{\partial^2 w}{\partial x^2} + v\frac{\partial^2 w}{\partial y^2}\right) \qquad M_y = -D\left(v\frac{\partial^2 w}{\partial x^2} + \frac{\partial^2 w}{\partial y^2}\right)$$

Substituting Eq. (5.3.8) into Eq. (5.3.7) gives the incremental strain energy as

$$dU_d = \frac{1}{2}C_x w_{mn}^2 D^2\pi^4\left(v\frac{m^2}{a^2} + \frac{n^2}{b^2}\right)^2 \left\{sin^2\left(\frac{m\pi x}{a}\right)sin^2\left(\frac{n\pi y_1}{b}\right)dx\right\} \tag{5.3.9}$$

The strain energy associated with the discontinuous rotation for the whole crack is, therefore.

$$U_d = \frac{1}{2}C_x w_{mn}^2 D^2\pi^4\left(v\frac{m^2}{a^2} + \frac{n^2}{b^2}\right)^2 \int_0^l \left\{sin^2\left(\frac{m\pi x}{a}\right)sin^2\left(\frac{n\pi y_1}{b}\right)dx\right\} \tag{5.3.10}$$

The integration in Eq. (5.3.10) can be simplified to give,

$$\int_0^l \left\{ sin^2\left(\frac{m\pi x}{a}\right) sin^2\left(\frac{n\pi y_1}{b}\right) dx \right\}$$

$$= \frac{1}{2}\sin^2\left(\frac{n\pi y_1}{b}\right)\int_{x_1}^{x_2}\left(1-\cos\left(\frac{2m\pi x}{a}\right)\right)dx$$

$$= \frac{1}{2}\sin^2\left(\frac{n\pi y_1}{b}\right)\left[x-\frac{a}{4m\pi}\sin\left(\frac{2m\pi x}{a}\right)\right]_{x_1}^{x_2}$$

$$= \sin^2\left(\frac{n\pi y_1}{b}\right)\left[\frac{x_2-x_1}{2}\right. \qquad (5.3.11)$$

$$\left. -\frac{a}{4m\pi}\left[\sin\left(\frac{2m\pi x_2}{a}\right)-\sin\left(\frac{2m\pi x_1}{a}\right)\right]\right]$$

Let x_0 and y_0 represent the midpoint of the crack. When the crack in the plate is parallel to the x-axis, the midpoint can be expressed as:

$$y_1 = y_2 = y_0$$

$$\frac{x_2-x_1}{2} = \quad x_0 = \frac{l}{2}$$

After integrating the strain energy for a finite part of the crack from zero to the overall length of the crack, the total change in strain energy can be expressed as:

$$U_d = \frac{1}{2}C_x w_{mn}^2 D^2\pi^4\left(v\frac{m^2}{a^2}+\frac{n^2}{b^2}\right)^2 \qquad (5.3.12)$$

$$sin^2\left(\frac{n\pi y_0}{b}\right)\left[l-\frac{a}{2m\pi}cos\left(\frac{2m\pi x_0}{a}\right)sin\left(\frac{m\pi l}{a}\right)\right]$$

The available mechanical strain energy at peak displacement for the cracked plate is

$$U_c = U_0 - U_d \qquad (5.3.13)$$

The cracked plate vibrates with a reduced natural frequency ω_{mnc} and at zero displacement has kinetic energy:

$$T_c = \frac{1}{2}\rho h\omega_{mnc}^2 w_{mn}^2\int_0^a\int_0^b sin^2\left(\frac{m\pi x}{a}\right)sin^2\left(\frac{n\pi y}{b}\right)dy\,dx \qquad (5.3.14)$$

Conservation of energy requires that $T_c = U_c$ and so

$$T_c - T_0 = U_c - U_0 = -U_d \tag{5.3.15}$$

$$\frac{1}{2}\rho h(\omega_{mnc}^2 - \omega_{mn0}^2)w_{mn}^2 \int_0^a \int_0^b sin^2\left(\frac{m\pi x}{a}\right) sin^2\left(\frac{n\pi y}{b}\right) dy\, dx = -U_d \tag{5.3.16}$$

Here, algebraic operations can be performed and difference between the square of the natural frequencies of the intact and cracked plate structures can be denoted by δ_{mn}, as expressed in Eq. (5.3.17) .

$$\omega_{mnc}^2 = \omega_{mn0}^2 - \delta_{mn} \tag{5.3.17}$$

The difference between the square of the natural frequencies of the intact and cracked plate can be provided using Eq. (5.3.18).

$$\delta_{mn} = \frac{C_n D^2 \pi^4 \left(v\frac{m^2}{a^2} + \frac{n^2}{b^2}\right)^2 \left[sin^2\left(\frac{n\pi y_1}{b}\right)\left[\frac{l}{2} - \frac{a}{2m\pi} cos\left(\frac{2m\pi x_0}{a}\right) sin\left(\frac{m\pi l}{a}\right)\right]\right]}{\rho h \int_0^a \int_0^b sin^2\left(\frac{m\pi x}{a}\right) sin^2\left(\frac{n\pi y}{b}\right) dy\, dx} \tag{5.3.18}$$

Note the double integral in the denominator of Eq. (5.3.18) is over the whole area of the plate and takes the value $(ab/4)$.

Similarly, the difference between the squares of the natural frequencies of a cracked and uncracked plate for a crack parallel to the *y*-axis can be expressed as:

$$\delta_{mn} = \frac{\left\{ C_n D^2 \pi^4 \left(\frac{m^2}{a^2} + v\frac{n^2}{b^2}\right)^2 sin^2\left(\frac{m\pi x_1}{a}\right)\left[\frac{l}{2} - \frac{b}{2n\pi} cos\left(\frac{2n\pi y_0}{b}\right) sin\left(\frac{n\pi l}{b}\right)\right]\right\}}{\rho h \int_0^a \int_0^b sin^2\left(\frac{m\pi x}{a}\right) sin^2\left(\frac{n\pi y}{b}\right) dy\, dx} \tag{5.3.19}$$

where

$$\frac{y_2 - y_1}{2} = \quad y_0 = \frac{l}{2} \qquad and \qquad x_1 = x_2 = x_0$$

5.3.1.2 Numerical Example.

This section explores the effects of a crack running parallel to either the *x* or *y* axis of the plate on the degradation of natural frequencies through a numerical example. The findings have been validated against prior research in the literature that employs Finite Element Analysis [20].

An isotropic square plate made of titanium has been considered for this demonstration as shown in Figure 5.6 The dimensions and the material properties are defined as: length $(a) = 0.1\text{m}$; width $(b) = 0.1\text{m}$; Young's modulus (E) = 110 x 10^9 Nm^{-2}; mass density $(\rho) = 4480\text{kgm}^{-3}$;

Two cases of cracks have been considered to observe the degradation in the natural frequencies in the plate. Case 1 (Figure 5.6 (a)) considers a crack running parallel to the *y*-axis from $(x_1, y_1) = (0.075, 0.05)$ to $(x_2, y_2) = (0.075, 0.1)$, i.e. along the quarter line of the plate. Similarly, case 2 considers the cracked plate presented in Figure 5.6 (b) which has a crack again running parallel to the *y*-axis but in this case located at the mid-line of the plate.

In both scenarios, crack depths vary between 10% and 60% of overall plate thickness. The difference between the squares of natural frequencies of the intact and cracked plate have been considered to conduct comparative studies. These results have been validated against findings from the advanced finite element method presented in earlier literature [20]. This earlier literature considered non-dimensional results regarding natural frequencies. For convenience of comparison, the obtained natural frequencies of the cracked plate have been converted into non-dimensional values using Eq. (5.3.20).

$$\bar{\omega}_{m,n} = \omega_{m,n} a^2 \sqrt{\frac{\rho h}{D}} \tag{5.3.20}$$

For comparison with respect to the finite element analyses performed, the relative change in natural frequencies (RCNF) has been employed. Relative changes in natural frequencies ($\delta^r{}_{(m,n)}$) can be obtained using Eq. (5.3.21).

$$\delta^r{}_{(m,n)} = 1 - \left(\frac{\omega^o{}_{(m,n)}}{\omega^c{}_{(m,n)}} \right) \tag{5.3.21}$$

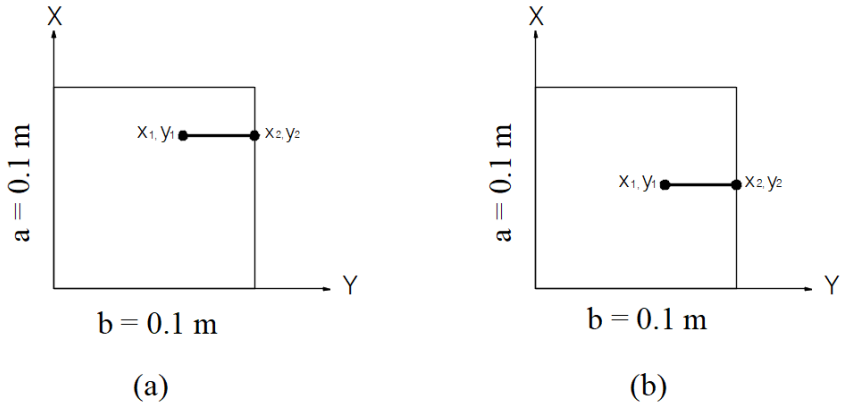

Figure 5.6 - An isotropic plate with a crack at, a) $(x_1, y_1) = (0.075, 0.05)$ and$(x_2, y_2) = (0.075, 0.1)$ b) $(x_1, y_1) = (0.05, 0.05)$ and $(x_2, y_2) = (0.05, 0.1)$.

5.3.1.3 Results

Table (5.1) displays the non-dimensional natural frequencies for the plate illustrated in Figure 5.6 which features a crack extending along the quarter line of the plate.

Table (5.2) provides relative changes in natural frequencies between the intact and cracked plates ($\delta^r{}_{(m,n)}$) resulting from the presence of this crack. Figure (5.7) shows the comparative analysis related to the finite element method.

Table 5.1 - non-dimensional natural frequencies of the cracked plate shown in Figure 5.6 (a)

d/h	**Mode (1,1)**	**Mode (2,1)**	**Mode (1,2)**	**Mode (2,2)**	**Mode (3,1)**	**Mode (1,3)**
0	19.739	49.348	49.348	78.956	98.696	98.696044
0.1	19.733	49.30	49.081	78.913	98.640	98.687
0.2	19.726	49.233	49.078	78.852	98.562	98.674
0.3	19.715	49.136	49.075	78.7637	98.448	98.656
0.4	19.697	48.986	49.072	78.626	98.273	98.629
0.5	19.669	48.735	49.064	78.398	97.9821	98.5833
0.6	19.617	48.271	49.0534	77.977	97.443	98.498

Table 5.2 – $\delta^{r}{}_{(m,n)}$ for partially through the depth of the crack for plate shown in Figure 5.6 (a)

d/h	**Mode (1,1)**	**Mode (2,1)**	**Mode (1,2)**	**Mode (2,2)**	**Mode (3,1)**	**Mode (1,3)**
0	0	0	0	0	0	0
0.1	0.00027	0.00096	0.00003	0.0005	0.000563	0.00008
0.2	0.00066	0.00231	0.00007	0.001321	0.00135	0.00021
0.3	0.0012	0.00428	0.0001	0.00244	0.0025	0.00039
0.4	0.00208	0.00733	0.00021	0.004181	0.00428	0.0006
0.5	0.00352	0.012404	0.0003	0.00706	0.007233	0.00114
0.6	0.00618	0.0218	0.0005	0.0123	0.01269	0.00199

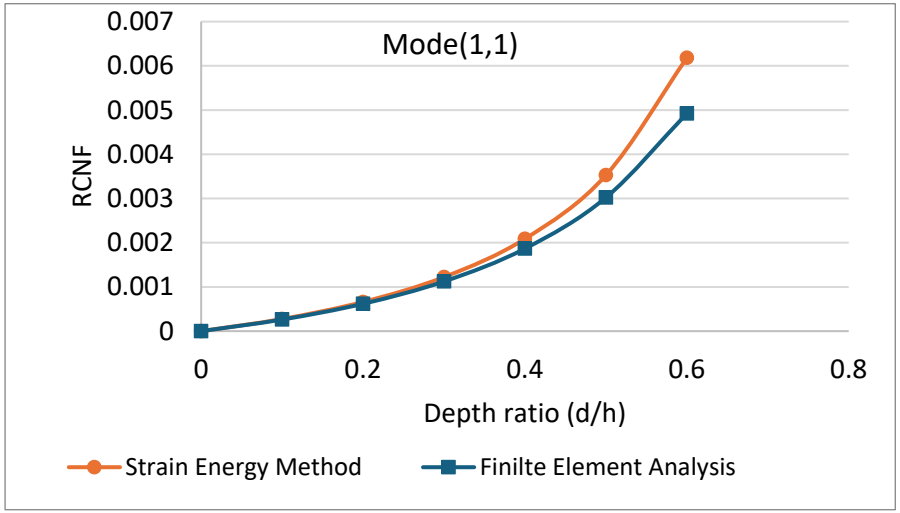
Mode(1,1)
RCNF
0.007
0.006
0.005
0.004
0.003
0.002
0.001
0
0
0.2
0.4
0.6
0.8
Depth ratio (d/h)
Strain Energy Method
Finilte Element Analysis

(a)

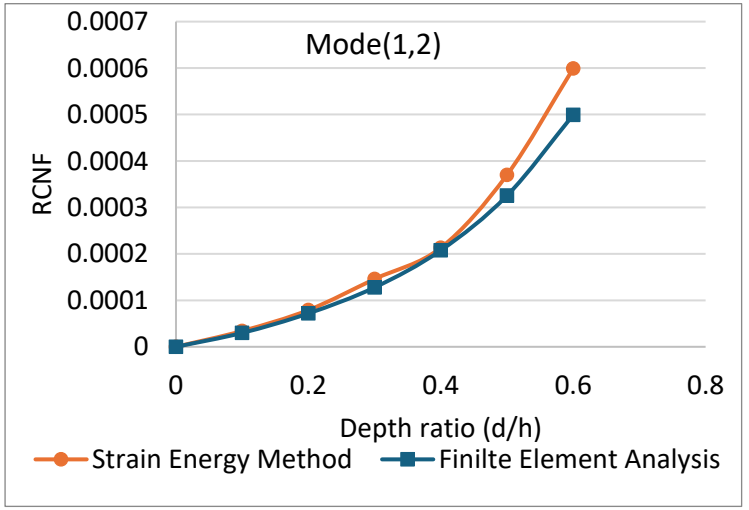
Mode(1,2)
RCNF
0.0007
0.0006
0.0005
0.0004
0.0003
0.0002
0.0001
0
0
0.2
0.4
0.6
0.8
Depth ratio (d/h)
Strain Energy Method
Finilte Element Analysis

(c)

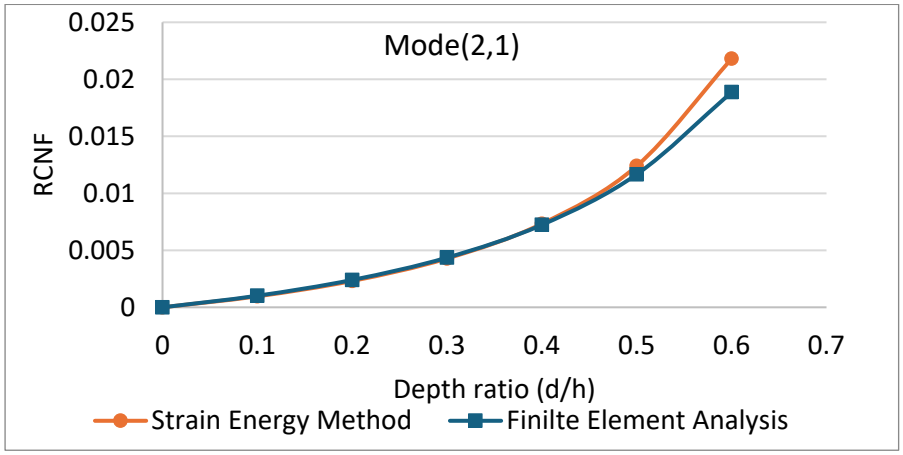
Mode(2,1)
RCNF
0.025
0.02
0.015
0.01
0.005
0
0
0.1
0.2
0.3
0.4
0.5
0.6
0.7
Depth ratio (d/h)
Strain Energy Method
Finilte Element Analysis

(b)

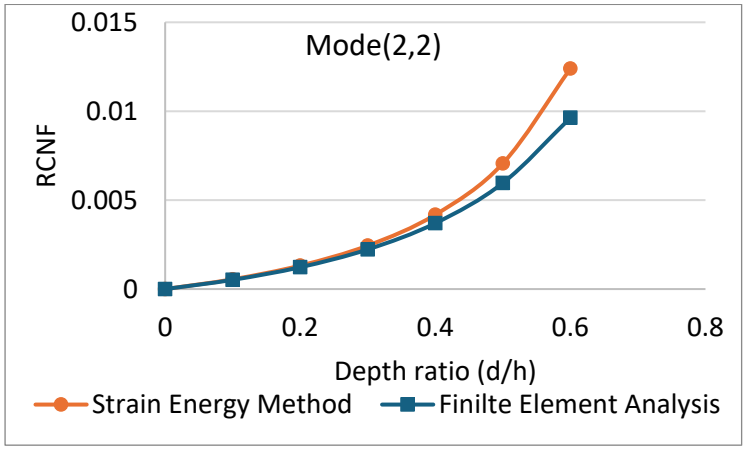
Mode(2,2)
RCNF
0.015
0.01
0.005
0
0
0.2
0.4
0.6
0.8
Depth ratio (d/h)
Strain Energy Method
Finilte Element Analysis

(d)

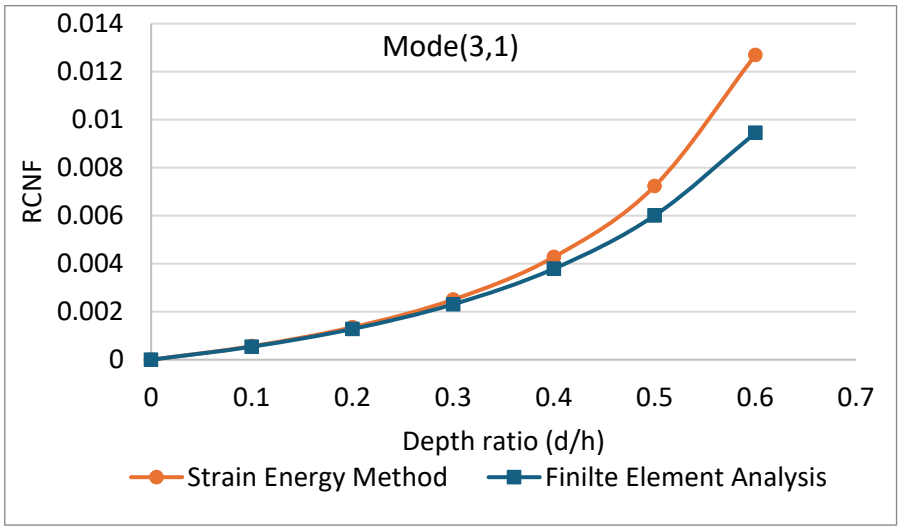

(e)

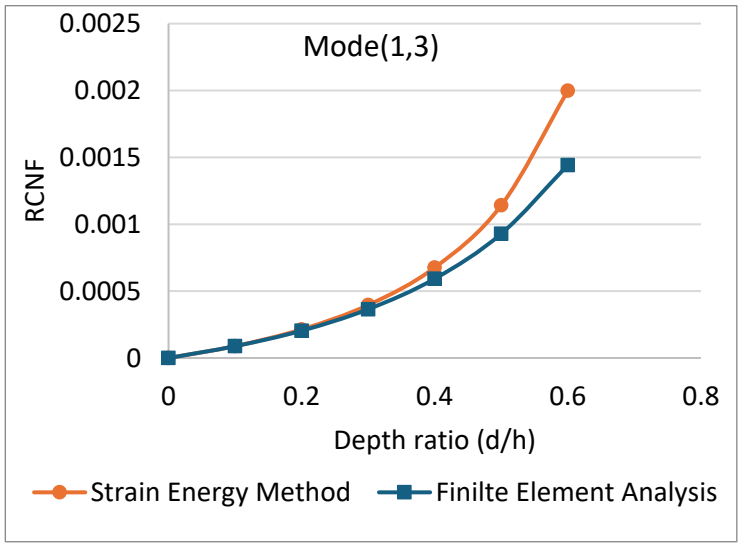

(f)

Figure 5.7 - Comparison of ' $\delta^{r}{}_{(m,n)}$ ' for a cracked plate shown in Figure 5.6 (a) with Finite Element analysis from the reference [20].

(*a*) Mode (1,1); (*b*) Mode (2,1) ;(*c*) Mode (1,2) ;(*d*) Mode (2,2) ;(*e*) Mode (3,1) ;(*f*) Mode (1,3).

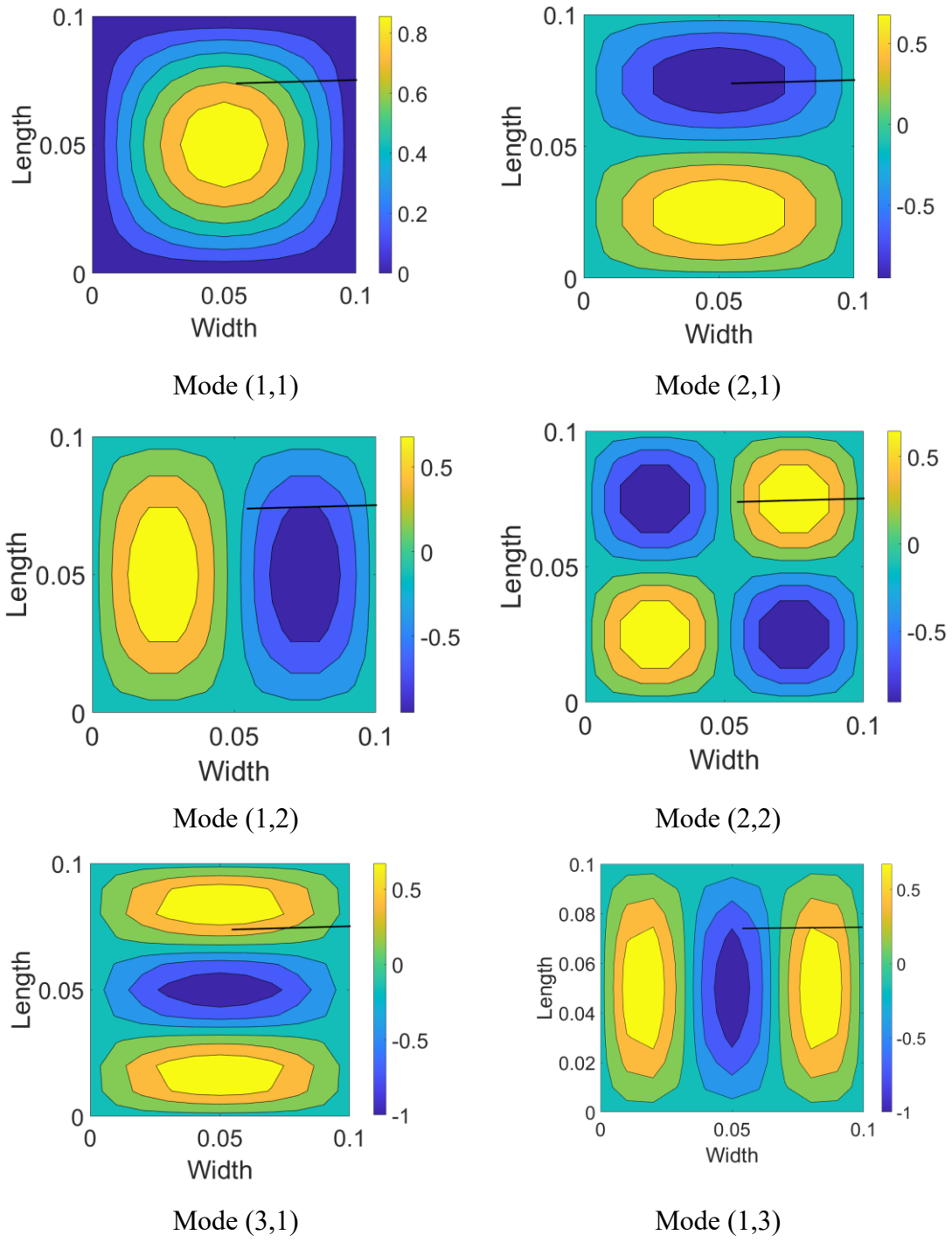

Figure 5.8 - Mode shapes for the plate shown in Figure 5.6 (a).

Figure 5.8 shows the mode shapes for the plate depicted in Figure 5.6(a), where the crack is located along the quarter line of the plate. The results show a match of 95% to 98% with the finite element model for crack depth ratios between 0.1 and 0.3. For crack depth ratios ranging from 0.4 to 0.6, this match varies between 91% and 81%.

Table 5.3 presents the non-dimensional natural frequencies for the plate illustrated in Figure 5.6 (b), with a crack extending along the mid-line of the plate. Table 5.4 provides the $\delta^{r}{}_{(m,n)}$ resulting from the presence of the crack.

Table 5.3 - non-dimensional natural frequencies of the cracked plate shown in Figure 5.6 (b)

d/h	Mode (1,1)	Mode (1,2)	Mode (2,1)	Mode (2,2)	Mode (3,1)	Mode (1,3)
0	19.739	49.348	49.348	78.956	98.696	98.696
0.1	19.728	49.335	49.348	78.956	98.584	98.678
0.2	19.713	49.318	49.348	78.956	98.429	98.653
0.3	19.690	49.292	49.348	78.956	98.201	98.617
0.4	19.656	49.253	49.348	78.956	97.849	98.562
0.5	19.599	49.188	49.348	78.956	97.262	98.470
0.6	19.494	49.068	49.348	78.956	96.1765	98.301

Table 5.4 - '$\delta^{r}{}_{(m,n)}$'for partially through the depth of the crack for plate shown in Figure 5.6 (b).

d/h	Mode (1,1)	Mode (1,2)	Mode (2,1)	Mode (2,2)	Mode (3,1)	Mode (1,3)
0	0	0	0	0	0	0
0.1	0.0005	0.0002	0	0	0.0011	0.00017
0.2	0.0013	0.0006	0	0	0.0027	0.00042
0.3	0.0024	0.0011	0	0	0.0050	0.00079
0.4	0.0041	0.0019	0	0	0.0085	0.0013
0.5	0.0070	0.0032	0	0	0.01452	0.0022
0.6	0.0123	0.0056	0	0	0.0255	0.0039

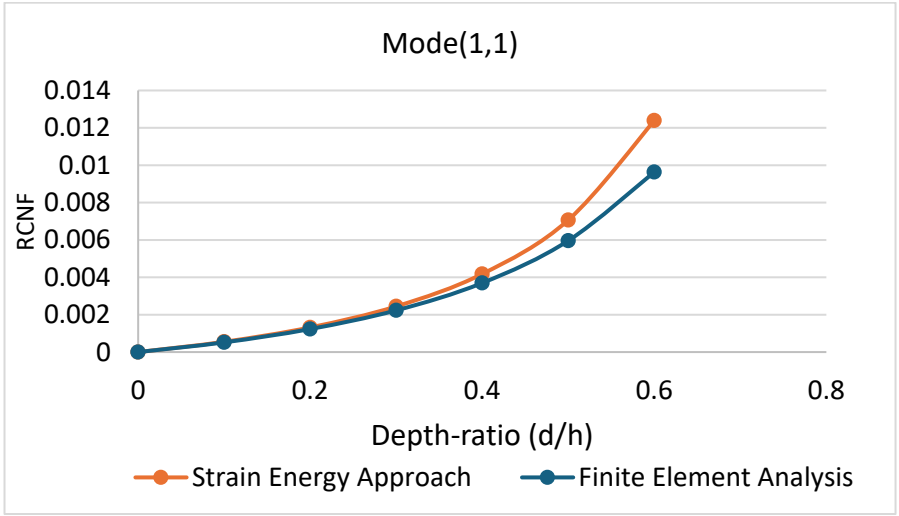
Mode(1,1)
RCNF
0.014
0.012
0.01
0.008
0.006
0.004
0.002
0
0
0.2
0.4
0.6
0.8
Depth-ratio (d/h)
Strain Energy Approach
Finite Element Analysis

(a)

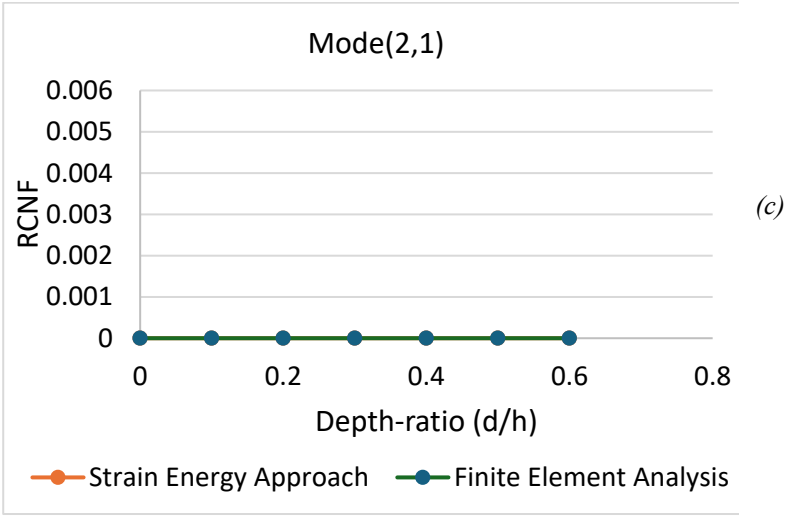
Mode(2,1)
RCNF
0.006
0.005
0.004
0.003
0.002
0.001
0
0
0.2
0.4
0.6
0.8
Depth-ratio (d/h)
Strain Energy Approach
Finite Element Analysis

(c)

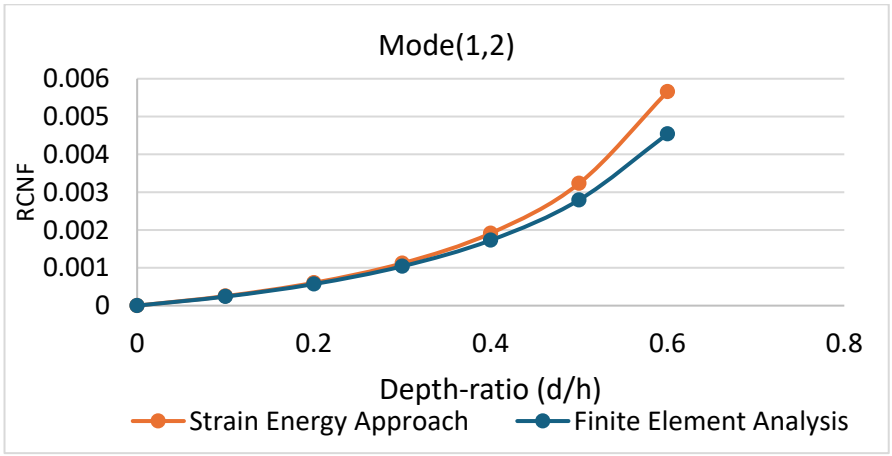
Mode(1,2)
RCNF
0.006
0.005
0.004
0.003
0.002
0.001
0
0
0.2
0.4
0.6
0.8
Depth-ratio (d/h)
Strain Energy Approach
Finite Element Analysis

(b)

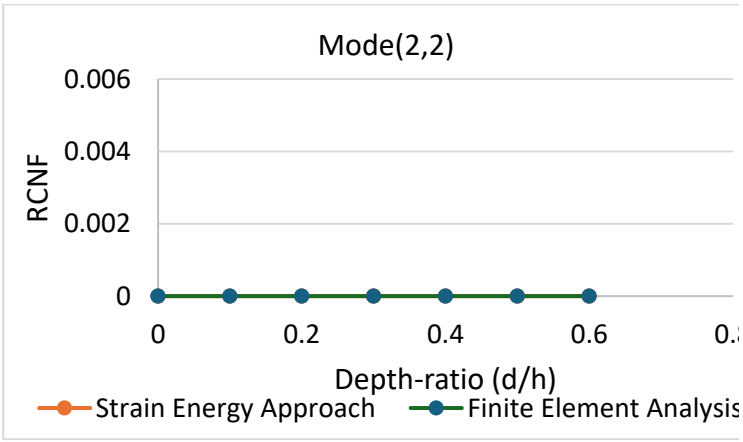
Mode(2,2)
RCNF
0.006
0.004
0.002
0
0
0.2
0.4
0.6
Depth-ratio (d/h)
Strain Energy Approach
Finite Element Analysis

(d)

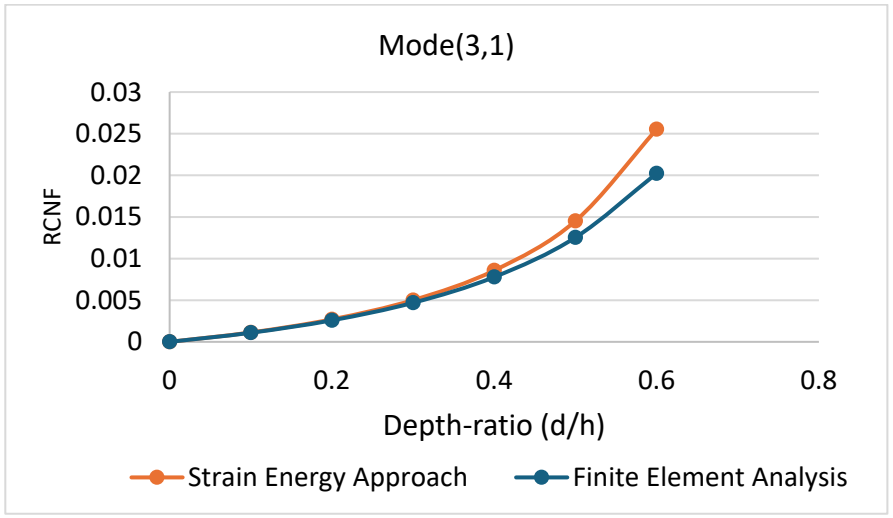

(e)

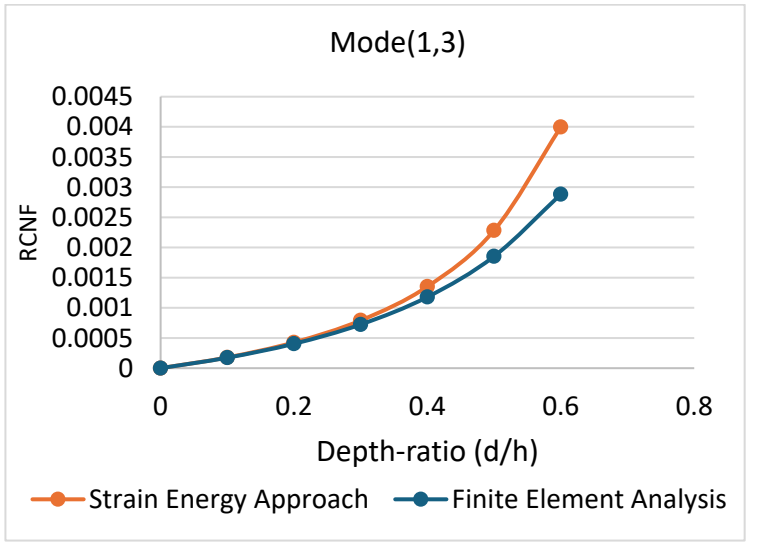

(f)

Figure 5.9 Comparison of RCNF for a cracked plate shown in Figure 5.6 (b) with Finite Element Model generated by [20], (*a*) Mode (1,1); (*b*) Mode (1,2); (*c*) Mode (2,1); (*d*) Mode (2,2); (*e*) Mode (3,1); (*f*) Mode (1,3).

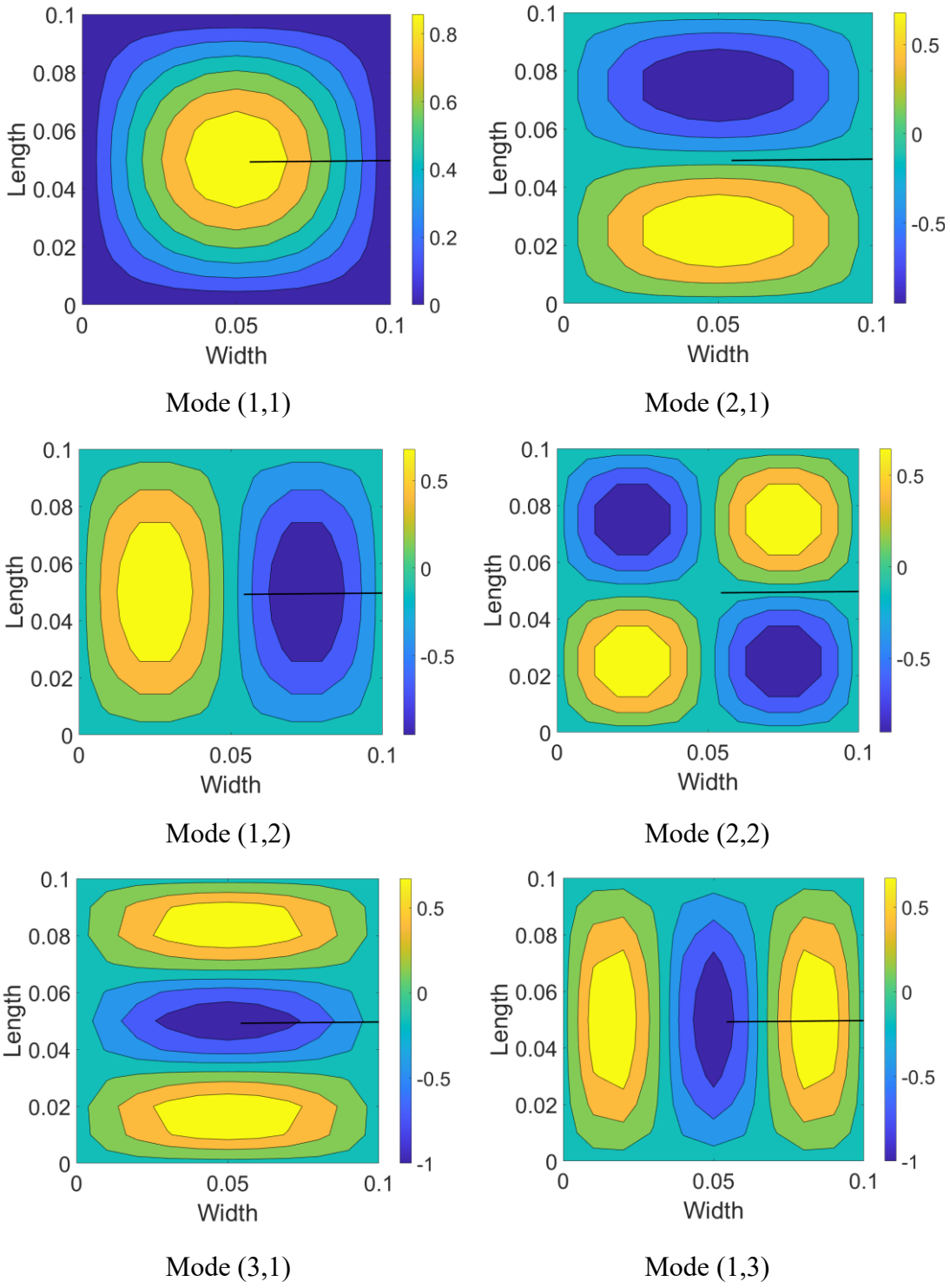

Figure 5.10 - Mode shapes for the plate shown in Figure 5.6 (b).

Figure (5.9) compares the strain energy approach and the finite element model results for a crack positioned along the mid-line of the plate. Figure 5.10 shows the mode shapes for the plate depicted in Figure 5.6(a), where the crack is located along the quarter line of the plate. The crack aligns precisely with the nodal line, resulting in no change in rotation, which in turn leads to no change in strain energy and negligible $\delta^{r}{}_{(m,n)}$ for modes (2,1) and (2,2).

The findings indicate a match of approximately 96% to 98% for crack depth ratios between 0.1 and 0.2. For crack depth ratios ranging from 0.3 to 0.5, the results show a variation of around 94 % to 86 %.

5.3.1.4 Discussion

This section has examined the degradation of natural frequencies in a square isotropic simply supported plate using the strain energy approach. The linear crack analysed here is partially through the depth and oriented parallel to the edge of the plate.

The obtained results were compared with prior research employing finite element analysis [20]. These studies revealed a significant correlation, with agreement levels ranging from 80% to 98% in terms of crack depth. However, an analytical approach to determining the degradation in natural frequencies offers a better match for crack depth ratios up to 0.4.

In the following Section, 5.3.2, a crack oriented in an arbitrary direction will be considered for modelling, along with parametric studies.

5.3.2 Case II – Arbitrary Oriented Crack.

5.3.2.1 Strain Energy Approach

In the previous Section 5.3.1, the case of a partial through-the-depth crack in an isotropic, simply supported plate, where the crack was parallel to the edges of the plate, was studied. An analytical solution was presented that provided the difference between the squares of the natural frequencies of the uncracked and cracked plates.

In earlier research studies [20], when modelling cracks using finite element analysis, for the case of an arbitrarily oriented crack, the effect was considered as a superposition of two cracks running parallel to the edges with the twisting moment being neglected.

This section presents the case of arbitrarily oriented, partially through-the-thickness crack, with the inclusion of the twisting effect in an analytical solution.

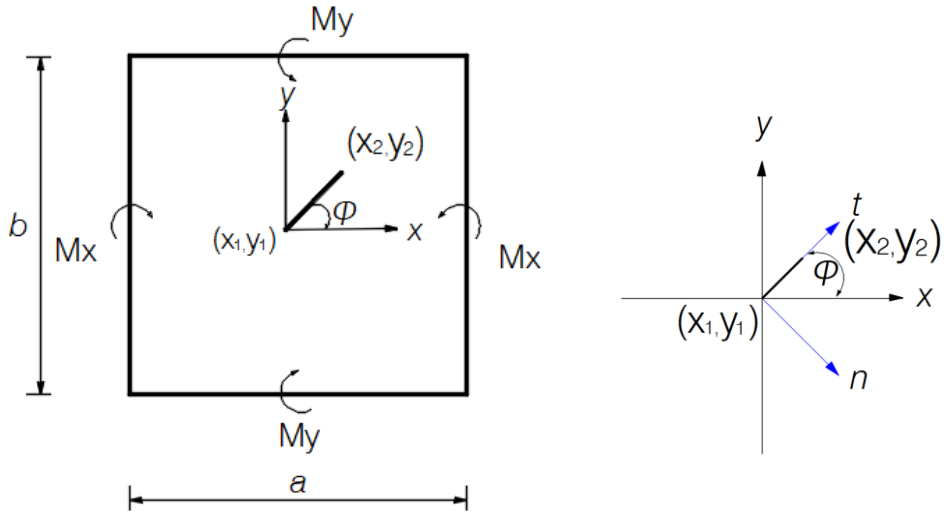

Figure 5.11 - a) Plate with an arbitrarily oriented crack. b) Axis transformation according to crack orientation.

.

An isotropic plate is considered with length *a*, breadth *b*, and thickness *h* as shown in Figure 5.11 (a).

A crack of depth *d* runs from the centre point of the plate with initial and final coordinates (x_1, y_1) and (x_2, y_2) respectively. $'l'$ denotes the length of the crack. The transformation of the crack to axes normal and tangential to the crack is shown is figure 5.10 (b).

The length of the crack and the orientation with respect to the *x* - axis can be calculated using Eq. (5.3.22) and (5.3.23).

$$l = \sqrt{(x_2 - x_1)^2 + (y_2 - y_1)^2} \tag{5.3.22}$$

$$\varphi = tan^{-1}\left(\frac{y_2 - y_1}{x_2 - x_1}\right) \tag{5.3.23}$$

If M_n and M_t represent the bending moments per unit length across and along the crack respectively, from Eq. (5.3.6) the change in rotation across the crack $\delta\theta_n$ for a small length of the crack (ds) can be represented by Eq. (5.3.24).

$$\delta\theta_n = (C_n)(M_n) \tag{5.3.24}$$

Here, C_n represents the compliance per unit length of the arbitrarily oriented crack. Similarly from Eq. (5.3.7) the change in strain energy for a small part of the crack 'ds' can be expressed as Eq. (5.3.25)

$$dU_d = \frac{1}{2}\delta\theta_n(M_n ds) = \frac{1}{2}C_n\left({M_n}^2 ds\right) \tag{5.3.25}$$

Here, M_n can be expressed as:

$$M_n = M_x(cos\varphi)^2 + M_y(sin\varphi)^2 + 2cos\varphi\, sin\,\varphi\, M_{xy} \tag{5.3.26}$$

The change in the strain energy can be obtained for a unit length ds by substituting Eq. (5.3.26) into Eq. (5.3.25).

$$dU_d = \frac{1}{2}C_n w_{mn}^2 D^2 \pi^4 \left[\left[\left(\frac{m^2}{a^2} + \nu \frac{n^2}{b^2} \right) (cos\varphi)^2 + \left(\nu \frac{m^2}{a^2} + \frac{n^2}{b^2} \right) (sin\varphi)^2 \right] sin\left(\frac{m\pi x}{a}\right) sin\left(\frac{n\pi y}{b}\right) ds + 2(1-\nu) cos\varphi \, sin\,\varphi \frac{mn}{ab} cos\left(\frac{m\pi x}{a}\right) cos\left(\frac{n\pi y}{b}\right) ds \right] \quad (5.3.27)$$

The strain energy associated with the discontinuous rotation over the whole crack is, therefore

$$U_d = \frac{1}{2}C_n w_{mn}^2 D^2 \pi^4 \int_0^l \left[\left[\left(\frac{m^2}{a^2} + \nu \frac{n^2}{b^2} \right) (\cos\varphi)^2 + \left(\nu \frac{m^2}{a^2} + \frac{n^2}{b^2} \right) (\sin\varphi)^2 \right] \sin\left(\frac{m\pi x}{a}\right) \sin\left(\frac{n\pi y}{b}\right) ds + 2(1-\nu)\cos\varphi \sin\varphi \frac{mn}{ab} \cos\left(\frac{m\pi x}{a}\right) \cos\left(\frac{n\pi y}{b}\right) ds \right] \quad (5.3.28)$$

While integrating Eq. (5.3.28), x and y can be substituted as:

$$x = x_1 + s(\cos\varphi) \ , y = y_1 + s(\sin\varphi) \quad (5.3.29)$$

and

$$\alpha_x = \frac{m\pi(x_1 + s\cos\varphi)}{a}, \alpha_y = \frac{n\pi(y_1 + \sin\varphi)}{b} \quad (5.3.30)$$

where, x_1 and y_1 are the starting points of the crack. Hence, the total strain energy due to the crack can be expressed as:

$$U_d = \frac{1}{2} C_n w_{mn}^2 D^2 \pi^4 \int_0^l \left[\begin{bmatrix} \left(\frac{m^2}{a^2} + \nu \frac{n^2}{b^2}\right) \cos^2 \varphi \\ + \left(\nu \frac{m^2}{a^2} + \frac{n^2}{b^2}\right) \sin^2 \varphi \end{bmatrix} \sin\left(\frac{m\pi x}{a}\right) \sin\left(\frac{n\pi y}{b}\right) ds \right.$$
$$\left. + 2(1-v)\cos\varphi \sin\varphi \frac{mn}{ab} \cos\left(\frac{m\pi x}{a}\right) \cos\left(\frac{n\pi y}{b}\right) ds \right]^2 \quad (5.3.31)$$

Using Eq. (5.3.30), Eq. (5.3.31) can be modified as:

$$U_d = \frac{1}{2} C_n w_{mn}^2 D^2 \pi^4 \left\{ \left[\left(\frac{m^2}{a^2} + \nu \frac{n^2}{b^2}\right) \cos^2 \varphi + \left(\nu \frac{m^2}{a^2} + \frac{n^2}{b^2}\right) \sin^2 \varphi \right]^2 \int_0^l \sin^2 \alpha_x \sin^2 \alpha_y \, ds \right.$$
$$+ \left(2(1-v)\cos\varphi \sin\varphi \frac{mn}{ab}\right)^2 \int_0^l \cos^2 \alpha_x \cos^2 \alpha_y \, ds$$
$$\left. + 4 \left[\left(\frac{m^2}{a^2} + \nu \frac{n^2}{b^2}\right) \cos\varphi + \left(\nu \frac{m^2}{a^2} + \frac{n^2}{b^2}\right) \sin\varphi \right] 2(1 - v)\cos\varphi \sin\varphi \frac{mn}{ab} \int_0^l \sin \alpha_x \sin \alpha_y \cos \alpha_x \cos \alpha_y \, ds \right\} \quad (5.3.32)$$

Using similar operations as performed from Eq. (5.3.12) to Eq. (5.3.17) the relationship for the difference between the squares of the natural frequencies of intact and cracked plates can be expressed in the form of Eq. (5.3.33). Simplification of integral terms has been presented in Appendix (A) and the function files are attached in the Appendix (G).

$$\delta_{mn} = \frac{C_n D^2 \pi^4 \begin{bmatrix} \left[\left(\frac{m^2}{a^2} + \nu\frac{n^2}{b^2}\right)cos^2\varphi + \left(\nu\frac{m^2}{a^2} + \frac{n^2}{b^2}\right)sin^2\varphi\right]^2 \\ \int_0^l sin^2\,\alpha_x sin^2\alpha_y\, ds + \\ \left(2(1-v)cos\varphi\, sin\,\varphi\frac{mn}{ab}\right)^2 \\ \int_0^l cos^2\,\alpha_x cos^2\alpha_y\, ds + \\ 4\left[\left(\frac{m^2}{a^2} + \nu\frac{n^2}{b^2}\right)cos^2\varphi + \left(\nu\frac{m^2}{a^2} + \frac{n^2}{b^2}\right)sin^2\varphi\right] \\ 2(1-v)cos\varphi\, sin\,\varphi\frac{mn}{ab} \\ \int_0^l sin\,\alpha_x sin\alpha_y\, cos\,\alpha_x cos\alpha_y\, ds \end{bmatrix}}{\rho h \int_0^a \int_0^b sin^2\left(\frac{m\pi x}{a}\right) sin^2\left(\frac{n\pi y}{b}\right) dy\, dx} \quad (5.3.33)$$

5.3.2.2 Modelling of Cracked Plate in ABAQUS

ABAQUS is a widely used commercial finite element analysis (FEA) software across various engineering fields. This section outlines a methodology for developing a cracked isotropic plate model using ABAQUS. The key purpose of these models is to validate the results obtained from a strain energy-based approach for analysing the degradation of natural frequencies due to arbitrarily oriented cracks in the plate for which there are no previous results in the literature [21].

In this study, the ABAQUS model uses homogeneous S4 shell elements to represent a simply supported isotropic rectangular plate. The model determines the vibration parameters, such as natural frequencies and mode shapes, of the plate. The plate can have a predefined crack that can be oriented either horizontally or vertically and positioned at any location on the plate, with varying crack depths. The mesh size and number of elements may vary depending on the meshing approach used. The ABAQUS model assigns six degrees of freedom to each node, but the analysis focuses only on the out-of-plane behaviour, suppressing the in-plane degrees of freedom. The study examines the first six natural frequencies of the cracked plate simply supported at the edges.

5.3.2.2.1 Intact and Cracked Plate Modelling in ABAQUS

While modelling the crack in a shell, there are many potential options. In this case the shell is divided in two parts with the division positioned to align with the crack. These

two parts are then joined together using two different methods corresponding to the intact and cracked parts of the shell along the join.

To model an intact plate using two separate parts, the interface nodes (or surfaces) are connected using tie constraints to ensure displacement compatibility and simulate perfect bonding between the parts. These constraints force all degrees of freedom of the nodes connected to be equivalent. So for example, the illustration in Figure 5.12 corresponds to two plates joined together using tie constraints which then behaves as a single plate. To validate the use of the tie constraint an intact square plate simply supported along all four edges is modelled with the obtained results compared with the previous studies for a perfect plate based on its non-dimensional natural frequencies. (Eq. (5.3.19)).

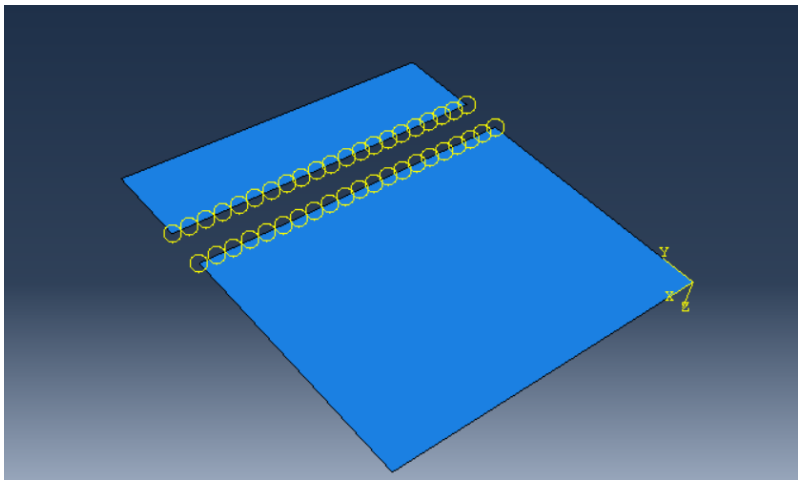

Figure 5.12 – Modelling of intact plate with two parts and tie constraints.

Table 5.3 - Comparison of non-dimensional natural frequencies of isotropic square plate simply supported at all ends with previous studies.

Mode	1,1	1,2	2,1	2,2	3,1	1,3
Rayleigh's Method	19.73	49.34	49.34	78.95	98.69	98.69
Liew *et al.* [90]	19.74	49.35	49.35	78.96	98.70	98.70
Stahl and Keer [80]	19.74	49.35	49.35	78.96	98.70	98.70
Huang *et al.* [96]	19.74	49.35	49.35	78.96	98.70	98.70
ABAQUS	19.73	49.68	49.68	79.36	100.81	100.81

For a plate with length a = 0.1m; width b = 0.1m; thickness h = 0.001m; modulus of elasticity E = 110 x 10^9 N m^{-2}; density ρ = 4480 kg · m^{-3} and Poisson's ratio v = 0.3, a comparison of natural frequency results is shown in Table 5.3. It can be seen that the non-dimensional natural frequencies match closely with the previous studies. Hence, the ABAQUS model is validated and can be used to model cracked plates,

To model the cracked part of the plate, two constraints are used. The first is a coupling constraint which restrains the rotation and displacements, with the exception of the rotation about the crack as shown in Figure 5.13.

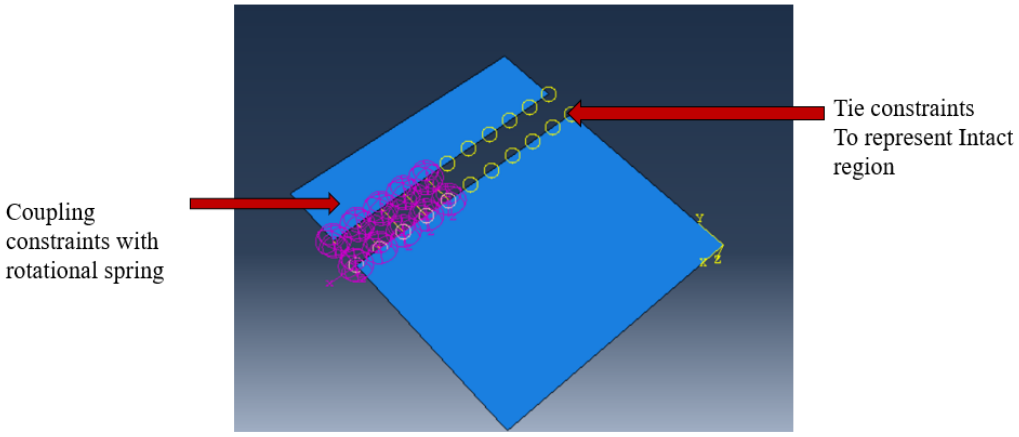

Figure 5.13 - a) Coupling Constraints and Rotational Spring model.

The second is a rotational spring as used by previous researchers [20], [35], [113]. The stiffness of the rotational spring can be obtained using Eq. (5.3.34).

$$K_{SP} = \frac{D\, l_e}{h\, C(d/h)} \tag{5.3.34}$$

Here, D is the flexural rigidity of the plate; l_e is the length of the element; h is the thickness of the plate and $C(d/h)$ is the non-dimensional compliance which can be obtained using Eq. (3.3.4).

5.3.2.2.2 Mesh convergence studies

Different mesh sizes have been considered for an intact square plate to select an appropriate mesh size for validation purposes. The relative change in natural frequencies (RCNF) has been calculated with respect to the natural frequencies obtained using the strain energy approach. A plate examined in section 5.3.2.2.1 has been used for mesh convergence studies.

Table 5.4 presents the natural frequencies of an intact plate using the analytical method (Eq. (5.2.10)) and FEM (ABAQUS) with four different mesh densities. Additionally, Table 5.5 presents the RCNF with respect to the analytical solution for plates modelled using ABAQUS.

Table 5.4 - Natural frequencies (Hz) of an intact plate using analytical solution and ABAQUS with different mesh sizes.

Mesh size	Mode (1,1)	Mode (2,1)	Mode (1,2)	Mode (2,2)	Mode (3,1)	Mode (1,3)
Analytical Method	471.08	1177.70	1177.70	1884.32	2355.40	2355.40
10 x 10	474.45	1219.30	1219.30	1943.00	2591.00	2591.30
15 x 15	472.02	1194.50	1194.50	1907.30	2451.90	2451.90
20 x 20	471.08	1185.90	1185.90	1894.10	2406.05	2406.05
25 x 25	471.05	1185.40	1185.40	1893.10	2406.00	2406.00

RCNF presented in table 5.5 have been calculated using Eq. (5.3.35)

$$\text{RCNF} = 1 - \frac{\text{Natural frequecy using strain energy approach}}{\text{Natural frequecy obatined using ABAQUS}} \tag{5.3.35}$$

Table 5.5 - RCNF with respect to analytical solution from Table 5.4.

Mesh size	10 x 10	15 x 15	20 x 20	25 x 25
Mode (1,1)	0.0071	0.0019	2.81×10^{-6}	2.81×10^{-6}
Mode (2,1)	0.0353	0.0142	0.0069	0.0065
Mode (1,2)	0.0353	0.0142	0.0069	0.0065
Mode (2,2)	0.03113	0.0121	0.0051	0.0046
Mode (3,1)	0.10002	0.0409	0.0215	0.0214
Mode (1,3)	0.1001	0.0409	0.0215	0.0214

A bar chart presented in Figure 5.14 illustrates the relative errors in the natural frequencies compared to the analytical solution for an intact square plate with four different mesh densities.

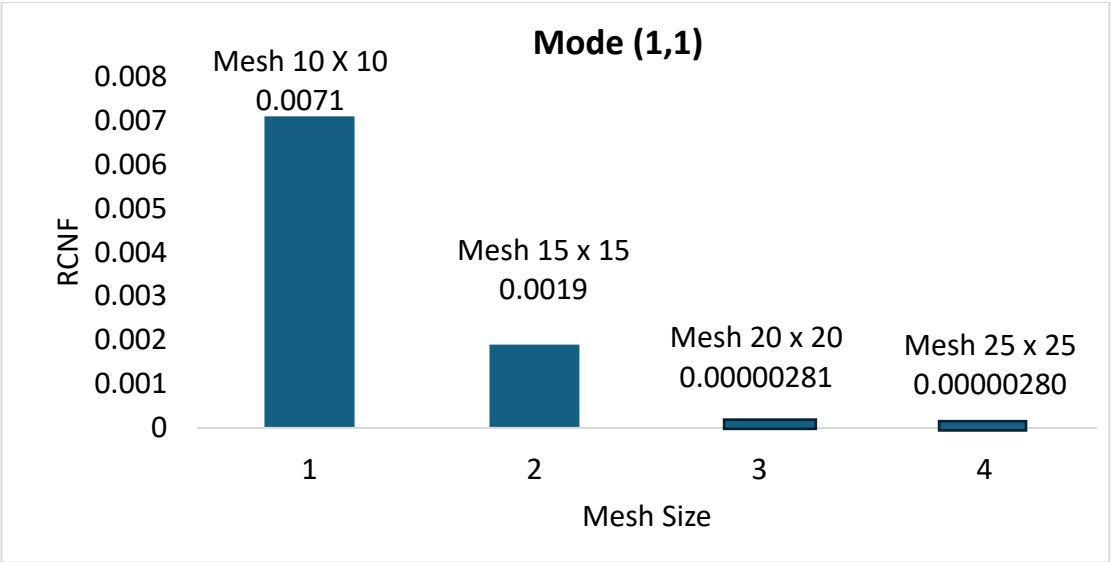
Mode (1,1)
Mesh 10 X 10
0.0071
Mesh 15 x 15
0.0019
Mesh 20 x 20
0.00000281
Mesh 25 x 25
0.00000280
RCNF
0.008
0.007
0.006
0.005
0.004
0.003
0.002
0.001
0
1
2
3
4
Mesh Size

(a)

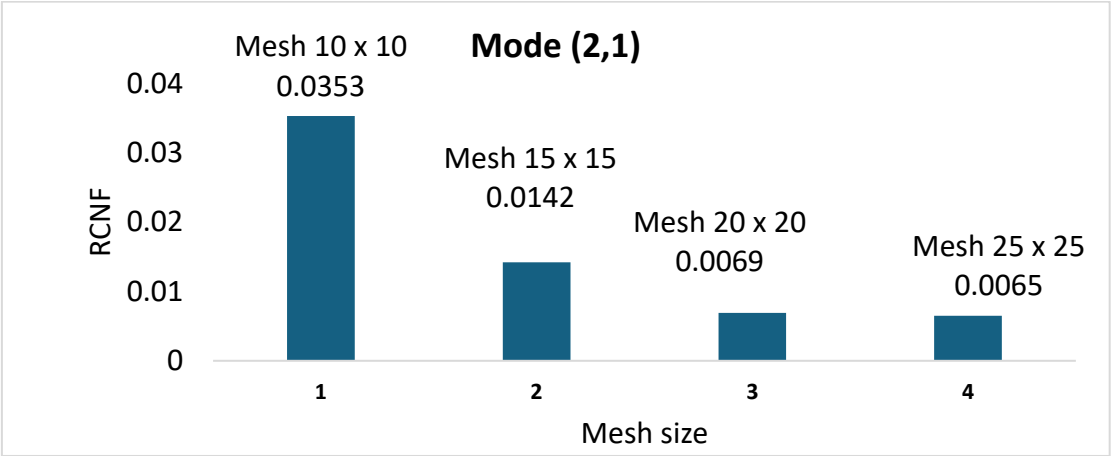
Mode (2,1)
Mesh 10 x 10
0.0353
Mesh 15 x 15
0.0142
Mesh 20 x 20
0.0069
Mesh 25 x 25
0.0065
RCNF
0.04
0.03
0.02
0.01
0
1
2
3
4
Mesh size

(b)

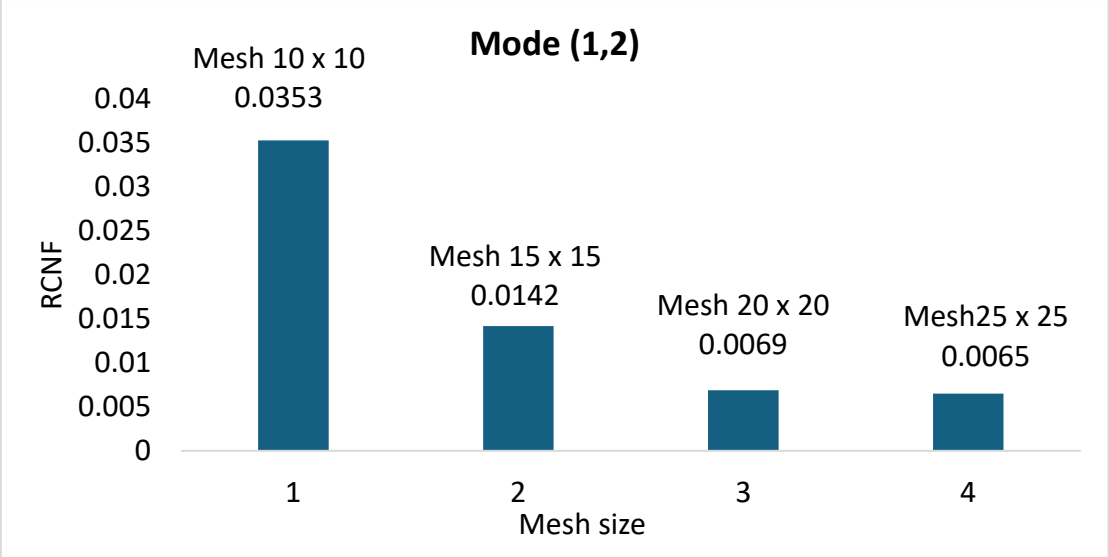
Mode (1,2)
Mesh 10 x 10
0.0353
Mesh 15 x 15
0.0142
Mesh 20 x 20
0.0069
Mesh25 x 25
0.0065
RCNF
0.04
0.035
0.03
0.025
0.02
0.015
0.01
0.005
0
1
2
3
4
Mesh size

(c)

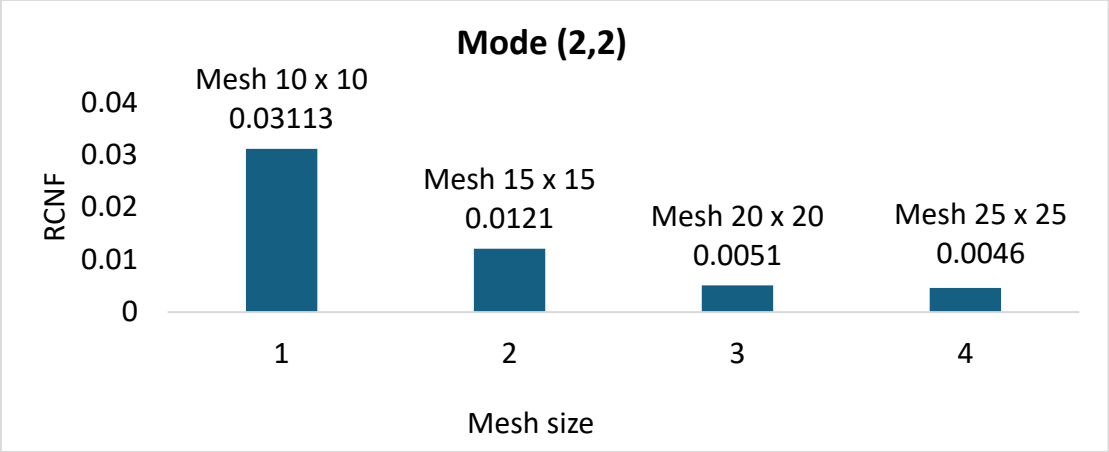
Mode (2,2)
Mesh 10 x 10
0.03113
Mesh 15 x 15
0.0121
Mesh 20 x 20
0.0051
Mesh 25 x 25
0.0046
RCNF
0.04
0.03
0.02
0.01
0
1
2
3
4
Mesh size

(d)

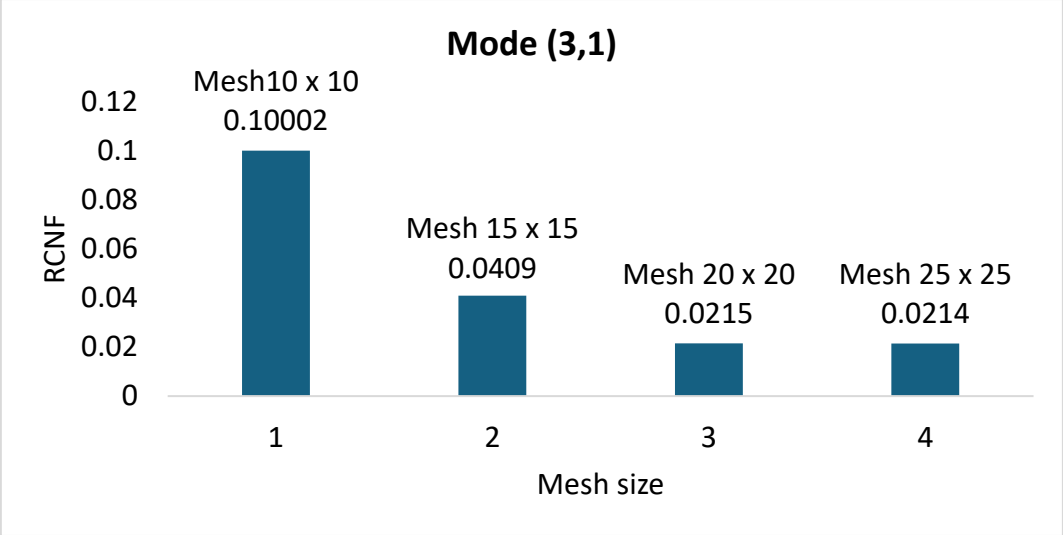

(e)

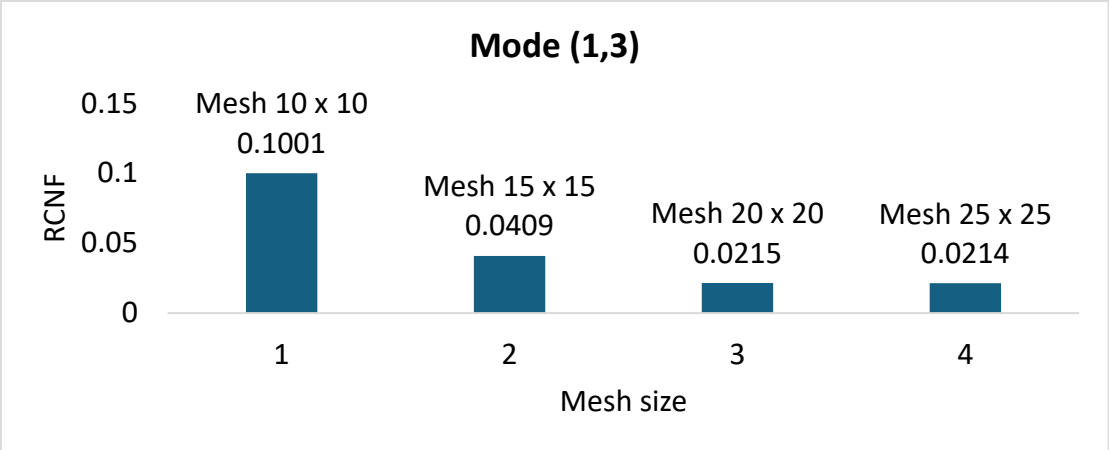

(f)

Figure 5.14 – Bar charts for mesh convergence studies: a) Mode (1,1), b) Mode (2,1), c) Mode (1,2), d) Mode (2,2), e) Mode (3,1), and f) Mode (1,3),

From Table 5.5 and Figure 5.14 , It can be observed that the average relative error for mesh sizes 10 x 10 and 15 x 15 varies from 5.14 % to 2.07 %. This percentage error has been further reduced to 1% using mesh sizes 20 x 20 and 25 x 25. The following section provides comparative studies and validation of the strain energy approach for modelling an arbitrary crack in simply supported square and rectangular plate structures. Mesh sizes 20 x 20 and 24 x 20 have been chosen from the references in Table 5.5 and Figure 5.14 for validation purpose.

.

5.3.2.3 Numerical Example and Validations

In this section, two numerical examples have been considered to demonstrate the effect of an arbitrary oriented crack on the natural frequencies of the plate. The material properties of the plates are as follows: Modulus of elasticity E = 110 x 10^9 N · m^{-2}; density ρ = 4480 kg · m^{-3}; Poisson's ratio v = 0.3. Both square and rectangular plates are considered for the comparison with those obtained from the ABAQUS model.

In both examples, the ratio of the depth of crack to the thickness of the plate varies from 0.1 to 0.6 in a discrete manner. The first six vibration modes are considered. Relative changes in natural frequencies (RCNF) with respect to a intact plate have been employed.

5.3.2.3.1 Numerical Example: Square Plate

The square plate presented in Figure 5.15 ,with length a = 0.1m, width b = 0.1, and thickness h = 0.001m is studied. A crack represented by the red line with initial coordinates (x_1, y_1) = (0.058,0.0553), and final coordinates (x_2, y_2) = (0.1,0.078) is introduced.

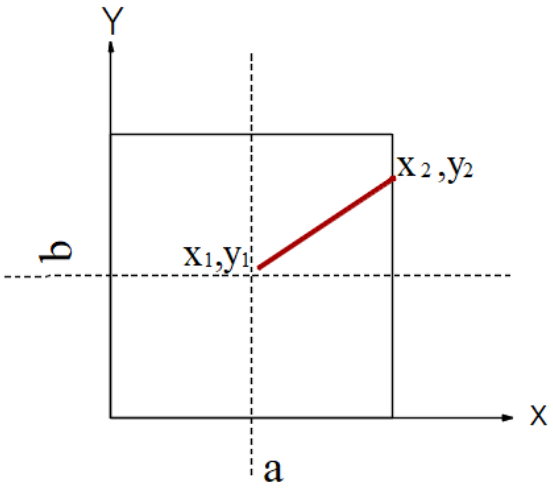

Figure 5.15 - Square isotropic simply supported cracked plate.

Table 5.6 presents the natural frequencies of the cracked plate, with respect to the change in depth of the crack. Table 5.7 presents the relative change in the natural frequencies with respect to a intact plate. Data represented in both tables is obtained using the proposed strain energy approach.

Table 5.6 - Natural frequencies of the cracked plate shown in Figure 5.15 using the proposed strain energy approach.

d/h	**Mode (1,1)**	**Mode (2,2)**	**Mode (3,1)**	**Mode (1,3)**
0	471.081	1884.32	2355.40	2355.40
0.1	470.93	1883.64	2354.90	2354.76
0.2	470.73	1882.68	2354.21	2353.87
0.3	470.44	1881.29	2353.19	2352.56
0.4	469.9	1879.13	2351.62	2350.55
0.5	469.24	1875.56	2349.01	2347.21
0.6	467.85	1868.96	2344.21	2341.05

Table 5.7 - RCNF for a plate shown in Figure 5.15 using strain energy approach.

d/h	**Mode (1,1)**	**Mode (2,2)**	**Mode (3,1)**	**Mode (1,3)**
0	0	0	0	0
0.1	0.000305	0.000363	0.000212	0.000271
0.2	0.000731	0.00087	0.000508	0.000651
0.3	0.001354	0.001611	0.00094	0.00120
0.4	0.002313	0.002753	0.001606	0.0020
0.5	0.003906	0.00465	0.002712	0.0034
0.6	0.006846	0.008152	0.004751	0.00609

The same cracked plate has been modelled using ABAQUS. Table 5.8 and 5.9 present the natural frequencies and relative change in natural frequencies with respect to intact plate based on this model.

Table 5.8 - Natural frequencies of a cracked plate shown in Figure 5.15 using ABAQUS.

d/*h*	Mode (1,1)	Mode (2,2)	Mode (3,1)	Mode (1,3)
0	471.2	1899.9	2364.4	2362.5
0.1	470.9	1899.1	2363.8	2361.8
0.2	470.48	1897.9	2363	2360.8
0.3	469.89	1896.4	2361.9	2359.4
0.4	469.01	1894	2360.3	2357.2
0.5	467.66	1890.4	2358.1	2354
0.6	465.42	1884.3	2354.6	2348.9

Table 5.9 - RCNF for a plate shown in Figure 5.15 using ABAQUS.

d/*h*	Mode (1,1)	Mode (2,2)	Mode (3,1)	Mode (1,3)
0	0	0	0	0
0.1	0.000637	0.000421	0.000254	0.000296
0.2	0.001528	0.001053	0.000592	0.00072
0.3	0.00278	0.001842	0.001057	0.001312
0.4	0.004648	0.003105	0.001734	0.002243
0.5	0.007513	0.005	0.002665	0.003598
0.6	0.012267	0.008211	0.004145	0.005757

The analytical solution and ABAQUS results do not match for modes (1,2) and (2,1) when a crack is present. This discrepancy arises because the location of the crack forces introduces an alternative mode shape, altering the RCNF and making a direct comparison invalid. As a result, these modes are excluded from the comparative analysis. This phenomenon is further illustrated in Figure 5.16, which shows how the presence of the crack influences the mode shapes, highlighting the limitations of both methods in capturing consistent results for these specific cases. This explanation is provided after introducing the tables for the energy method and ABAQUS results, as it directly addresses the challenges associated with these modes.

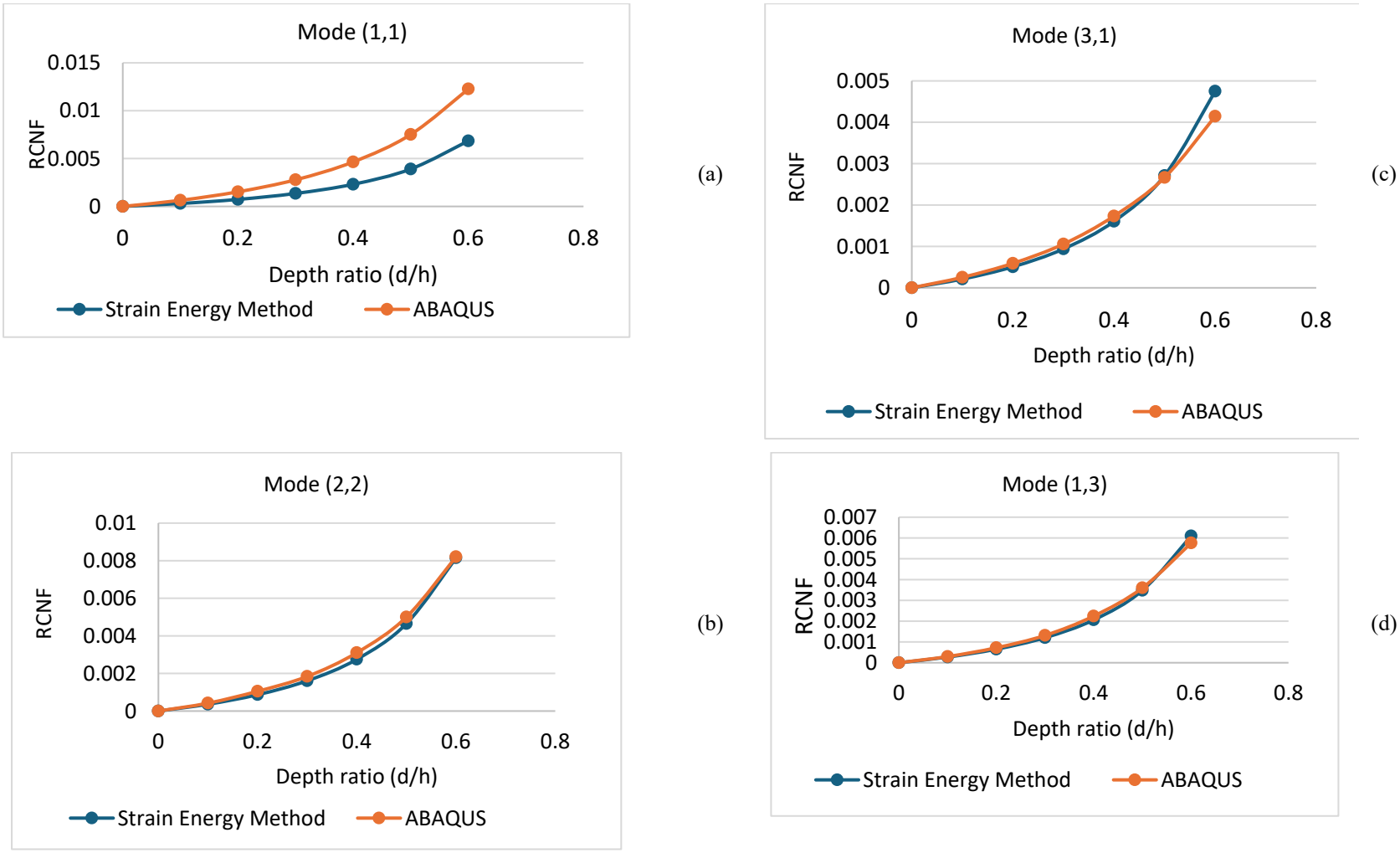

Figure 5.16 - Comparison of RCNF for a cracked plate shown in Figure 5.15 with Finite Element Model generated by ABAQUS (a) Mode (1,1); (b) Mode (2,2);(c) Mode (3,1);(d) Mode (1,3).

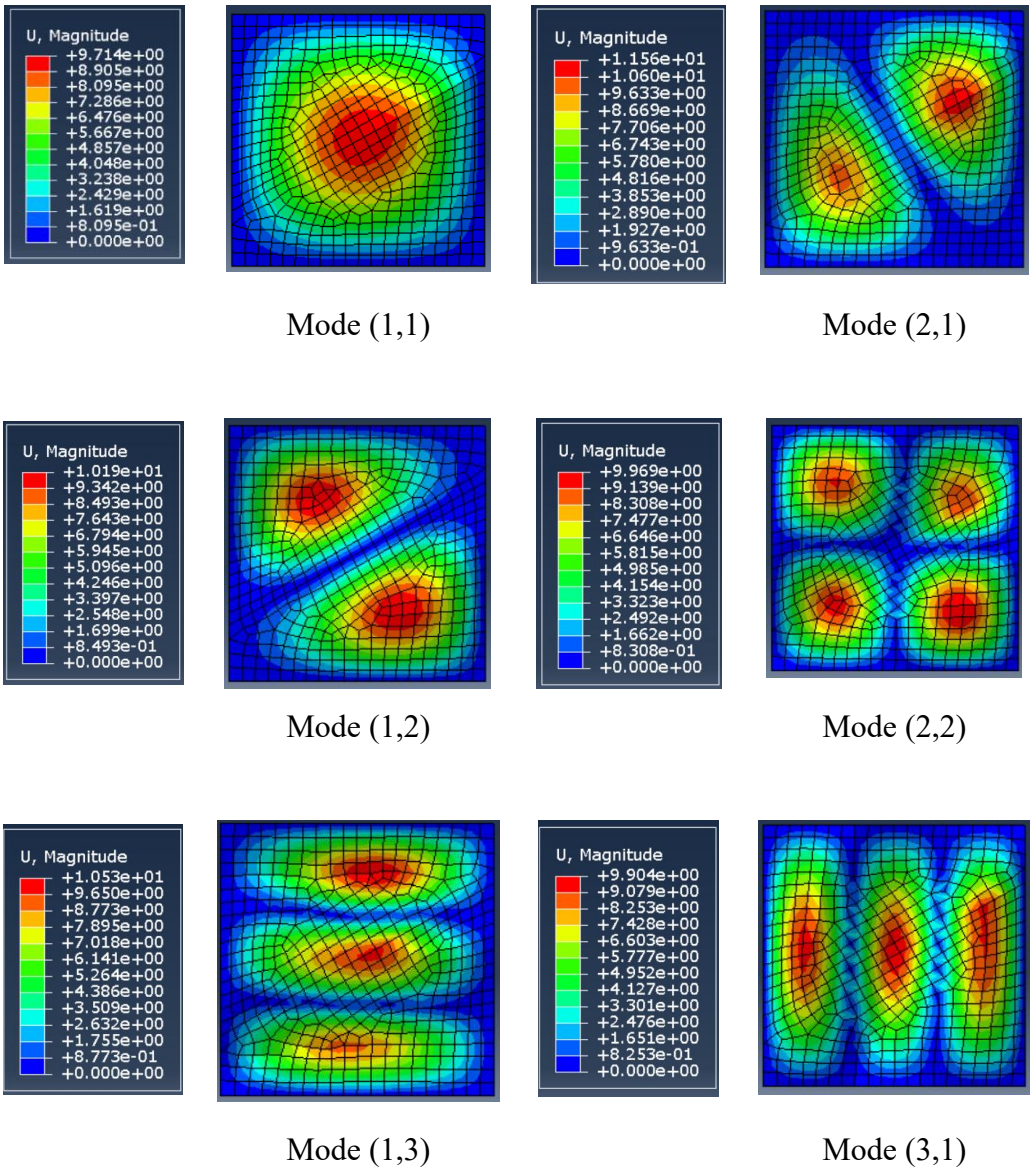

Figure 5.17 – Mode shapes of square cracked plate shown in Figure 5.14 using ABAQUS.

Figure 5.17 represents the first six mode shapes for a square cracked plate obtained from ABAQUS. Due to discrepancies observed in modes (1,2) and (2,1) when a crack is present beyond a crack depth ratio of 0.2, these modes have been excluded from the comparative studies with the strain energy approach. The effect of the crack on the mode shapes for a range of vibration modes are shown including for the mode shapes for the second and third natural frequencies which do not correspond to any combination of m and n in the shape function used to represent the plate displacement in the analytical solution.

It is noted that in Figure 5.17, the displacement appears different on either side of the crack. This variation is not physical, but rather a result of shading and nodal averaging effects during post-processing. The actual displacement field remains consistent with the expected behaviour across the crack.

To provide a further example for validation of the analytical solution for which the modes corresponding to the full range of values of *m* and *n*, a rectangular plate has been considered in the next section.

5.3.2.3.2 Numerical Example: Rectangular Plate

A rectangular plate is considered in this section with the same material properties used in Section 5.3.2.3.1. The plate has a length a of 0.12 m, a width b of 0.1 m, and a thickness h of 0.001 m. The crack is represented by the red line with initial coordinates (x_1, y_1) of (0.03088, 0.02995) and final coordinates (x_2, y_2) of (0.03699, 0.06985), shown in Figure 5.18.

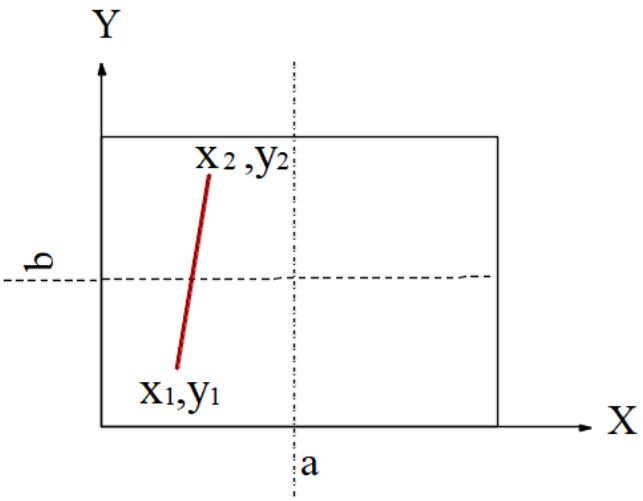

Figure 5.18 - Rectangular isotropic simply supported cracked plate.

Table 5.10 shows the natural frequencies of the plate, with the frequencies varying depending on the depth of the crack. Additionally, Table 5.11 presents the relative change in the natural frequencies compared to the intact (uncracked) plate. The data shown in both Table 5.10 and Table 5.11 was obtained using the strain energy approach.

Table 5.10 - Natural frequencies of a cracked plate shown in Figure 5.18 using strain energy approach.

d/*h*	Mode (1,1)	Mode (2,1)	Mode (1,2)	Mode (2,2)	Mode (3,1)	Mode (1,3)
0	399.11	889.82	1105.73	1596.44	1707.67	2283.43
0.1	398.98	888.98	1105.65	1596.08	1707.20	2283.29
0.2	398.80	887.81	1105.54	1595.59	1706.55	2283.10
0.3	398.54	886.097	1105.38	1594.86	1705.59	2282.82
0.4	398.14	883.45	1105.14	1593.75	1704.12	2282.38
0.5	397.47	879.045	1104.73	1591.90	1701.68	2281.67
0.6	396.24	870.87	1103.98	1588.48	1697.18	2280.34

Table 5.11 - RCNF for a plate shown in Figure 5.18 using strain energy approach.

d/*h*	Mode (1,1)	Mode (2,1)	Mode (1,2)	Mode (2,2)	Mode (3,1)	Mode (1,3)
0	0	0	0	0	0	0
0.1	0.00032	0.000941	0.0000707	0.000222	0.000273	0.0000605
0.2	0.000768	0.002259	0.000169	0.000533	0.000656	0.000145
0.3	0.001422	0.004184	0.000314	0.000986	0.001214	0.000268
0.4	0.002429	0.007158	0.000536	0.001685	0.002074	0.000458
0.5	0.004103	0.012109	0.000904	0.002845	0.003503	0.000774
0.6	0.007191	0.021289	0.001583	0.004984	0.006138	0.001354

A similar crack has been modelled using ABAQUS. Table 5.12 presents the natural frequencies obtained using ABAQUS. Additionally, Table 5.13 presents the relative change in the natural frequencies with respect to intact plate. Figure 5.19 shows validation between strain energy approach and results obtained using ABAQUS.

Table 5.12 - Natural frequencies of a cracked plate shown in Figure 5.18 using ABAQUS.

d/*h*	Mode (1,1)	Mode (2,1)	Mode (1,2)	Mode (2,2)	Mode (3,1)	Mode (1,3)
0	399.14	893.23	1114.7	1604.5	1730.9	2335.9
0.1	399	892.3	1114.6	1604	1730.4	2335.8
0.2	398.8	891.03	1114.5	1603.4	1729.8	2335.6
0.3	398.52	889.22	1114.3	1602.6	1729	2335.3
0.4	398.09	886.57	1114	1601.5	1727.7	2334.9
0.5	397.43	882.45	1113.6	1599.7	1725.7	2334.3
0.6	396.32	875.72	1113	1597	1722.6	2333.3

Table 5.13 - RCNF for a plate shown in Figure 5.18 using ABAQUS.

d/*h*	Mode (1,1)	Mode (2,1)	Mode (1,2)	Mode (2,2)	Mode (3,1)	Mode (1,3)
0	0	0	0	0	0	0
0.1	0.000351	0.001041	0.0000897	0.000312	0.000289	0.0000428
0.2	0.000852	0.002463	0.000179	0.000686	0.000636	0.000128
0.3	0.001553	0.004489	0.000359	0.001184	0.001098	0.000257
0.4	0.002631	0.007456	0.000628	0.00187	0.001849	0.000428
0.5	0.004284	0.012069	0.000987	0.002992	0.003004	0.000685
0.6	0.007065	0.019603	0.001525	0.004674	0.004795	0.001113

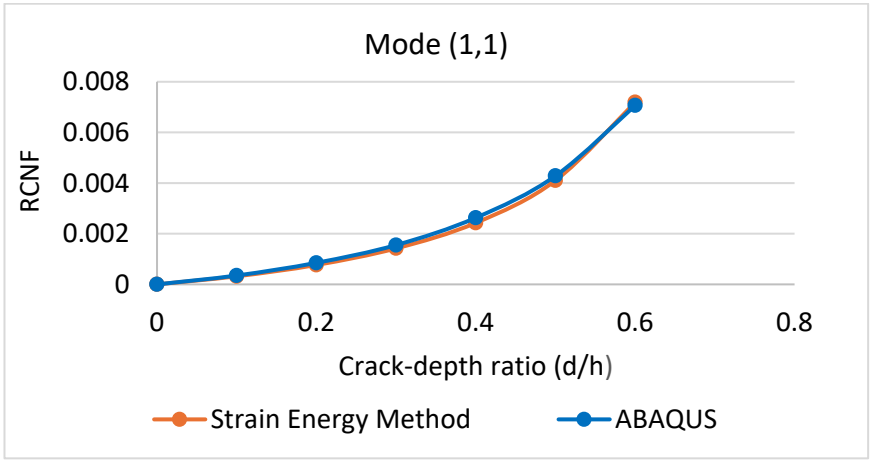
Mode (1,1)
RCNF
0.008
0.006
0.004
0.002
0
0
0.2
0.4
0.6
0.8
Crack-depth ratio (d/h)
Strain Energy Method
ABAQUS

(a)

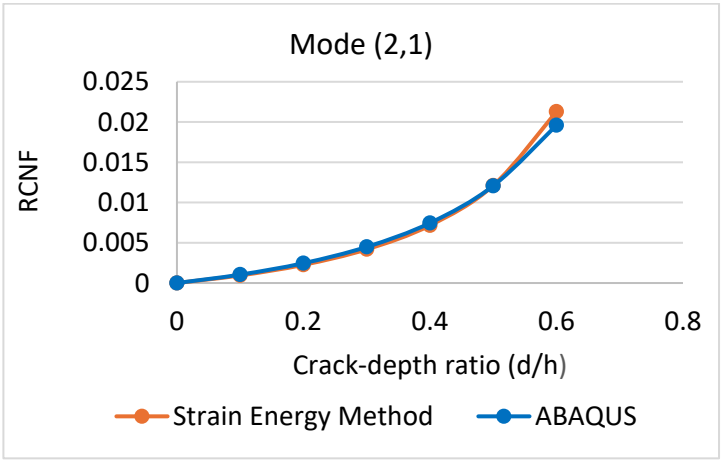
Mode (2,1)
RCNF
0.025
0.02
0.015
0.01
0.005
0
0
0.2
0.4
0.6
0.8
Crack-depth ratio (d/h)
Strain Energy Method
ABAQUS

(c)

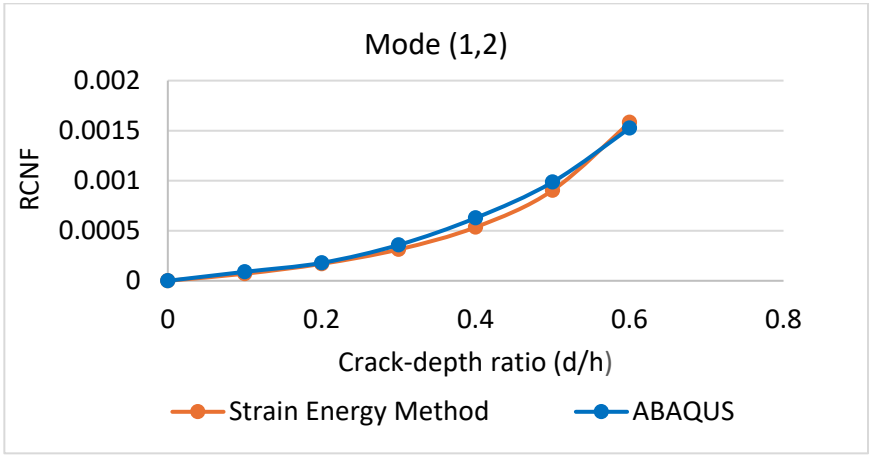
Mode (1,2)
RCNF
0.002
0.0015
0.001
0.0005
0
0
0.2
0.4
0.6
0.8
Crack-depth ratio (d/h)
Strain Energy Method
ABAQUS

(b)

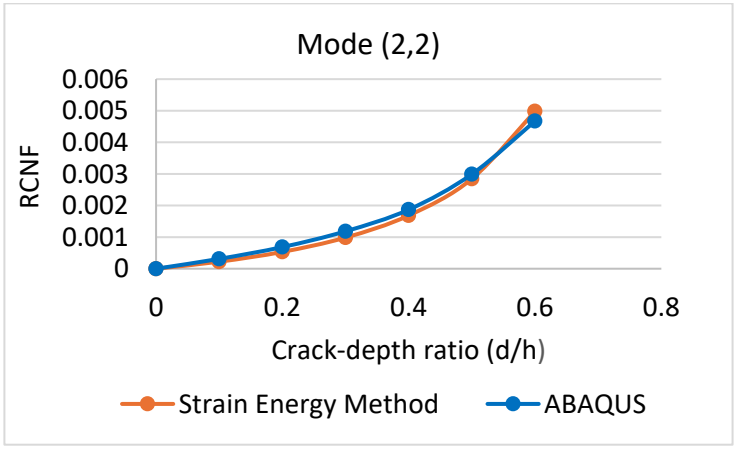
Mode (2,2)
RCNF
0.006
0.005
0.004
0.003
0.002
0.001
0
0
0.2
0.4
0.6
0.8
Crack-depth ratio (d/h)
Strain Energy Method
ABAQUS

(d)

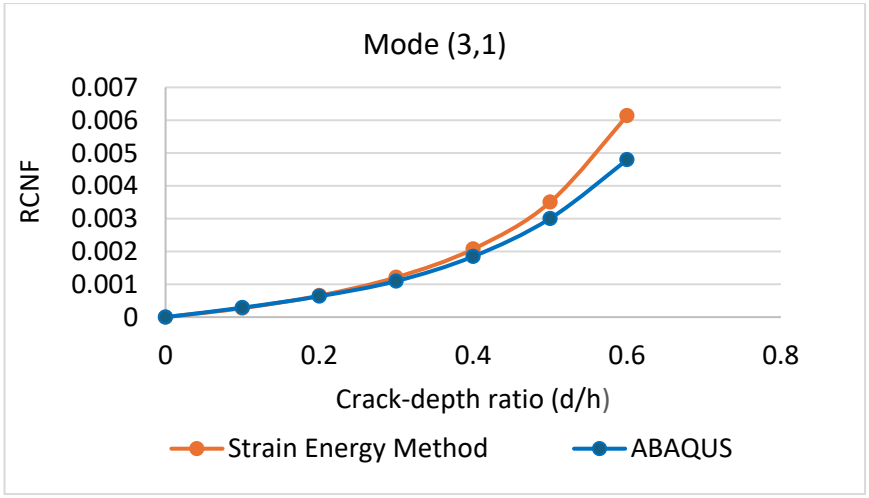

(e)

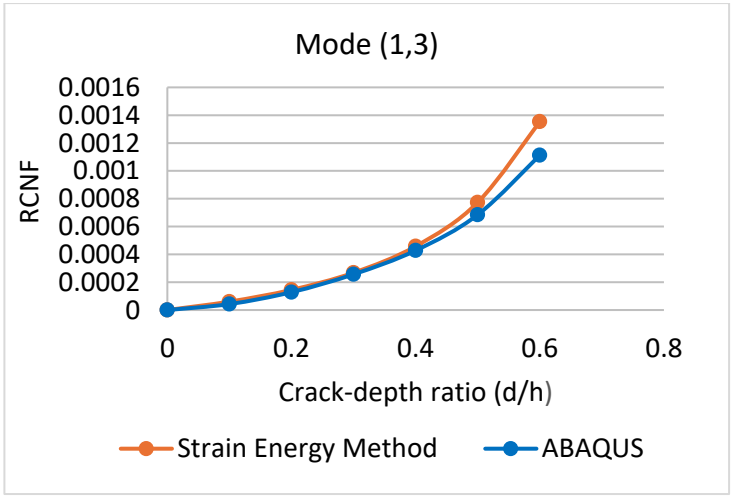

(f)

Figure 5.19 – Comparison of RCNF for a cracked plate shown in Figure 5.18 with Finite Element Model generated by ABAQUS (a) Mode (1,1); (b) Mode (2,1);(c) (1,2);(d) Mode (2,2);(e)Mode (3,1).(f) Mode (1,3).

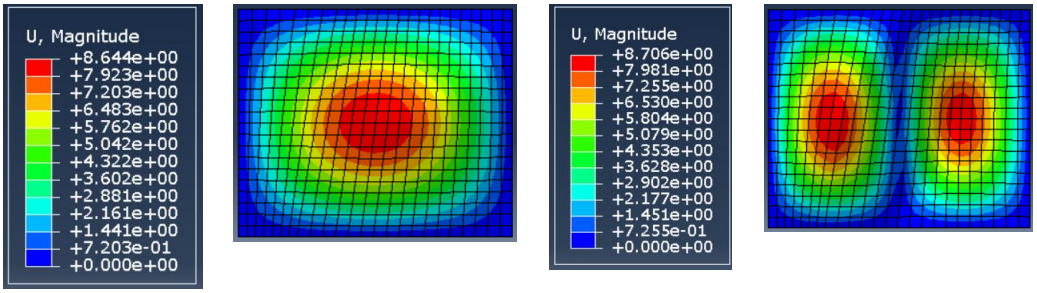

Mode (1,1) Mode (2,1)

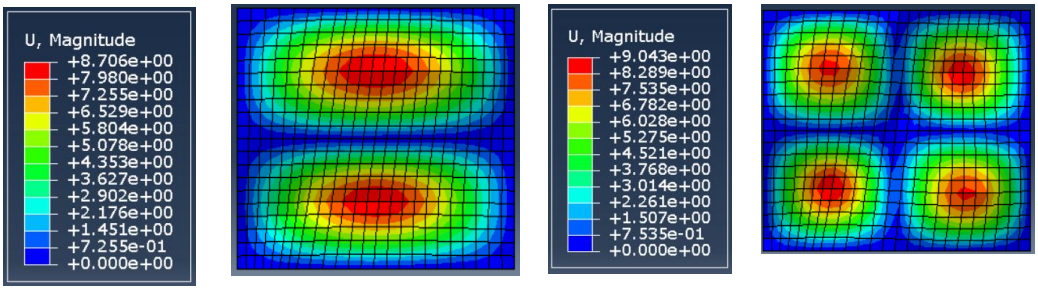

Mode (1,2) Mode (2,2)

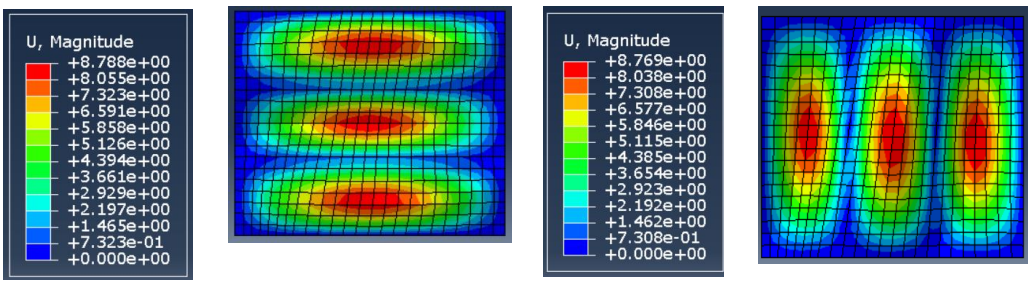

Mode (1,3) Mode (3,1)

Figure 5.20 – Mode shapes of rectangular cracked plate shown in Figure 5.18, using ABAQUS.

Figure 5.20 shows the first six mode shapes for the plate, using ABAQUS. The mode shapes remain close to the uncracked plate. In contrast to those for the rectangular square plate presented in Figure 5.17.

5.3.2.4 Discussion

Comparing the analytical and ABAQUS results for the square plates, it is observed that even for an intact plate, the natural frequencies do not match precisely, likely due to meshing inaccuracies. For the cracked plate the correlation is good with 2.32% error, up to a crack depth of 0.6 after which the difference between the analytical solution and the ABAQUS results gradually increases. This is due to the fact that we assume no change in mode shape due to the crack in the analytical solution whereas the crack clearly does have an effect (as seen in Figure 5.16 and Figure 5.19) which becomes more significant as it becomes deeper. This was also found by previous authors [20]. More significantly, the crack causes a complete change in modes 1,2 and 2,1 which realign such that the nodal line runs along the crack. However, for a crack less than 0.5 of the thickness the remainder of the modes correlate well with the ABAQUS model.

In the case of rectangular plates, the nodal lines do not shift to correspond to the direction of the crack. This may be attributed to the removal of any symmetry between the geometry and the orientation of the crack. These findings highlight a potential limitation of the energy method which is not able to model modes not corresponding to integers of m and n.

5.3.3 Parametric Studies.

To utilize the significant efficiency of the developed analytical expression, parametric studies are carried out to explore the effect of different crack parameters on the natural frequencies.

The degradation of the natural frequencies for an isotropic simply supported square plate with crack at centre of the plate with an orientation varying from 0^0 to 180^0 will now be explored.

A square plate with the same material properties used in Section 5.3.2 is considered in this Section. From Figure 5.21 it can be seen that, the starting point of the crack is considered to be the centre of the plate, and the effects of the crack with discrete clockwise orientations for this crack will now be obtained. The length of the crack is 0.0283 m and the crack-depth ratio 0.2.

Table 5.14 - Degradation of the natural frequencies $\delta_{m,n}(Hz^2)$ vs orientation (φ).

φ	0^0	10^0	20^0	30^0	40^0	45^0
$\delta_{(1,1)}$	514.2114	506.9277	488.983	469.450	457.201	455.552
$\delta_{(1,2)}$	0	255.0035	846.731	1411.9	1690.988	1709.304
$\delta_{(2,1)}$	1057.508	1108.76	1256.887	1471.001	1664.935	1709.3048
$\delta_{(2,2)}$	0	301.3337	1015.200	1744.93	2176.477	2233.012

φ	50^0	60^0	70^0	80^0	90^0
$\delta_{(1,1)}$	457.2013	469.4502	488.983	506.927	514.211
$\delta_{(1,2)}$	1664.936	1471.001	1256.884	1108.760	1057.507
$\delta_{(2,1)}$	1690.989	1411.9	846.731	255.003	0
$\delta_{(2,2)}$	2176.478	1744.93	1015.200	301.33	0

φ	100^0	110^0	120^0	130^0	135^0	140^0
$\delta_{(1,1)}$	506.927	488.98	469.450	457.201	455.552	457.201
$\delta_{(1,2)}$	1108.76	1256.88	1471.001	1664.93	1709.305	1690.98
$\delta_{(2,1)}$	255.0035	846.731	1411.9	1690.989	1709.305	1664.93
$\delta_{(2,2)}$	301.333	1015.201	1744.93	2176.478	2233.012	2176.47

φ	150^0	160^0	170^0	180^0
$\delta_{(1,1)}$	469.4502	488.98	506.9277	514.2114
$\delta_{(1,2)}$	1411.9	846.731	255.0035	0
$\delta_{(2,1)}$	1471.001	1256.88	1108.76	1057.508
$\delta_{(2,2)}$	1744.93	1015.201	301.3337	0

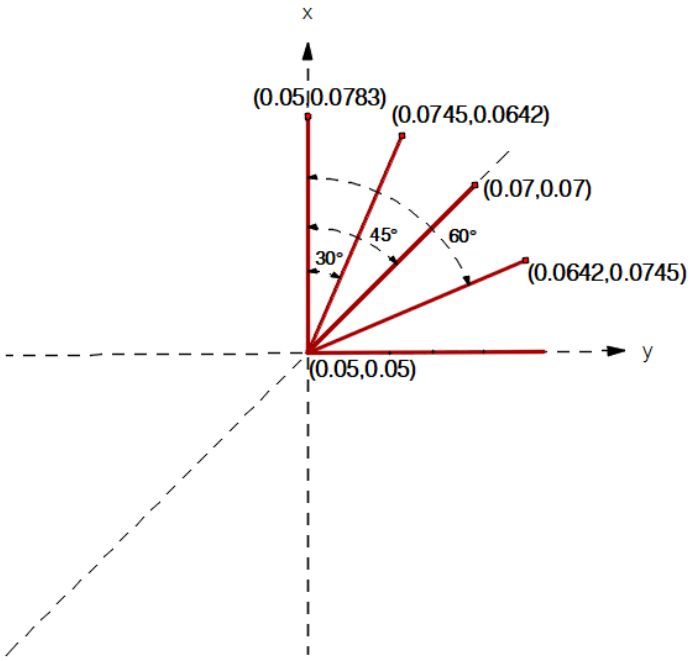

Figure 5.21 - Crack orientations.

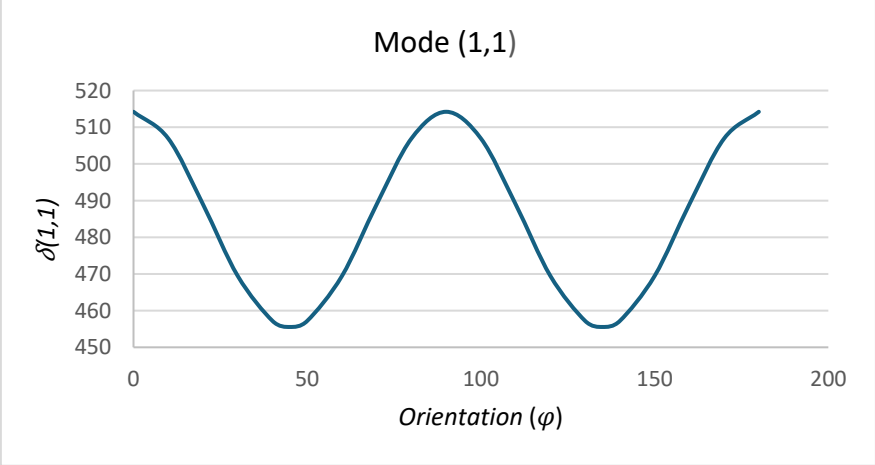

(a)

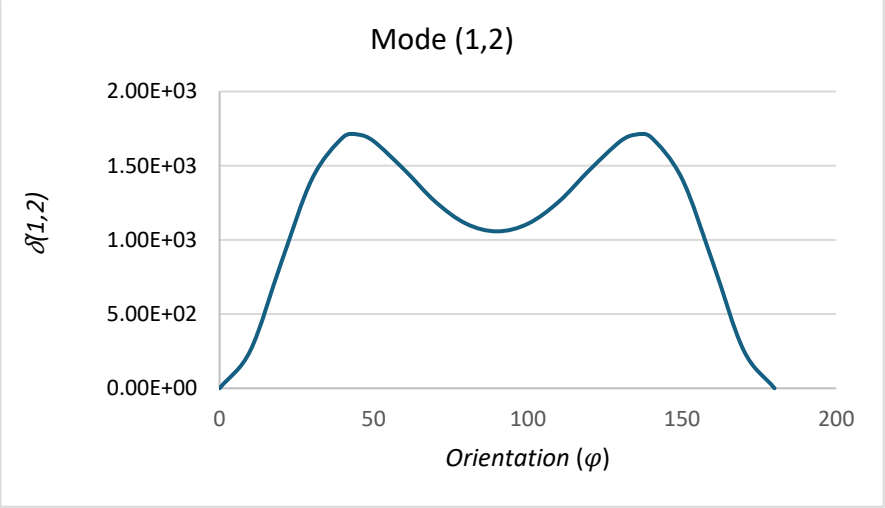
Mode (1,2)
2.00E+03
1.50E+03
1.00E+03
5.00E+02
0.00E+00
δ(1,2)
0
50
100
150
200
Orientation (φ)

(b)

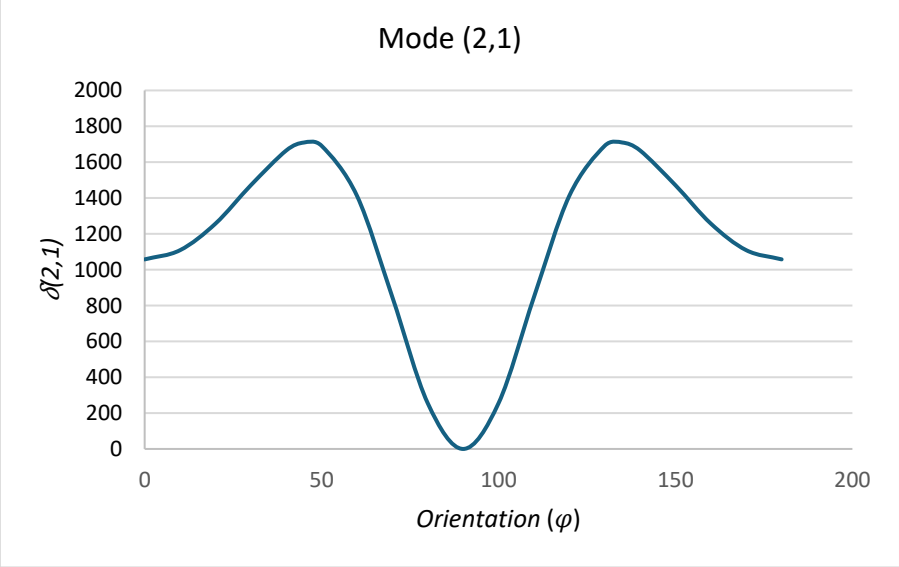
Mode (2,1)
2000
1800
1600
1400
1200
1000
800
600
400
200
0
δ(2,1)
0
50
100
150
200
Orientation (φ)

(c)

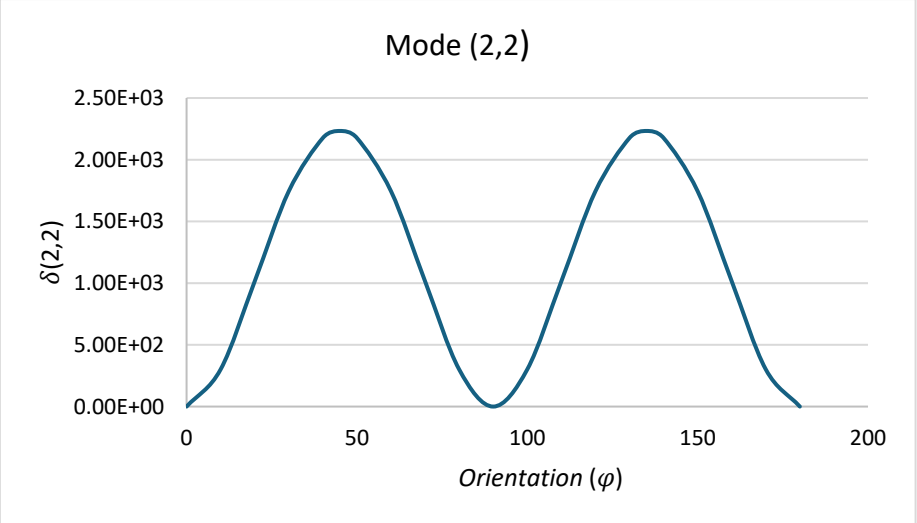

(d)

Figure 5.22 – Degradation in the square of the natural frequencies ($\delta_{m,n}$) vs orientation (φ). (a)Mode (1,1) ;(b) Mode (2,1); (c) Mode (1,2); (d) Mode (2,2).

Table 5.14 and Figure 5.22 presents the variation of the degradation in the square of the natural frequencies between intact and damaged plates with respect to the orientation with angle. Cracks located at symmetric locations as would be expected have the same level degradation in the natural frequencies. For example, cracks with orientations 0°, 10°, 20°, 30°, and 40° have the same amount of degradation in the natural frequencies as cracks with orientations 90°, 80°, 70°, 60°, and 50° contribute, respectively.

5.3.4 Conclusion

The numerical examples provided in this study demonstrate a strong agreement with results from prior research. For cracks aligned in arbitrary orientations, where comparable research is scarce, a model has been developed using the finite element software ABAQUS which shows good agreement with the analytical results further validating the proposed methodology.

Overall, the analytical solution for degradation in natural frequencies serves as a foundational approach for damage quantification in isotropic plate structures. This framework is further employed in the following Chapter as the basis for a damage identification technique. Here the benefits of the significantly increased computational efficiency are particularly apparent since the problem requires a large number of calculations to be completed to converge on a solution.

For example, while the ABAQUS model can take several hours to simulate a single case, the analytical solution produces results within seconds. Moreover, the analytical method eliminates the need to create a new model for each individual case. Instead, users can simply input the plate dimensions and crack location, making the process faster and more practical. This computational efficiency is especially important for handling complex problems or large datasets.

6 Chapter 6: Crack Identification in Plate Structures.

6.1 Introduction

In the past, different methodologies have been adapted for damage detection in plate structures. Different damage detection methods can be classified as model-based approaches or as response-based approaches. Along with that, consideration of different domains can further differentiate the use of vibration analysis in damage identification procedures.

In Section 2.5, the importance of identifying damage in plate structures was discussed. For isotropic beams, locating damage is more straightforward because it is a one-dimensional problem. Damage localization in beam structures can be achieved using a single parameter (i.e. location of crack). However, for plate structures, the challenge becomes two-dimensional when it comes to crack localization. To identify a crack in an isotropic plate, four coordinates: two for the start point and two for the endpoint of the crack or the two start point coordinates, the angle and the length are needed. The depth of the crack can be considered as a fifth parameter to measure the severity of the damage caused by the crack.

In this chapter, the identification of the crack parameters of an isotropic simply supported square plate has been demonstrated using a gradient-based optimization procedure. A similar demonstration has been provided for obtaining the 2 parameters for a beam structure in Section 4.5. In this chapter, the problem has been set up to obtain the 5 crack parameters using the sum of least squares technique.

6.2 Methodology

Eq. (5.3.33) of chapter 5, can be used to model a crack in any arbitrary direction, including cracks parallel to the edges of the plate. It was derived to model the changes in natural frequencies of plates due to cracks in any arbitrary direction, including cracks parallel to the edges of the plate. This equation can be employed to calculate the difference in the square of the natural frequencies between an intact and a cracked, simply supported, isotropic plate.

For simplicity Eq. (5.3.33) can be expressed in the form of Eq. (6.2.1)

$$\delta_{mn} = \frac{2U_d}{\rho h \int_0^a \int_0^b sin^2\left(\frac{m\pi x}{a}\right) sin^2\left(\frac{n\pi y}{b}\right) dy\, dx} \tag{6.2.1}$$

where U_d is the change in the strain energy due to the presence of the crack based on compliance (C_n), the initial location of the crack (x_1, y_1), and the final location (x_2, y_2) of the crack.

For an isotropic plate that is simply supported at all edges, the presence of a crack degrades the natural frequencies of the plates. The notation ${\delta^M}_{mn}$ can be used to represent the difference between the square of the natural frequencies of the intact and cracked plates. The superscript 'M' denotes the measured natural frequencies, while the subscripts *m* and *n* define the number of half-wavelengths along the *x* and *y* axes of the plate, respectively.

$$f(x, y, d) = min \sum_{m,n} \left\{ \frac{\delta_{mn} - {\delta^M}_{mn}}{{\delta^{MS}}_{mn}} \right\}^2 \rightarrow 0 \tag{6.2.2}$$

Section 5.3 highlights that cracks at different locations affect the degradation of natural frequencies in varying ways. For instance, cracks along the nodal lines do not cause any degradation in the natural frequencies. To address this, considering the first six or more modes of vibration can help achieve a unique solution.

In Eq. (6.2.2) , δ_{mn} represents the difference in the square of the natural frequencies between the intact and cracked plate for each set of trial crack parameters. This value is calculated using Eq. (6.2.1). A trial set consists of five parameters: the start (x_1, y_1) and end coordinates (x_2, y_2) of the crack (four parameters) and the crack depth ratio (d/h - 5th parameter). Multiple sets of trial values can be used. Based on these, an optimization problem is formulated using the least squares difference between δ_{mn} and the measured difference ${\delta^M}_{mn}$ from the real cracked plate structure. This approach helps to identify the crack parameters effectively. The formulated function presented in Eq. (6.2.2) can be minimised using optimization toolbox.

The data for the first six differences in the squares of the natural frequencies ($\delta^M{}_{mn}$) for cracks with a known set of parameters can be utilised to set up an optimization problem based on the error function in Eq. (6.2.2) .

To implement the optimization procedure,δ_{mn} can be defined in the form of function file in MATLAB. It can produce the data as per the sets of the crack parameters. To perform optimization. The set of $\delta^M{}_{mn}$ needs to be provided. To consider the noise free simulation, the set of $\delta^M{}_{mn}$ has been obtained using Eq. (5.3.33) for the known crack parameters ($x_1, y_1, x_2, y_2,$ and , d/h). The data can be referred as synthetic data.

For this kind of noiseless simulation, due to the higher numerator, the computational time is high. To reduce its computational time, a scaling factor has been added in the denominator ($\delta^{MS}{}_{mn}$). This factor can be obtained using Eq. (5.3.33) for any arbitrary crack in the plate. The purpose of the scaling factor is only to scale the numerator of Eq. (6.2.2).

To implement the optimization procedure, δ_{mn} is defined as a function file in MATLAB, allowing it to generate data based on various sets of crack parameters. To perform optimization, a set of $\delta^M{}_{mn}$ values is required. For noise-free simulation, these values are generated using Eq. (5.3.33) for known crack parameters ($x_1, y_1, x_2, y_2,$ and *d/h)*, referred to as synthetic data.

To address the high computational time caused by the large numerator in Eq. (6.2.2) a scaling factor, ($\delta^{MS}{}_{mn}$), is introduced in the denominator. This factor is calculated for known arbitrary crack parameters using Eq. (5.3.33). It ensures that no particular natural frequency dominates the optimization problem by scaling the numerator appropriately. Without affecting the overall procedure.

The optimization is carried out using the optimization toolbox, FMINCON in MATLAB which was explained in Section 4.5.2.

To perform the optimization process, constraints must be defined. In this case, the geometrical boundaries of the plate are used as constraints for the identification of the crack localization and severity. For a plate having a length *a* and width *b*, the search area for the crack location can be defined by constraining the parameters (x_1, y_1, x_2, y_2) between 0 and *a*, and 0 and *b*, respectively. In terms of the crack depth the crack-depth ratio (d/h) is theoretically constrained between 0 and 1, with 0 being the lower limit

and 1 being the upper limit. However, the model presented in Eq. (5.3.33) is not valid for cracks that extend fully through the depth of the plate, so an upper limit of 0. 9999 is used instead. These constraints ensure that the optimization process can accurately identify both the crack location and severity.

The optimisation is initialised using random values as trials for the crack parameter. For example, if the parameters of the cracks are, $x_1, y_1, x_2, y_2,$ and crack-depth ratio (d/h).The range for the random trial value for each parameter is given in Table 6.1.

Table 6.1 - Values of upper and lower limit for the Latin hypercube sample to produce trial values for optimization.

Parameters	x_1	y_1	x_2	y_2	d/h
Upper limit	a	b	a	b	0.9999
Lower limit	0	0	0	0	0

In the next two sections, numerical examples demonstrating the parameter quantification for a parallel crack and an arbitrary crack will be reported.

6.3 Numerical Example: Crack location and Characterization.

In the following examples, changes in the natural frequencies due to two different cracks in two distinct plates are calculated using Eq. (5.3.33) and subsequently used as test data to solve the inverse problem, i.e., to determine the crack parameters.

6.3.1 Crack Parallel to the Edges

Consider an isotropic simply supported isotropic square plate made of titanium as shown in Figure 6.1. The dimensions and the material properties are defined as: length $(a) = 0.1\text{m}$; width $(b) = 0.1\text{m}$; Young's modulus (E) = 110 x 10^9 Nm^{-2}; mass density $(\rho) = 4480\text{kgm}^{-3}$;

The crack parameters are: Start $(x_1 = 0.02, y_1 = 0.02)$; End point $(x_2 = 0.02, y_1 = 0.04)$; Crack-depth ratio (d/h) = 0.3.

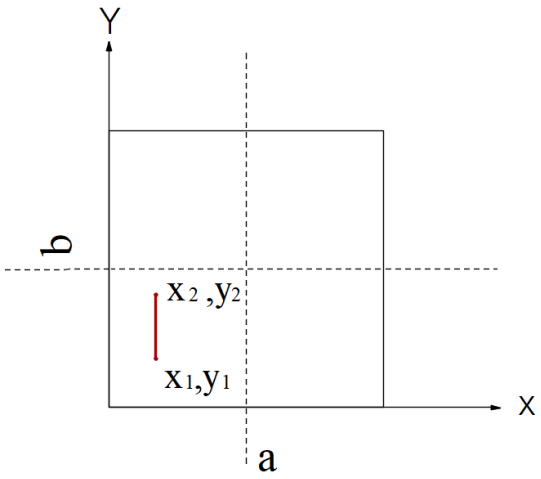

Figure 6.1 – Isotropic plate with a crack parallel to edge.

The differences between the squares of the natural frequencies of intact and cracked plate are the input along with the constraints for crack detection. For optimization purpose, this data were generated using Eq. (6.2.1) and is referred as a synthetic data in this chapter.

Table 6.2 - Obtained synthetic data for ($\overline{\delta}_{mn}$) the plate shown in the Figure 6.1, used for the optimization.

Modes $(\boldsymbol{m,n})$	(1,1)	(1,2)	(2,1)	(2,2)	(1,3)	(3,1)
$\overline{\boldsymbol{\delta}}_{\boldsymbol{mn}}(\boldsymbol{rad^2s^{-2}})$	7625.841	27315.42	218430.5	399525.4	28359.98	1021744

Synthetic data presented in Table 6.2 is employed in Eq. (6.2.1) to develop an error function using modes of vibration from $(m,n) = (1,1)$, (1,2)…..(3,1).

To provide the trial values for the crack parameters to initialise the optimization, Latin hypercube sampling is utilised to choose parameters between the upper and lower limits shown in Table 6.3

Table 6.3 - Range for the trial values of the crack parameters.

Parameters	$\boldsymbol{x_1}$	$\boldsymbol{y_1}$	$\boldsymbol{x_2}$	$\boldsymbol{y_2}$	$\boldsymbol{d/h}$
Upper limit	0.1	0.1	0.1	0.1	0.9999
Lower limit	0	0	0	0	0

After providing the ranges for the trial values followed by the search space and a tolerance of 10^{-6}, the crack parameters can be determined using the gradient-based optimization approach available in the FMINCON toolbox, which is part of the MATLAB software.

The decision to use ten independent chains was made to improve the robustness of the optimization process. Using multiple trial values helps reduce the impact of poor initial guesses, which often converge to local minima instead of the global minimum. This increases the likelihood of accurately identifying the crack parameters.

The error function may have several local minima, making it difficult to converge to the global minimum. When the initial guesses are close to the true parameters, the optimization is more likely to succeed. However, if the initial guesses are far from the solution, they may fail to converge to the correct values.

From Table 6.4 it can be observed that, set number 4,7 and 8 converged with much lower values of the error function $f(x, y, d)$ than set numbers 1,2,3,5,6,9, and 10.

Table 6.4 - Converged values of crack parameters and error function for 10 sets of trial values for the plate shown in Figure 6.1.

Set No.	x_1	y_1	x_2	y_2	d/h	$f(x, y, d)$
1	0.0798	0.0149	0.0798	0.0850	0.1185	0.577905
2	0.0201	0.0149	0.0201	0.0850	0.1185	0.577905
3	0.0798	0.0850	0.0798	0.0149	0.1185	0.577905
4	0.0799	0.06	0.08	0.08	0.2999	1.08×10^{-6}
5	0.0798	0.0149	0.0798	0.0850	0.1185	0.577905
6	0.020	0.01499	0.0201	0.085	0.1185	0.577905
7	0.08	0.02	0.08	0.04	0.3	5.95×10^{-6}
8	0.0199	0.04	0.02	0.02	0.3	8.45×10^{-6}
9	0.0201	0.0149	0.0201	0.085	0.1185	0.577905
10	0.0798	0.0850	0.0798	0.014	0.1185	0.577905

For crack localization, the first four converged crack parameters (x_1, x_2, y_1, y_2), for each of the sets are plotted in Figure 6.2.

Set number 8 converges at the exact crack location, where set numbers 4 and 7 converge at symmetric locations to the crack. However, set numbers 1,2,3,5,6,9, and 10 do not converge at either the exact location of the crack or any of the symmetric locations.

The thickness of the lines in Figure 6.2 is inversely proportional to the final error value. Consequently, the results which converge with lower error values are represented by higher thickness lines.

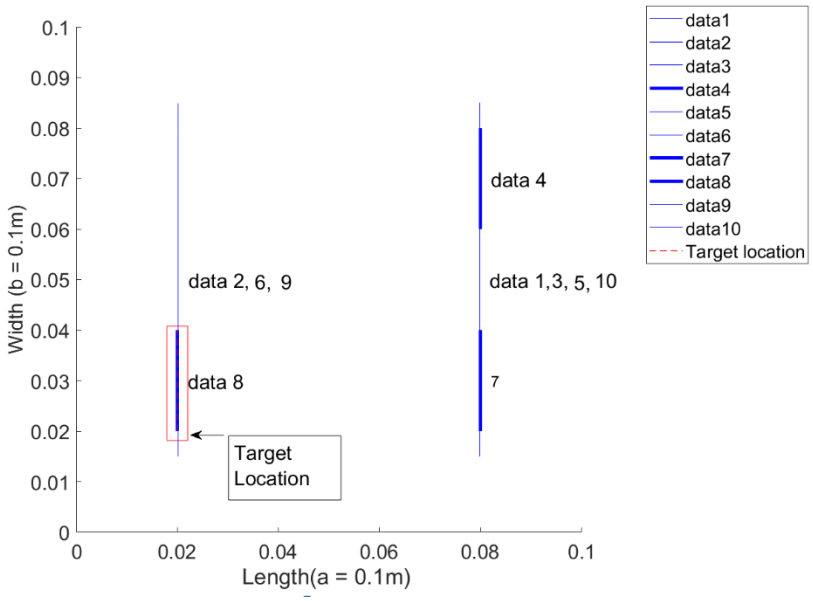

Figure 6.2 - Optimized crack location for 10 sets of trial values.

The convergence of the crack depth ratios derived from the optimization of each of the 10 sets of trial values is illustrated in Figure 6.3. The 'Target depth' represents the crack depth ratio for the modelled crack. In this graph, it is evident that several sets of trial values have converged according to the optimality criteria, specifically those that also converged based on location parameters (sets 4, 7 and 8). The data that align with the actual crack depth ratio (0.3) are highlighted with thick lines.

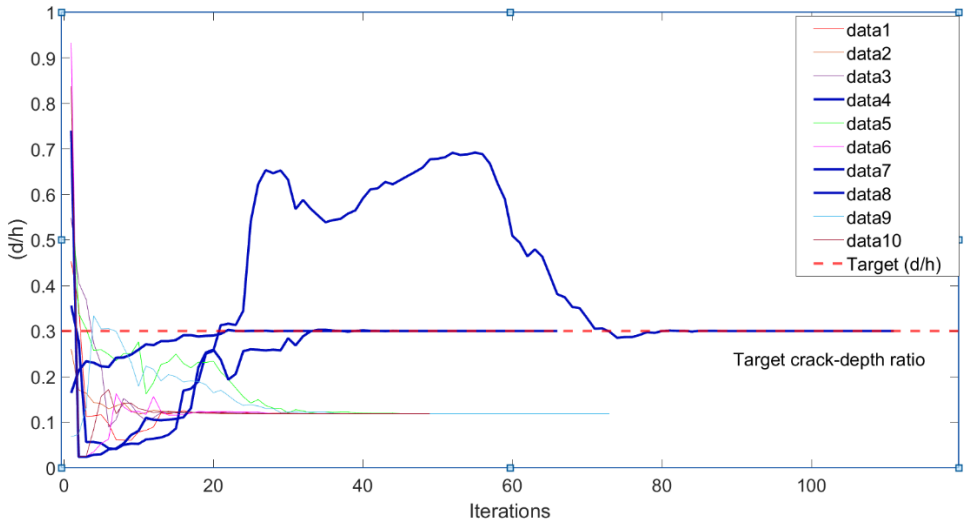

Figure 6.3 - Converge of crack depth-ratio crack depth vs iterations for 10 set of trial values for plate shown in Figure 6.1.

6.3.2 Crack in an Arbitrary Direction

In this section, a similar crack identification method is considered for an arbitrarily oriented crack as was used for the parallel crack. The same plate is used with the same material property. The parameters of crack shown in Figure 6.4 are: start point ($x_1 = 0.023, y_1 = 0.027$); end point ($x_2 = 0.043, y_1 = 0.04$); Crack-depth ratio (d/h) = 0.3.

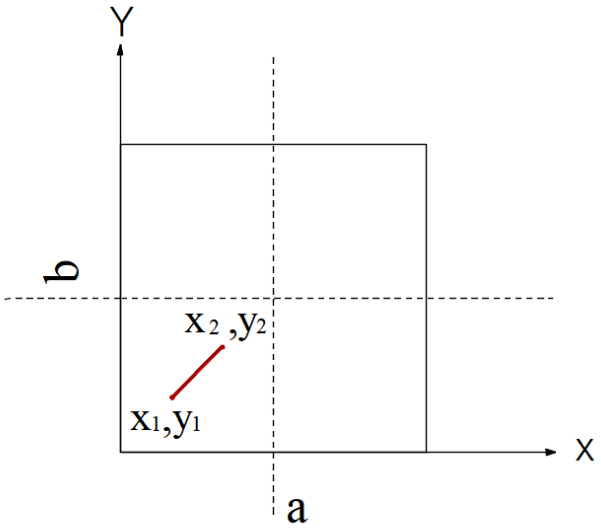

Figure 6.4 – Arbitrarily oriented crack in a square isotropic plate.

Table 6.5 - Obtained synthetic data for ($\overline{\delta}_{mn}$) the plate shown in Figure 6.4, and used in the optimization.

Modes (m, n)	(1,1)	(1,2)	(2,1)	(2,2)	(1,3)	(3,1)
$\overline{\delta}_{mn}(rad^2 s^{-2})$	22895.9	146094	189709	286910	303291	293621

Table (6.5) presents synthetic data obtained using Eq. (6.2.1) to develop an error function based on modes of vibration from $(m, n) = (1,1)$, (1,2)…..(3,1).

Table 6.6 summarizes the crack parameters after the optimization process was completed. Examination of both Figure 6.4 and Figure 6.5 reveals that crack parameter sets 1, 3,5 and 8 converged with lower error values compared to sets 2,4,6,7,9, and 10. Furthermore, set number 1 converged precisely at the actual crack location, while sets 3,5, and 8 converged at symmetric locations. This is due to the fact that symmetric cracks have a similar effect on the degradation of natural frequencies, depending on frequencies compared.

Table 6.6 : Converged values of crack parameters and error function for 10 set of trial values for the plate shown in Figure 6.4.

Set No.	x_1	y_1	x_2	y_2	d/h	$f(x, y, d)$
1	0.043	0.047	0.023	0.027	0.3	3.31×10^{-6}
2	0.0548	0.0025	0.0768	0.0459	0.225	3.53×10^{-1}
3	0.0229	0.073	0.043	0.053	0.30	8.55×10^{-6}
4	0.0734	0.0403	0.0742	0.0401	0.849	1.32×10^{-1}
5	0.0569	0.047	0.077	0.027	0.299	8.06×10^{-6}
6	0.0267	0.059	0.0255	0.059	0.8112	1.32×10^{-1}
7	0.0267	0.059	0.025	0.059	0.8112	3.53×10^{-1}
8	0.0769	0.073	0.057	0.053	0.2999	4.12×10^{-6}
9	0.0999	0.0742	0.0756	0.098	0.3589	6.16×10^{-1}
10	0.0231	0.0459	0.0451	0.0025	0.225	3.53×10^{-1}

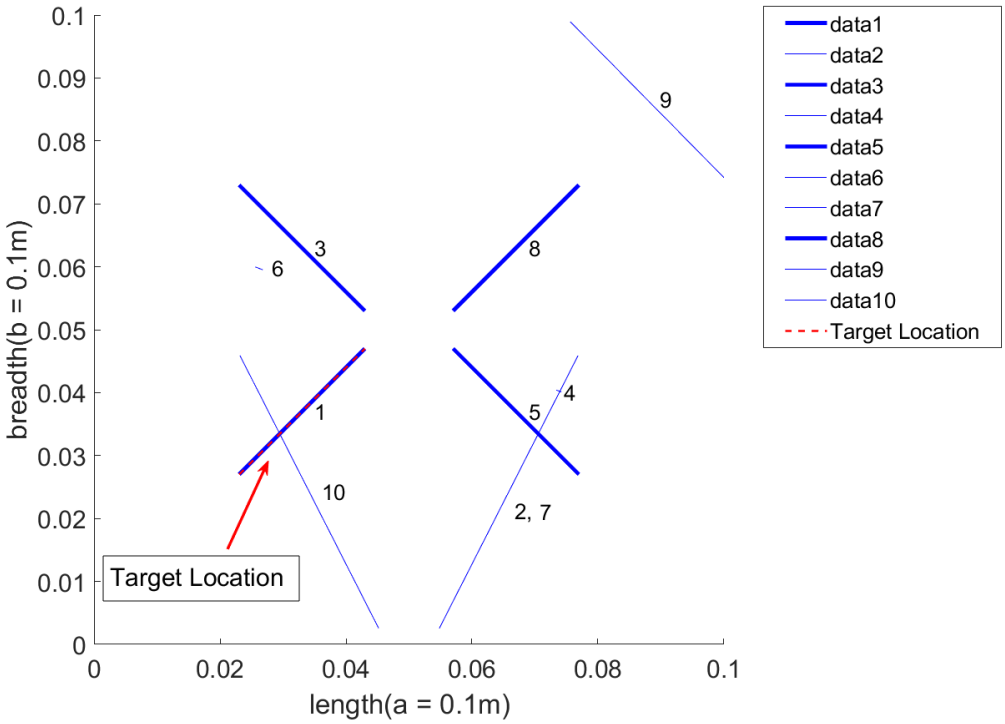

Figure 6.5 - Optimized location of crack for 10 sets of trial values for Figure 6.4.

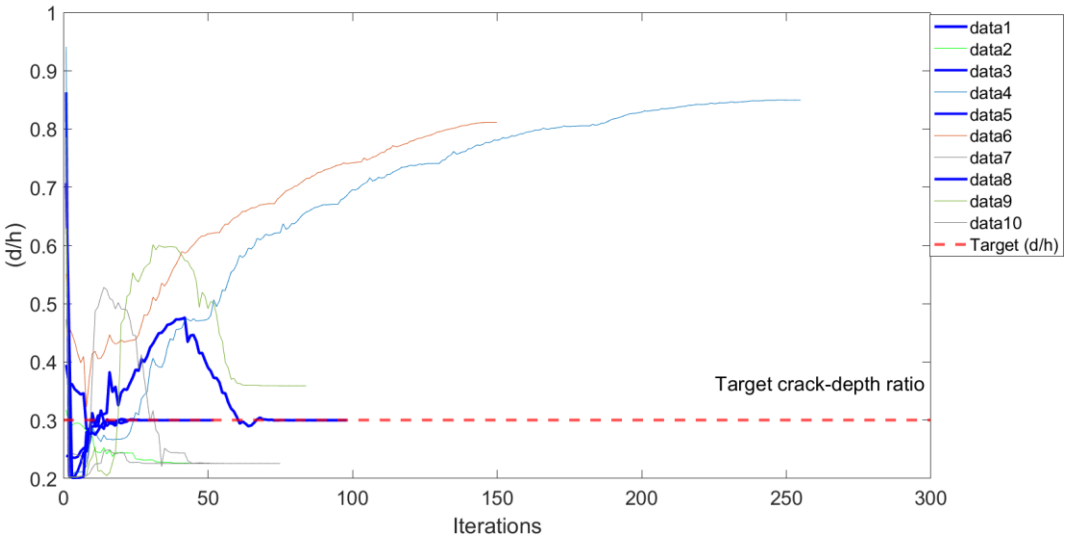

Figure 6.6 - Convergence of crack depth-ratio for 10 sets of trial values for the plate shown in Figure 6.4.

From Table 6.6 and Figure 6.5 it can be observed that, set numbers 4,7, and 8 converge with much lower values of the error function $f(x, y, d)$ than se numbers 1,2,3,5,6,9 and 10.

Figure 6.6 presents the convergence of the crack depth parameter. Crack parameter sets 1, 3, 5, and 8 converge at the target crack-depth ratio of 0.3. The same set numbers also converged at the target location and at the symmetric locations of the crack. On the other hand, set numbers 2, 4, 6, 7, 9, and 10 do not converge at the target depth or locations. The function files are attached in the Appendix (H).

6.4 Discussion

The numerical examples presented in the Section 6.3 demonstrate that crack location and characterisation can be achieved using the proposed analytical solutions, specifically Rayleigh's quotient, and gradient-based optimization procedures, implemented in MATLAB. Increasing the number of sets of trial values and adding more mode shapes could enhance the probability of converging to the expected crack parameters.

Furthermore, the data were obtained from the optimization process can be leveraged as a prior in a Bayesian approach to develop a robust crack identification algorithm.

The framework used for crack identification is the strain energy approach, which assumes that the mode shapes of cracked plate structures are the same as those of intact plates. A similar plate with a crack aligned parallel to the edges is shown in Figure 5.6. Therefore, the mode shapes of the plate structures illustrated in Figures 6.1 and 6.4 are similar to those shown in Figures 5.8 and 5.10.

6.5 Conclusion

In this chapter, a strain energy-based method combined with a gradient-based optimization process is used to find and describe cracks. An analytical solution was used to create a framework for modelling and detecting cracks, allowing the calculation of changes in natural frequencies. This method improved computational efficiency, with the simulation taking around 50–55 seconds. The efficiency is due to using an analytical solution; if a numerical method were used instead, the time could range from several minutes to hours, depending on the complexity of the problem.

This method holds promise for further improvement and expansion. It could be extended to address plates with different boundary conditions, as well as plate assemblies. Additionally, the incorporation of experimental noise should be considered as part of the future research scope. This would improve the reliability of the crack detection and quantification approach by enabling it to better handle real-world complexities and uncertainties.

The results yield three additional possible crack locations due to the geometric symmetry of the square plate and the symmetric boundary conditions, with all edges simply supported. The solution obtained through optimization can serve as a preliminary estimate of the crack location, thereby reducing the need for exhaustive inspection across the entire plate and narrowing the search area. However, in real-world scenarios, it is often impractical to have plates with simply supported conditions along all edges. When the structure features non-symmetric boundary conditions, the phenomenon of multiple equivalent solutions in crack localization is significantly reduced, enabling more accurate and unique identification of damage locations.

The ability to accurately model crack-induced changes in natural frequencies, and the implementation of optimization techniques to obtain crack characteristics, represents a valuable contribution to the field of structural health monitoring. Continued improvements of this approach, including the considerations mentioned, could lead to more reliable and practical tools for the non-destructive evaluation of cracked structures.

7 Chapter 7 - Conclusions and suggestion for future work.

7.1 Conclusions

Structural damage, such as cracks, can lead to catastrophic failure, resulting in significant economic losses and potential loss of life. Developing methods to detect cracks in structures is essential for assessing the severity of damage and predicting the remaining lifespan of the structure.

In beam structures, both through-width and partial-depth cracks have been modelled using rotational springs. Natural frequencies were determined using both analytical and numerical methods. The simplicity of the developed analytical solution based on the strain energy approach enhances computational efficiency. This analytical solution has also served as a framework for solving inverse problems in beams for crack localization and quantification. The inverse problem was addressed using vector calculus, interval arithmetic, and gradient-based optimization methods.

Building on the validated results from the beam studies, an analytical solution was developed to determine the degradation in natural frequencies due to cracks in plate structures. Partial-depth cracks were modelled using rotational springs, and both arbitrarily oriented cracks and those parallel to the plate edges were considered in the numerical studies. The results for edge-parallel cracks were validated against existing literature, while the results for arbitrarily oriented eccentric cracks were validated using a finite element model developed in ABAQUS. Furthermore, the developed solution was extended as a framework for inverse problems in plates using gradient-based optimization.

The proposed methods demonstrate high efficiency and offer a promising tool for damage detection, particularly in preliminary analyses. The outcomes of each part of the study are presented chapter-wise, as outlined below.

Chapter 3 demonstrated the application of the Newton-Raphson method to determine the eigenvalues of a cracked beam by solving the dynamic stiffness matrix. The results obtained were validated against previous research using the Wittrick-Williams algorithm. An alternative method based on the strain energy

approach was also explored. A comparative study of the cracked beam highlighted the accuracy of the Newton-Raphson method, particularly for deeper cracks, as it accounts for significant changes in the beam's mode shapes caused by presence of cracks. Conversely, for shallow cracks, the strain energy approach provides a reliable match with the Newton-Raphson method. Considering computational efficiency and potential applications in damage detection for beams, the strain energy approach was further emphasized.

In Chapter 4, simulations involving both noise-free and noise-contaminated data were examined for single-crack detection in isotropic beam structures. For noise-free simulations, vector analysis and gradient-based optimization were successfully employed. In the case of noise-contaminated simulations, interval arithmetic operations were utilized to estimate a range of crack locations. Additionally, gradient-based optimization, combined with an error function developed using the least squares method, proved efficient for crack characterization based on noiseless data. These findings serve as an effective reference for extending crack detection methods to isotropic plate structures.

Chapter 5 investigated the free vibration analysis of cracked isotropic plates using a strain energy approach. A novel method, developed as part of this research, leverages the strain energy approach to derive analytical solutions that demonstrate the degradation in the natural frequencies of a plate due to the presence of cracks. Results were validated against finite element analysis methods documented in previous literature. For scenarios lacking comparative studies, a cracked plate model was developed in ABAQUS. The developed method exhibited an exceptionally accurate match with finite element analysis results for crack depth ratios up to 0.4. However, a key limitation of this approach is the assumption that the mode shapes of cracked plates are identical to those of intact plates. Despite this limitation, the proposed method offers a significant advancement and provides a robust framework for developing crack detection techniques.

Chapter 6 focused on the use of the least squares method to formulate an error function for crack parameter estimation. Gradient-based optimization techniques

were employed to minimize the error function and optimize crack parameters using the MATLAB optimization toolbox FMINCON.

7.2 Future Scope

Several areas in the work presented offer opportunities for further development and refinement of the proposed techniques. Building upon the methods introduced in this thesis, future research can explore advanced approaches to enhance the accuracy, efficiency, and applicability of crack detection methodologies in structural analysis

The methodologies presented in Chapter 5 for calculating shifts in the natural frequencies of plates using analytical solutions can be extended to composite and functionally graded plates under various boundary conditions. Incorporating the effects of damping and the changes in mode shapes caused by the presence of cracks could further enhance the accuracy of the developed approach. In future work, this method can be applied to structures composed of plate assemblies, enabling broader application to more complex and practical structural configurations.

The results of the direct problem, presented in Chapters 3 and 5 and obtained using the strain energy approach for beam and plate structures, need to be validated through experimental analysis in future work. The discrepancies between the experimental data and the developed analytical solution may serve as a basis for formulating a more robust inverse problem solution that incorporates varying levels of noise.

In this thesis, a crack quantification method proposed for plate structures using gradient-based optimization and an error function developed by integrating the analytical solution with synthetic data representing shifts in natural frequencies for known crack parameters in Chapter 6 showed promising results. However, incorporating noise due to environmental conditions, sensor inaccuracies, or

human errors into the analytical solution remains a critical area for improvement. To address these practical challenges, experimental data will be required.

On other hand, for a more comprehensive approach, Gaussian noise could be introduced into the error function. This modification would make the method more robust and suitable for real-world scenarios, facilitating experimental validation in future studies. Additionally, the current method focuses on single crack detection. Future work could explore its applicability to multiple cracks or interacting defects in both beam and plate structures.

Appendices

Appendix (A): Algebraic operations (Chapter 5)

The integrals from Eq. (5.3.32) are provided in this section.

$$\int_0^l sin^2\,\alpha_x sin^2\alpha_y\,ds = \frac{1}{4}\int_0^l (1-cos2\alpha_x)\big(1-cos2\alpha_y\big)\,ds \tag{A1}$$

Further simplification can be provided in Eq. A2

$$= \frac{1}{4}\int_0^l \Big[1-\cos2\alpha_x-\cos2\alpha_y + \frac{1}{2}\Big(\cos\big(2\alpha_x-2\alpha_y\big)+\cos\big(2\alpha_x+2\alpha_y\big)\Big)\Big]\,ds$$

$$= \frac{1}{4}\Bigg[s-\frac{\sin2\alpha_x}{2\beta_x}-\frac{\sin2\alpha_y}{2\beta_y} + \frac{1}{2}\Bigg(\frac{\sin\big(2\alpha_x-2\alpha_y\big)}{2\big(\beta_x-\beta_y\big)}+\frac{\sin\big(2\alpha_x+2\alpha_y\big)}{2\big(\beta_x+\beta_y\big)}\Bigg)\Bigg]_0^l$$

$$= \frac{l}{4}-\frac{\sin\left(\frac{2m\pi x_2}{a}\right)-\sin\left(\frac{2m\pi x_1}{a}\right)}{8\beta_x}-\frac{\sin\left(\frac{2n\pi y_2}{b}\right)-\sin\left(\frac{2n\pi y_1}{b}\right)}{8\beta_y} + \frac{\sin\left(\frac{2m\pi x_2}{a}-\frac{2n\pi y_2}{b}\right)-\sin\left(\frac{2m\pi x_1}{a}-\frac{2n\pi y_1}{b}\right)}{16\big(\beta_x-\beta_y\big)} + \frac{\sin\left(\frac{2m\pi x_2}{a}+\frac{2n\pi y_2}{b}\right)-\sin\left(\frac{2m\pi x_1}{a}+\frac{2n\pi y_1}{b}\right)}{16\big(\beta_x+\beta_y\big)} \tag{A2}$$

Here,

$$\beta_x = \frac{d\alpha_x}{ds} = \frac{m\pi}{a}cos\varphi\ , \quad \beta_y = \frac{d\alpha_y}{ds} = \frac{n\pi}{b}sin\varphi \tag{A3}$$

$$x_0 = \frac{x_1+x_2}{2}\ , \quad y_0 = \frac{y_1+y_2}{2} \tag{A4}$$

$$l_x = x_2-x_1 = l\,cos\varphi,\ l_y = y_2-y_1 = l\,sin\varphi \tag{A5}$$

After modification, Eq. (A2) Can be expressed in the form of Eq. (A6)

$$\int_0^l sin^2\,\alpha_x sin^2\alpha_y\,ds$$
$$= \frac{l}{4} - \frac{cos\left(\frac{2m\pi x_0}{a}\right) sin\left(\frac{m\pi l\,cos\varphi}{a}\right)}{4\beta_x}$$
$$- \frac{cos\left(\frac{2n\pi y_0}{b}\right) sin\left(\frac{n\pi l\,sin\varphi}{b}\right)}{4\beta_y}$$
$$+ \frac{cos\left(\frac{2m\pi x_0}{a} - \frac{2n\pi y_0}{b}\right) sin\left(\frac{m\pi l\,cos\varphi}{a} - \frac{n\pi l\,sin\varphi}{b}\right)}{8(\beta_x - \beta_y)}$$
$$+ \frac{cos\left(\frac{2m\pi x_0}{a} + \frac{2n\pi y_0}{b}\right) sin\left(\frac{m\pi l\,cos\varphi}{a} + \frac{n\pi l\,sin\varphi}{b}\right)}{8(\beta_x + \beta_y)} \quad \text{(A6)}$$

Integral expressed in Eq. (A6) are further updated for two different cases.

CASE 1: When the crack oriented +45^0, $\beta x = \beta y$

$$\int_0^l \sin^2\,\alpha_x \sin^2\alpha_y\,ds$$
$$= \frac{l}{4} - \frac{\cos\left(\frac{2m\pi x_0}{a}\right) \sin\left(\frac{m\pi l\,cos\varphi}{a}\right)}{4\beta_x}$$
$$- \frac{\cos\left(\frac{2n\pi y_0}{b}\right) \sin\left(\frac{n\pi l\,sin\varphi}{b}\right)}{4\beta_y}$$
$$+ \frac{1}{8} cos\left(\frac{2m\pi x_1}{a} - \frac{2n\pi y_1}{b}\right)$$
$$+ \frac{\cos\left(\frac{2m\pi x_0}{a} + \frac{2n\pi y_0}{b}\right) \sin\left(\frac{m\pi l\,cos\varphi}{a} + \frac{n\pi l\,sin\varphi}{b}\right)}{8(\beta_x + \beta_y)} \quad \text{(A7)}$$

CASE 2: When the crack oriented -45^0, $\beta x = -\beta y$

$$\int_0^l \sin^2\alpha_x \sin^2\alpha_y \, ds$$

$$= \frac{l}{4} - \frac{\cos\left(\frac{2m\pi x_0}{a}\right)\sin\left(\frac{m\pi l\cos\varphi}{a}\right)}{4\beta_x} - \frac{\cos\left(\frac{2n\pi y_0}{b}\right)\sin\left(\frac{n\pi l\sin\varphi}{b}\right)}{4\beta_y} + \frac{\cos\left(\frac{2m\pi x_0}{a} - \frac{2n\pi y_0}{b}\right)\sin\left(\frac{m\pi l\cos\varphi}{a} - \frac{n\pi l\sin\varphi}{b}\right)}{8(\beta_x - \beta_y)} + \cos\left[\frac{2m\pi x_1}{a} + \frac{2n\pi y_1}{b}\right] \quad \text{(A8)}$$

Similarly, $\int_0^l \cos^2\alpha_x \cos^2\alpha_y \, ds$ are expressed for arbitrary orientation of crack with Case 1 and Case 2 in Eq. A9, A10, and A11 respectively

$$\int_0^l \cos^2\alpha_x \cos^2\alpha_y \, ds$$

$$= \frac{l}{4} + \frac{\cos\left(\frac{2m\pi x_0}{a}\right)\sin\left(\frac{m\pi l\cos\varphi}{a}\right)}{4\beta_x} + \frac{\cos\left(\frac{2n\pi y_0}{b}\right)\sin\left(\frac{n\pi l\sin\varphi}{b}\right)}{4\beta_y} + \frac{\cos\left(\frac{2m\pi x_0}{a} - \frac{2n\pi y_0}{b}\right)\sin\left(\frac{m\pi l\cos\varphi}{a} - \frac{n\pi l\sin\varphi}{b}\right)}{8(\beta_x - \beta_y)} + \frac{\cos\left(\frac{2m\pi x_0}{a} + \frac{2n\pi y_0}{b}\right)\sin\left(\frac{m\pi l\cos\varphi}{a} + \frac{n\pi l\sin\varphi}{b}\right)}{8(\beta_x + \beta_y)} \quad \text{(A9)}$$

CASE 1: When the crack oriented +45^0, $\beta x = \beta y$

$$\int_0^l \cos^2 \alpha_x \cos^2 \alpha_y \, ds$$
$$= \frac{l}{4} + \frac{\cos\left(\frac{2m\pi x_0}{a}\right) \sin\left(\frac{m\pi l \cos\varphi}{a}\right)}{4\beta_x}$$
$$+ \frac{\cos\left(\frac{2n\pi y_0}{b}\right) \sin\left(\frac{n\pi l \sin\varphi}{b}\right)}{4\beta_y} + \frac{1}{8} cos\left(\frac{2m\pi x_1}{a} - \frac{2n\pi y_1}{b}\right)$$
$$+ \frac{\cos\left(\frac{2m\pi x_0}{a} + \frac{2n\pi y_0}{b}\right) \sin\left(\frac{m\pi l \cos\varphi}{a} + \frac{n\pi l \sin\varphi}{b}\right)}{8(\beta_x + \beta_y)} \quad \text{(A10)}$$

CASE 2: When the crack oriented -45^0, $\beta x = -\beta y$

$$\int_0^l \cos^2 \alpha_x \cos^2 \alpha_y \, ds$$
$$= \frac{l}{4} + \frac{\cos\left(\frac{2m\pi x_0}{a}\right) \sin\left(\frac{m\pi l \cos\varphi}{a}\right)}{4\beta_x}$$
$$+ \frac{\cos\left(\frac{2n\pi y_0}{b}\right) \sin\left(\frac{n\pi l \sin\varphi}{b}\right)}{4\beta_y}$$
$$+ \frac{\cos\left(\frac{2m\pi x_0}{a} - \frac{2n\pi y_0}{b}\right) \sin\left(\frac{m\pi l \cos\varphi}{a} - \frac{n\pi l \sin\varphi}{b}\right)}{8(\beta_x - \beta_y)}$$
$$+ \cos\left[\frac{2m\pi x_1}{a} + \frac{2n\pi y_1}{b}\right] \quad \text{(A11)}$$

Integral $\int_0^l \sin(\alpha_x) \cos(\alpha_x) \sin(\alpha_x) \cos(\alpha_y) \, ds$ simplified in Eq. (A12). Case 1 and 2 further expressed in Eq. (A13) and (A14).

$$\int_0^l \sin(\alpha_x)\cos(\alpha_x)\sin(\alpha_x)\cos(\alpha_y)\,ds$$

$$= \frac{1}{8}\left[\begin{array}{l} \dfrac{2cos\left(\dfrac{2m\pi\, x_0}{a} - \dfrac{2n\pi y_0}{b}\right) sin\left(\dfrac{m\pi l cos\varphi}{a} - \dfrac{n\pi l sin\varphi}{b}\right)}{2(\beta_x - \beta_y)} \\ - \dfrac{2cos\left(\dfrac{2m\pi l\, x_0}{a} + \dfrac{2n\pi y_0}{b}\right) sin\left(\dfrac{m\pi\, l\, cos\varphi}{a} + \dfrac{n\pi\, l\, sin\varphi}{b}\right)}{2(\beta_x + \beta_y)} \end{array}\right] \quad \text{(A12)}$$

CASE 1: When the crack oriented $+45^0$, $\beta x = \beta y$

$$\int_0^l \sin(\alpha_x)\cos(\alpha_x)\sin(\alpha_x)\cos(\alpha_y)\,ds \;=$$

$$= \frac{l}{8} cos\left(\frac{2m\pi x_1}{a} - \frac{2n\pi y_1}{b}\right)$$
$$- \frac{1}{8}\left[\frac{2cos\left(\dfrac{2m\pi x_0}{a} + \dfrac{2n\pi y_0}{b}\right) sin\left(\dfrac{m\pi\, l\, cos\varphi}{a} + \dfrac{n\pi l\, sin\varphi}{b}\right)}{2(\beta_x + \beta_y)}\right] \quad \text{(A13)}$$

CASE 2: When the crack oriented -45^0, $\beta x = -\beta y$

$$\int_0^l \sin(\alpha_x)\cos(\alpha_x)\sin(\alpha_x)\cos(\alpha_y)\,ds \;=$$

$$= \frac{1}{8}\left[\frac{2cos\left(\dfrac{2m\pi\, x_0}{a} - \dfrac{2n\pi y_0}{b}\right) sin\left(\dfrac{m\pi\, l\, cos\varphi}{a} - \dfrac{n\pi l\, sin\varphi}{b}\right)}{2(\left(\beta_x - \beta_y\right)}\right]$$
$$- \frac{l}{8} cos\left(\frac{2m\pi x_1}{a} + \frac{2n\pi y_1}{b}\right) \quad \text{(A14)}$$

Appendix (B): Free vibration analysis in cracked beam structures using Newton-Raphson Method (Chapter 2).

- MATLAB codes to obtain function (Eq. (3.4.7)) to further use Newton-Raphson Method with the help of symbolic toolbox available in MATLAB.

```
syms A
k = 2.3696e+08;% Stiffness of the rotational spring
E=2*(10^11);% Modulus of elasticity
I = 0.198*((0.122)^3)/12; % Moment of inertia
l1=1.0; %1st Element
l2=2.0; % 2nd Element
lamda1=A*(l1);% A is the factor associated with the eigen %
values
lamda2=A*(l2);
% part 1 of tge beam
hyC1 = cosh(lamda1);
c1 = cos(lamda1);
hyS1 = sinh(lamda1);
s1 = sin(lamda1);
D1 = 1 - (hyC1*c1);
alpha1 = A* E*I * (hyC1*s1-hyS1*c1)/D1;
beta1 = A*E*I * (hyS1-s1)/D1;
v1 = ((A)^2)*E*I* hyS1*s1/D1;
delta1 = (A)^2*E*I*(hyC1-c1)/D1;
gama1 = (A)^3*E*I*( hyC1*s1 + hyS1* c1)/D1;

% part 2 of the beam %
hyC2 = cosh(lamda2);
c2 = cos(lamda2);
hyS2 = sinh(lamda2);
s2 = sin(lamda2);
D2 = 1 - (hyC2*c2);
alpha2 = A*E*I * (hyC2*s2-hyS2*c2)/D2;
beta2 = A*E*I * (hyS2-s2)/D2;
v2 = (A)^2*E*I*hyS2*s2/D2;
delta2 = (A^2)*E*I*(hyC2-c2)/D2;
gama2 = (A^3)*E*I*( hyC2*s2 + hyS2* c2)/D2;
f1 = (gama1+gama2)*((alpha1+k)*(alpha2+k)-k^2);
f2 = v1*((k*v2)-v1*(alpha2+k));
f3 = v2*((k*v1)-v2*(alpha1+k));
f = f1 + f2 + f3
df = diff(f)
```

Appendix (C): Stran energy approach for beams (Chapter 3).

- MATLAB Function file to calculate degradation in natural frequencies due to crack in an isotropic beam fixed at both ends: Using Strain energy approach. (Section 3.6.1)

```
function   DELTA = beamfunc_deltaVec(X)
fa = X(1)
x  = X(2)

L = 1.5;
E = 2*10^11;
b = 0.198;
h = 0.122;
I = 0.198*((0.122)^3)/12;
% d =0.01;
kr = E*I*((fa)-1)^2/(h*fa*(2-(fa)))

mu = 184.4;
cc = (E*I)^2/(kr*mu);

Wu  = 1.0e+03*[0.4481   1.2353   2.4217 … 4.0031];%Undamaged
natural frequencies.
%Wu = 1.0e+03*(0.4481);
l(1)= 1.5; % 1st beam
l(2)= 1.5; % second beam
factor = (E*I)/(kr*mu);

constant1 = zeros(4,4);
constant2 = zeros(4,4);
curvature = zeros(1,4);
J = zeros(1,4);
A = zeros (1,4);

Rdelta = zeros(1,4); % (W0^2- Wc^2)

for n =1:length(Wu);
       W = Wu(n);
       lamda = (E*I/(mu*W^2))^0.25;
       zeta = 1/lamda;
       g1= l(1)*(zeta);
       g2= l(2)*(zeta);
       mat1 = [1 0 1 0;0 1 0 1;cos(g1) sin(g1) cosh(g1)
sinh(g1);-sin(g1) cos(g1) sinh(g1) cosh(g1)];
       mat2 = [1 0 1 0;0 1 0 1;cos(g2) sin(g2) cosh(g2)
sinh(g2);-sin(g2) cos(g2)  sinh(g2) cosh(g2)];

            if rem(n,2)==0
                dis1  = [0; 0; 0; 1];
```

```
                dis2 = [0;1;0;0];% anti symeric modes
            else
                dis1  = [0; 0 ; 1; 0]; % symetric modes
                 dis2 = [1; 0; 0; 0];
            end

            con1 = inv(mat1)*dis1;
            con2 = inv(mat2)*dis2;
            a1 = con1(1,1);
            b1= con1(2,1);
            c1 = con1(3,1);
            d1 = con1(4,1);

            a2 = con2(1,1);
            b2 = con2(2,1);
            c2 = con2(3,1);
            d2= con2(4,1);

            cona = [a1  b1  c1  d1];
            constant1(n,:) = cona;

            conb = [a2  b2  c2  d2];
            constant2(n,:) = conb;

end
% in constant 1,all rows are the values of  the constats
a,b,c,d for first memeber ,for first 4
% natural frequencies
% in constant 2,all rows are the values of  the constats
a,b,c,d for second memeber ,for first 4
% natural frequencies
constant1;
constant2;
A = zeros (1,4);
% the constants has cheacked and verified.

for  n = 1:length(Wu);
    W = Wu(n);
     lamda = (E*I/(mu*W^2))^0.25;
         k = constant1(n,:);
         j = constant2(n,:);

             a1 = k(1);
             b1 = k(2);
             c1 = k(3);
             d1 = k(4);

             a2 = j(1);
             b2 = j(2);
```

```
            c2 = j(3);
            d2 = j(4);

t1 = l(1)/lamda;

i1 = (a1)^2*((t1/2)+(sin(2*t1)/4)) + (b1)^2*(((t1/2)-
sin(2*t1)/4)) +...
    (c1)^2*((t1/2)+(sinh(2*t1)/4)) + (d1)^2*((-
t1/2)+(sinh(2*t1)/4))+...
    (a1)*(b1)*(-(cos(2*t1)/2)) + ((c1)*(d1)*(cosh(2*t1)/2))
+...
    (a1)*(c1)*((cos(t1)*sinh(t1)) + (sin(t1)*cosh(t1)))+...
    (a1)*(d1)*((cos(t1)*cosh(t1)) + (sin(t1)*sinh(t1)))+...
    (b1)*(c1)*(-cos(t1)*cosh(t1) + sin(t1)*sinh(t1))+...
    (b1)*(d1)*(-cos(t1)*sinh(t1) + sin(t1)*cosh(t1));

t2 = 0;

i2 =  (a1)^2*((t2/2)+(sin(2*t2)/4)) + (b1)^2*(((t2/2)-
sin(2*t2)/4)) +...
    (c1)^2*((t2/2)+(sinh(2*t2)/4)) + (d1)^2*((-
t2/2)+(sinh(2*t2)/4))+...
    (a1)*(b1)*(-(cos(2*t2)/2)) + ((c1)*(d1)*(cosh(2*t2)/2))
+...
    (a1)*(c1)*((cos(t2)*sinh(t2)) + (sin(t2)*cosh(2)))+...
    (a1)*(d1)*((cos(t2)*cosh(t2)) + (sin(t2)*sinh(t2)))+...
    (b1)*(c1)*(-cos(t2)*cosh(t2) + sin(t2)*sinh(t2))+...
    (b1)*(d1)*(-cos(t2)*sinh(t2) + sin(t2)*cosh(t2));

J1 = (lamda)*(i1-i2) ;

t3 = l(2)/lamda;
ii1 =  (a2)^2*((t3/2)+(sin(2*t3)/4)) + (b2)^2*(((t3/2)-
sin(2*t3)/4)) +...
    (c2)^2*((t3/2)+(sinh(2*t3)/4)) + (d2)^2*((-
t3/2)+(sinh(2*t3)/4))+...
    (a2)*(b2)*(-(cos(2*t3)/2)) + ((c2)*(d2)*(cosh(2*t3)/2))
+...
    (a2)*(c2)*((cos(t3)*sinh(t3)) + (sin(t3)*cosh(t3)))+...
    (a2)*(d2)*((cos(t3)*cosh(t3)) + (sin(t3)*sinh(t3)))+...
    (b2)*(c2)*(-cos(t3)*cosh(t3) + sin(t3)*sinh(t3))+...
    (b2)*(d2)*(-cos(t3)*sinh(t3) + sin(t3)*cosh(t3));

t4 = 0;

ii2 =  (a2)^2*((t4/2)+(sin(2*t4)/4)) + (b2)^2*(((t4/2)-
sin(2*t4)/4)) +...
    (c2)^2*((t4/2)+(sinh(2*t4)/4)) + (d2)^2*((-
t4/2)+(sinh(2*t4)/4))+...
```

```
    (a2)*(b2)*(-(cos(2*t4)/2)) + ((c2)*(d2)*(cosh(2*t4)/2))
+...
    (a2)*(c2)*((cos(t4)*sinh(t4)) + (sin(t4)*cosh(t4)))+...
    (a2)*(d2)*((cos(t4)*cosh(t4)) + (sin(t4)*sinh(t4)))+...
    (b2)*(c2)*(-cos(t4)*cosh(t4) + sin(t4)*sinh(t4))+...
    (b2)*(d2)*(-cos(t4)*sinh(t4) + sin(t4)*cosh(t4));

J2 = (lamda)*(ii1-ii2) ;
AJ = J1+J2;

            J(n) = AJ;
            AA = 1/(AJ*W^2);
          A(n) = AA ;

end
J; % verified
A; % verified

   for  n = 1:length(Wu)
  W = Wu(n);
  lamda = (E*I/(mu*W^2))^0.25;
   zeta = 1/lamda;

   k = constant1(n,:);
   j = constant2(n,:);
   a1 = k(1); b1 = k(2); c1 = k(3);d1 = k(4);
   a2 = j(1);b2 = j(2);c2 = j(3);d2 = j(4);
 one = [a1 b1 c1 d1];% no direct use of one and two
two = [a2 b2 c2 d2];% just to see the values of a,b,c,d.    kk
= (zeta)^2*((-a1)*cos(zeta*x)-
(b1)*sin(zeta*x)+(c1)*cosh(zeta*x)+(d1)*sinh(zeta*x));%
verified
      ddelta = cc*A(1,n)*(kk)^2
 Rdelta(1,n) = ddelta
    end

  for m = 1:length(Wu)
 WC = (Wu(1,m)*sqrt(1-Rdelta(1,m))) ;
 Wc(1,m) = WC
  end

DELTA = zeros(1,4)
for  ii = 1:length(Wu)
    sqdiffw = (Wu(1,ii))^2-(Wc(1,ii))^2;
    DELTA(1,ii) =  sqdiffw
end
end
```

Appendix (D): Crack localisation with Vector operations (Chapter 4).

- MATLAB codes for damage localisation with noise-less simulation, using Vector operations. (Section 4.3)

```
clear all;
clc; % provide any name to the file and save i.e.
 % DeltaVec.m
kr = 2.3624e+07;% stiffness of rotational spring
% Due to normalisation procedure we can use it for any %crack depth
L = 1.5;
E = 2*10^11 % Young's Modulus;b =0.122 %width; h = 0.122 % depth of beam
I = b*((d)^3)/12;% moment of inertia
mu = 184.4; % mass density
cc = (E*I)^2/(kr*mu);
Wu = 1.0e+03*[0.4481   1.2353   2.4217  4.0031];%Undamaged %natural
frequencies.
%Wu = 1.0e+03*(0.4481);
l(1)= 1.5; % 1st beam
l(2)= 1.5; % second beam
factor = (E*I)/(kr*mu);
 loc = [0:0.01:1.5];% location
maxiter=20;
constant1 = zeros(4,4);constant2 = zeros(4,4);curvature = zeros(1,4);
J = zeros(1,4);A = zeros (1,4);
% Mv is the vector contains noramailised delta Eq.4.2.1 from %thesis, for
demonstration the values in the matrix are for %crack location 0.5
MV =  [0.108939247  0.0917893   0.54003686  0.829498134];%
Crckloc = 0.5;% lOctaion of crack
kprime = zeros(1,4);
kdoublepr = zeros(1,4);
Rdelta = zeros(1,4); % Relative delta
wdsq = zeros(1,4); % Damaged natural frequencies
delta = zeros(1,4);
deltaprime = zeros(1,4);
deltadoublepr = zeros(1,4);
alldeltabar = zeros(4,length(loc));
alldeltadoublebar = zeros(4,length(loc));
floc = zeros(1,length(loc));
fderiv = zeros(1,length(loc));
f2deriv = zeros(1,length(loc));
Y = zeros(1,length(loc));
 for m = 1:length(loc)
%x=xtrial
% for m = 1:maxiter
   x = loc(m);
for n =1:length(Wu);
```

```
      W = Wu(n);
      lamda = (E*I/(mu*W^2))^0.25;
      zeta = 1/lamda;
      g1= l(1)*(zeta);
      g2= l(2)*(zeta);
      mat1 = [1 0 1 0;0 1 0 1;cos(g1) sin(g1) cosh(g1) sinh(g1);-sin(g1) cos(g1) sinh(g1)
cosh(g1)];
      mat2 = [1 0 1 0;0 1 0 1;cos(g2) sin(g2) cosh(g2) sinh(g2);-sin(g2) cos(g2)  sinh(g2)
cosh(g2)];
          if rem(n,2)==0
             dis1  = [0; 0; 0; 1];
             dis2 = [0;1;0;0];% anti symeric
          else
             dis1  = [0; 0 ; 1; 0]; % symetric
              dis2 = [1; 0; 0; 0];
          end
         con1 = inv(mat1)*dis1;con2 = inv(mat2)*dis2;
  a1 = con1(1,1);b1= con1(2,1);c1 = con1(3,1);d1 = con1(4,1);
  a2 = con2(1,1);b2 = con2(2,1);c2 = con2(3,1);d2= con2(4,1);
          cona = [a1  b1  c1  d1];
          constant1(n,:) = cona;
          conb = [a2  b2  c2  d2];
          constant2(n,:) = conb;
end
% in constant 1,all rows are the values of  the constats a,b,c,d for first memeber ,for
first 4
% natural frequencies
% in constant 2,all rows are the values of  the constats a,b,c,d for second memeber
,for first 4
% natural frequencies
constant1; constant2;
A = zeros (1,4);
% the constants has cheacked and verified.
for  n = 1:length(Wu);
    W = Wu(n);
     lamda = (E*I/(mu*W^2))^0.25;
        k = constant1(n,:);
        j = constant2(n,:);
       a1 = k(1);b1 = k(2);c1 = k(3);d1 = k(4);a2 = j(1);
       b2 = j(2);c2 = j(3);d2 = j(4);
t1 = l(1)/lamda;
i1 = (a1)^2*((t1/2)+(sin(2*t1)/4)) + (b1)^2*(((t1/2)-sin(2*t1)/4)) +...
    (c1)^2*((t1/2)+(sinh(2*t1)/4)) + (d1)^2*((-t1/2)+(sinh(2*t1)/4))+...
    (a1)*(b1)*(-(cos(2*t1)/2)) + ((c1)*(d1)*(cosh(2*t1)/2)) +...
    (a1)*(c1)*((cos(t1)*sinh(t1)) + (sin(t1)*cosh(t1)))+...
    (a1)*(d1)*((cos(t1)*cosh(t1)) + (sin(t1)*sinh(t1)))+...
    (b1)*(c1)*(-cos(t1)*cosh(t1) + sin(t1)*sinh(t1))+...
```

```
   (b1)*(d1)*(-cos(t1)*sinh(t1) + sin(t1)*cosh(t1));
t2 = 0;
i2 =  (a1)^2*((t2/2)+(sin(2*t2)/4)) + (b1)^2*(((t2/2)-sin(2*t2)/4)) +...
   (c1)^2*((t2/2)+(sinh(2*t2)/4)) + (d1)^2*((-t2/2)+(sinh(2*t2)/4))+...
   (a1)*(b1)*(-(cos(2*t2)/2)) + ((c1)*(d1)*(cosh(2*t2)/2)) +...
   (a1)*(c1)*((cos(t2)*sinh(t2)) + (sin(t2)*cosh(2)))+...
   (a1)*(d1)*((cos(t2)*cosh(t2)) + (sin(t2)*sinh(t2)))+...
   (b1)*(c1)*(-cos(t2)*cosh(t2) + sin(t2)*sinh(t2))+...
   (b1)*(d1)*(-cos(t2)*sinh(t2) + sin(t2)*cosh(t2));
J1 = (lamda)*(i1-i2) ;
t3 = l(2)/lamda;
ii1 =  (a2)^2*((t3/2)+(sin(2*t3)/4)) + (b2)^2*(((t3/2)-sin(2*t3)/4)) +...
   (c2)^2*((t3/2)+(sinh(2*t3)/4)) + (d2)^2*((-t3/2)+(sinh(2*t3)/4))+...
   (a2)*(b2)*(-(cos(2*t3)/2)) + ((c2)*(d2)*(cosh(2*t3)/2)) +...
   (a2)*(c2)*((cos(t3)*sinh(t3)) + (sin(t3)*cosh(t3)))+...
   (a2)*(d2)*((cos(t3)*cosh(t3)) + (sin(t3)*sinh(t3)))+...
   (b2)*(c2)*(-cos(t3)*cosh(t3) + sin(t3)*sinh(t3))+...
   (b2)*(d2)*(-cos(t3)*sinh(t3) + sin(t3)*cosh(t3));
t4 = 0;
ii2 =  (a2)^2*((t4/2)+(sin(2*t4)/4)) + (b2)^2*(((t4/2)-sin(2*t4)/4)) +...
   (c2)^2*((t4/2)+(sinh(2*t4)/4)) + (d2)^2*((-t4/2)+(sinh(2*t4)/4))+...
   (a2)*(b2)*(-(cos(2*t4)/2)) + ((c2)*(d2)*(cosh(2*t4)/2)) +...
   (a2)*(c2)*((cos(t4)*sinh(t4)) + (sin(t4)*cosh(t4)))+...
   (a2)*(d2)*((cos(t4)*cosh(t4)) + (sin(t4)*sinh(t4)))+...
   (b2)*(c2)*(-cos(t4)*cosh(t4) + sin(t4)*sinh(t4))+...
   (b2)*(d2)*(-cos(t4)*sinh(t4) + sin(t4)*cosh(t4));
J2 = (lamda)*(ii1-ii2) ;
AJ = J1+J2;
         J(n) = AJ;
         AA = 1/(AJ*W^2);
        A(n) = AA ;
end
J; % verified
A; % verified
         for  n =1:length(Wu)
                W = Wu(n);
                lamda = (E*I/(mu*W^2))^0.25;
                zeta = 1/lamda;
k = constant1(n,:);j = constant2(n,:);a1 = k(1);b1 = k(2);c1 = k(3);d1 = k(4);a2 = j(1);b2
= j(2);c2 = j(3);d2 = j(4);
one = [a1 b1 c1 d1]; % no direct use of one and two
two = [a2 b2 c2 d2]; % just to see the values of a,b,c,d.
        kk = (zeta)^2*((-a1)*cos(zeta*x)-
(b1)*sin(zeta*x)+(c1)*cosh(zeta*x)+(d1)*sinh(zeta*x));% verified
            kkprime = (zeta)^3*((a1)*sin(zeta*x)-
(b1)*cos(zeta*x)+(c1)*sinh(zeta*x)+(d1)*cosh(zeta*x));
```

```
kkdoublepr=zeta^4*((a1)*cos(zeta*x)+(b1)*sin(zeta*x)+(c1)*cosh(zeta*x)+(d1)*sinh(
zeta*x));
            ddelta = A(1,n)*(kk)^2
           % Awdsq = sqrt(W^2*(1-ddelta));
            ddeltaprime = 2*A(1,n)*kk*kkprime; ddeltadoublepr = 2*A(1,n)*(
(kkprime)^2 + (kk*kkdoublepr));
            curvature(n) = kk;
            kprime(n)=  kkprime;
            kdoublepr(n) =kkdoublepr ;
            Rdelta(n) = ddelta
            %wdsq(n) = Awdsq;
            deltaprime(n) = ddeltaprime;
            deltadoublepr(n) =  ddeltadoublepr;
            end
            G  = cc*Rdelta;
            Wc = (Wu -(G.*Wu))';
            sk = sqrt(sum(Rdelta.*Rdelta));
            p  = sum(Rdelta.*deltaprime);
            skprime = p/sk;
           X = sum(deltaprime.*deltaprime);
           Y = sum(Rdelta.*deltadoublepr);
           skdoublepr = (X+Y-((skprime)^2))/sk;
         deltaBAR = zeros(1,4);
         deltaBARprime = zeros(1,4);
         deltadoubleBARprime = zeros(1,4);
     for n = 1:length(Wu)
        Adeltabar = Rdelta(n)/sk;
        Adeltabarprime = (deltaprime(n)/sk) - (Rdelta(n)*skprime/(sk)^2);
        Adeltadoublebarprime = (deltadoublepr(n)/sk)-
(2*(deltaprime(n)*skprime/(sk)^2))-...
 (Rdelta(n)*skdoublepr/(sk)^2)+ ((2*Rdelta(n)*(skprime)^2)/(sk)^3);

        deltaBAR(1,n)=Adeltabar ;
        deltaBARprime(1,n)= Adeltabarprime ;
        deltadoubleBARprime(1,n) =Adeltadoublebarprime ;
     end
alldeltabar (1:4,m) =deltaBAR'
 alldeltadoublebar(1:4,m) = deltaBARprime';

 f = sum(MV.*deltaBAR);% used formulation for vector operations
 fprime = sum(MV.*deltaBARprime);
 fdoublepr = sum(MV.*deltadoubleBARprime);
 YY =(sum(MV.*deltaBAR)-1)*sum(MV.*deltaBARprime);
  floc(m) = f;
  fderiv(m) = fprime;
 f2deriv(m) =  fdoublepr;
      Y(m) = YY;
```

```
      result = [floc;fderiv];
     end
plot(loc,floc,'-b','LineWidth',2);
      hold on
      xline(Crckloc,'--r', 'LineWidth',1)
      hold off
      title('Noise free simulation for crack ,0.3 meters')
      xlabel('location in meters','FontSize',12)
      ylabel('f(X)','FontSize',12)
      xlim([0 1.5])
      ylim([0 1])
      grid off
%
```

Appendix (E): Crack localisation using interval arithmetic method (Chapter 4).

- MATLAB codes for Damage localisation in beam with noise with interval arithmetic operations, From Section (4.4).

```
clear all;
clc;
DeltaVec;
 wo =  1.0e+03*[0.4481   1.2353   2.4217  4.0031];% Natural
frequencies of intact beam.
% Wc Natural frequencies of cracked beam.
wc = [444.184910676421     1226.21246976088 2314.91582628476
      3728.53320419325];% Location  = 0.5,depth of crack =0.05;

e = 0.5;% Error
n = length(wo);
 wol = [wo(1)-e ,wo(2)-e, wo(3)-e, wo(4)-e] ;
 wou = [wo(1)+e ,wo(2)+e, wo(3)+e, wo(4)+e] ;
 wcl = [wc(1)-e ,wc(2)-e, wc(3)-e, wc(4)-e] ;
 wcu = [wc(1)+e ,wc(2)+e, wc(3)+e, wc(4)+e] ;
 DL  = zeros(1,4);
 DU  = zeros(1,4);
 DLBAR = zeros(1,4);% lower limit for normalised natural
%frequencies
 DUBAR = zeros(1,4); );% Upper limit for normalised natural
%frequencies
 for i = 1:n
dl = 1 - (wcu(i))/(wol(i));
du = 1 - (wcl(i))/(wou(i));
DL(1,i) = dl;
DU(1,i) = du;
```

```
 end
 DLsq = DL.^2;
 DUsq = DU.^2;
 SL = sum(DLsq);
 s = sqrt(SL);
 SU = sum(DUsq);
 q = sqrt(SU)
 epsi = DUsq - DLsq

 for i =1:n
      DLB = DL(i)/sqrt(SU-epsi(i))
      if DLB < 0;
          dlbar =0;
      else
          dlbar = DLB;
      end
     dubar = DU(i)/sqrt(SL-epsi(i))

     DLBAR(i) = dlbar;
     DUBAR(i) = dubar;
 end

 figure()
  for  i =1:4
    subplot(2,2,i)
xloc = alldeltabar(i,:);%change mode
 plot(loc,xloc,'-b','LineWidth',1.5);
xlabel('location (m)','FontSize',20,'FontName','Times new
Roman')
 grid off
 ylabel(' (f(x/l)','FontSize',20,'FontName','Times new Roman')
 hold on
  yline(DUBAR(1,i),'LineWidth',1.3)% chnage mode
 hold on
 yline(DLBAR(1,i),'LineWidth',1.3)%change mode
 hold on
xline(0.5,'--r', 'LineWidth',1.5)
 hold on
 str1 = {' Upper Limit'};
 str2 = {' Lower Limit'};
text(0.75,0.5,str1,'FontSize',17,'FontName','Times new Roman')
text(0.75,0.2,str2,'FontSize',17,'FontName','Times new Roman')
hold on
legend(' f(x)',' U.L.',' L.L.',' Target
Location','FontSize',17,'FontName','Times new Roman')
hold off
 xlim([0 1.5])
  ylim([0 1])
  end
```

Appendix (F): Inverse problem in beam structures using gradient based optimisation (Chapter 4).

- MATLAB Function file to calculate the error function which employed for minimisation using FMINCON for beam structure.

```
function errVal = beaminversequations(X,deltaSyn,deltaScale)
% Cy = X(1);
deltaVal = beamfunc_deltaVec(X); % vector eith 4 elements
errVal = norm((deltaVal - deltaSyn)./deltaScale);
end
```

- MATLAB codes for the inverse problem: beam structure using gradient based optimisation.

```
clc;
clear;
close all;
P = 10 % Number of sample points
N = 2 % Number of dimensions
lb = [0  0]; % lower bounds for crack depth ratio and location
ub = [1  1.5];
Y  = lhsdesign(P,N,'criterion','correlation');
M0 = bsxfun(@plus,lb,bsxfun(@times,Y,(ub-lb)));

loc = 0.6;% Target location
deFac = 0.4098;% Target depth of crack/thickness


deltaSyn = [583.78 73282.40 737558.419… 1758286.76877513];%
Synthetic data
% obtained using ‘beamfunc_deltaVec(X)’ with target % location
and target crack depth ratio

deltaScale  =[17637.0041984586   24023.0825807091
     4821.68261841498 421616.003938783];
% Scaling factor employed to scale the numerator and
% obtained for any random crack location and crack -depth %
ratio using ‘beamfunc_deltaVec(X)’. Strictly for
% scaling purpose

XSOL = zeros(P,N)
  Options =
optimoptions('fmincon','Display','iter','Algorithm','interior-
point','PlotFcn',...
    'optimplotfvalconstr', 'OutputFcn',@outfun);
  options = optimoptions(options,'StepTolerance',1e-50);
  options = optimoptions(options,'ConstraintTolerance',1e-40);
%   edit optimplotfval
```

```
%   set(gca, 'YScale', 'log');
%   options = optimset(options,'PlotFcns',{… @optimplotlogfval
}
fval = zeros(1,P); exitflag = zeros(1,P); output = {};
display = {};
for i = 1:P
T0 = M0(i,:);
A = [];
b = [];
Aeq = [];
beq = [];
nonlcon = [];
lb = [0.015  0.1];
ub = [0.97  1.4];
% Set up shared variables with outfun
global history searchdir
history.x = [];
history.fval = [];
searchdir = [];
[Xsol,fval(i),exitflag(i),output{i}] = fmincon(@(X)
beaminversequations(X,...
    deltaSyn,deltaScale), T0,
A,b,Aeq,beq,lb,ub,nonlcon,options);
XSOL(i,:) = Xsol;
xhist{i} = history.x;
fvalhist{i} = history.fval;
searchdirhist{i} = searchdir;
end
colScale = -log10(fval./(max(fval)+1e-2));
colScale = colScale./max(colScale);

figure ()
h = [128 128 128]/255;
jj=1;
        plot(xhist{1}(:,jj),'-','Color',...
       h,'LineWidth',2*colScale(1));
         hold on
        plot(xhist{2}(:,jj),'-','Color',...
     [0.6350 0.0780 0.1840],'LineWidth',2*colScale(2));
         hold on
          plot(xhist{3}(:,jj),'-','Color',...
        h,'LineWidth',2*colScale(3));
         hold on
          plot(xhist{4}(:,jj),'-','Color',...
       h,'LineWidth',2*colScale(4));
         hold on
          plot(xhist{5}(:,jj),'-','Color',...
        [0 0 1],'LineWidth',2*colScale(5));
         hold on
```

```
          plot(xhist{6}(:,jj),'-','Color',...
         [0.4660 0.6740 0.1880 ],'LineWidth',2*colScale(6));
          hold on
           plot(xhist{7}(:,jj),'-','Color',...
         [1 0 1],'LineWidth',2*colScale(7));
          hold on
           plot(xhist{8}(:,jj),'-','Color',...
        [0.9290 0.6940 0.1250],'LineWidth',2*colScale(8));
          hold on
           plot(xhist{9}(:,jj),'-','Color',...
         [0.4940 0.1840 0.5560],'LineWidth',2*colScale(9));
          hold on
           plot(xhist{10}(:,jj),'-','Color',...
         h,'LineWidth',2*colScale(10))
 hold on
 yline(deFac,'--r','LineWidth',2.5);
     hold off
     alpha(0.1)
     xlabel('iterations','FontSize',15,'FontName','Times new
Roman');
     ylabel('d/h','FontSize',15,'FontName','Times new Roman');
     xt = [0.5];
     yt = [0.22];
str = {' Target depth'};

text(xt,yt,str,'FontSize',15,'FontName','Times new Roman')
title('crack depth ratio  vs convergence set
','FontSize',15,'FontName','Times new Roman')
figure()
jj=2;
       plot(xhist{1}(:,jj),'-','Color',...
       h,'LineWidth',2*colScale(1));
         hold on
        plot(xhist{2}(:,jj),'-','Color',...
     [0.6350 0.0780 0.1840],'LineWidth',2*colScale(2));
         hold on
          plot(xhist{3}(:,jj),'-','Color',...
        h,'LineWidth',2*colScale(3));
         hold on
          plot(xhist{4}(:,jj),'-','Color',...
       h,'LineWidth',2*colScale(4));
         hold on
          plot(xhist{5}(:,jj),'-','Color',...
        [0 0 1],'LineWidth',2*colScale(5));
         hold on
          plot(xhist{6}(:,jj),'-','Color',...
        [0.4660 0.6740 0.1880 ],'LineWidth',2*colScale(6));
         hold on
          plot(xhist{7}(:,jj),'-','Color',...
```

```
        [1 0 1],'LineWidth',2*colScale(7));
         hold on
          plot(xhist{8}(:,jj),'-','Color',...
       [0.9290 0.6940 0.1250],'LineWidth',2*colScale(8));
         hold on
          plot(xhist{9}(:,jj),'-','Color',...
        [0.4940 0.1840 0.5560],'LineWidth',2*colScale(9));
         hold on
          plot(xhist{10}(:,jj),'-','Color',...
        h,'LineWidth',2*colScale(10));
 hold on
     yline(loc,'--r','LineWidth',1.5);
     hold off
     alpha(0.1)
     xlabel({'iterations'},'FontSize',15,'FontName','Times new
Roman');
     ylabel({'location'},'FontSize',15,'FontName','Times new
Roman');
     xt = [0.5];
     yt = [0.22];
str = {' Target location'};

text(xt,yt,str,'FontSize',15,'FontName','Times new Roman')
title('Location  vs convergence set
','FontSize',15,'FontName','Times new Roman')
```

Appendix (G): Damage modelling in plate structures (Chapter 5).

- MATLAB Function file to calculate degradation in natural frequencies due to crack in a simply supported isotropic plate.

```
function DELTA = func_deltaVec(X)
x1 = X(1);y1 = X(2);x2 = X(3);y2 = X(4);fa = X(5);
E = 110e9; % Modulus of elasticity
roe = 4480; % Weight density
v = 0.3; % Poisson's ratio
a = 0.1; % length of crck
b = 0.1; % width of crack
h = 0.001; % thickness of plate
D = E*h^3/(12*(1-v^2));% flexural rigidity
M = [1 1 2 2 1 3]; % Number of half wavelengths in X-axis
N = [1 2 1 2 3 1]; % Number of half wavelengths in Y-axis
DELTA = zeros (1, length(M));
WO = zeros (1, length(M));
WC = zeros (1, length(M));
l = sqrt((x2-x1)^2 + (y2-y1)^2);% Crack length.
```

```
fi = atan((y2-y1)/(x2-x1));
d=fa*h; % Depth of crack
 S = (d/h)*(2-(d/h))/(0.9*(1-(d/h))^2);%new
Cy = (h*S/D);   % Compliance
x0 = (x1+x2)/2 ;  y0 = (y1+y2)/2;Midpoint of the crack
for i = 1:length(M)
    m = M(i); n = N(i);
% alphax = m*pi*(x1+(l*cos(fi)))/a;
% alphay = n*pi*(y1+(l*sin(fi)))/b;
Bx = (m*pi/a)*cos(fi);
By = (n*pi/b)*sin(fi);
BCASE1 = Bx-By; BCASE2 = Bx+By;
t1 = ((m^2/a^2) + (v*(n^2/b^2)))*((sin(fi)^2));
t2 = ((v*(m^2/a^2)) + (n^2/b^2))*((cos(fi)^2));
d1 = (Cy*4/(roe*h*a*b));
A = l/4;
B = cos(2*m*pi*x0/a)*sin(m*pi*l*cos(fi)/a)/(4*Bx);
C = cos(2*n*pi*y0/b)*sin(n*pi*l*sin(fi)/b)/(4*By);
if  abs(BCASE1)< 0.000000001;
%    x1 = input('put value of x1 for +45 =');
%    y1 = input('put value of y1 for +45 =');
  De = (l/8)*(cos((2*m*pi*x1/a)-(2*n*pi*y1/b)));
 else
%
D1 = cos((2*m*pi*x0/a)-(2*n*pi*y0/b));
D2 = sin((m*pi*l*cos(fi)/a)-(n*pi*l*sin(fi)/b));
De = D1*D2/(8*(Bx-By));
 end
if abs(BCASE2)<0.000000001%if crack have alignment 45⁰ or 135⁰
%    x1 = input('put value of x1 for -45 =');
%    y1 = input('put value of y1 for -45 =');
E = (l/8)*(cos((2*m*pi*x1/a)+(2*n*pi*y1/b)));
else
E1 = cos((2*m*pi*x0/a)+(2*n*pi*y0/b));
E2 = sin((m*pi*l*cos(fi)/a)+(n*pi*l*sin(fi)/b));
E = E1*E2/(8*(Bx+By));
end

if abs(Bx)<0.000000001
    finaldtr1 = 0;
    d11 =(sin(m*pi*x0/a))^2;
 d22 = ((l/2)-((b/(2*n*pi))*cos(2*n*pi*y0/b)*sin(n*pi*l/b)));
 d2 = D^2*pi^4*((t1+t2)^2)*d11*d22;
elseif abs(By)<0.000000001
 finaldtr1 = 0;
d2 = D^2*pi^4*((t1+t2)^2)*(sin(n*pi*y0/b))^2*((l/2)-
((a/(2*m*pi))*cos(2*m*pi*x0/a)*sin(m*pi*l/a)));
else
  d2 =  D^2*pi^4*((t1+t2)^2)*(A - B - C + De + E) ;
```

```
dtr1 = (2*D*pi^2*(1-v)*sin(fi)*cos(fi)*m*n/(a*b))^2;
finaldtr1 = dtr1*(A+B+C+De+E);
end
if abs(Bx) < 0.0000000001
    dtr2 = 0;
    elseif abs(By) <0.00000001
    dtr2 = 0;
else
    dtr2 = 4*D^2*pi^4*(t1+t2)*(1-v)*sin(fi)*cos(fi)*m*n/(a*b);
end
intdtr1 = (2*m*pi*x0/a);
intdtr2 = (2*n*pi*y0/b);
intdtr3 = m*pi*l*cos(fi)/a;
intdtr4 = n*pi*l*sin(fi)/b;
if abs(BCASE1)<0.0000001
%    x1 = input('put value of x1 for +45  =');
%    y1 = input('put value of y1 for +45  =');
   term1 = l*(cos((2*m*pi*x1/a)-(2*n*pi*y1/b)));
term2 =
(2*cos(intdtr1+intdtr2)*sin(intdtr3+intdtr4))/(2*(Bx+By));
finaldtr2 = (dtr2)*(1/8)*(term1-term2);
elseif abs(BCASE2)<0.0000001
%   x1 = input('put value of x1 for -45 =');
%   y1 = input('put value of y1  for -45 =');
  term1 = (2*cos(intdtr1-intdtr2)*sin(intdtr3-
intdtr4))/(2*(Bx-By));
term2 = l*cos((2*m*pi*x1/a)+(2*n*pi*y1/b));
finaldtr2 = (dtr2)*(1/8)*(term1-term2);
else
    term1 = (2*cos(intdtr1-intdtr2)*sin(intdtr3-
intdtr4))/(2*(Bx-By));
   term2 =
(2*cos(intdtr1+intdtr2)*sin(intdtr3+intdtr4))/(2*(Bx+By));
    finaldtr2 = dtr2*(1/8)*(term1-term2);
end
delta = d1*( d2 + finaldtr1 - finaldtr2); % BY SING NOTS
wo = sqrt((D*pi^4*((m^2/a^2)+(n^2/b^2))^2)/(roe*h));
wcsq =(wo^2-delta);
wc = sqrt(wcsq)
edelta = wo^2 - wc^2;
DELTA(1,i) = edelta
 WO(i)=wo;
 WC(i)=wc;
end
% CH1 = WO';
% CH2 = WC';
% CH3 = DELTA';
% check = [CH1 CH2 CH3];
% REUSE = CH3'
```

```
end
```

Appendix (H): Inverse problem in plat structures using gradient based optimisation (Chapter 6).

- MATLAB Function file to calculate the error function which employed for minimisation using FMINCON.

```
function errVal = inversequations(X,deltaSyn,deltaScale)
% Cy = X(1);
deltaVal = func_deltaVec(X);% vector with 5 elements
errVal = norm ((deltaVal - deltaSyn)./deltaScale);
end
```

- MATLAB codes for the inverse problem : plate structure.

```
clear;
close all;
P = 10  % Number of sample points
N = 5;   % Number of dimensions
lb = [0 0 0 0 0]; %lower bounds for x1,y1,x2,y2
ub = [0.1 0.1 0.1 0.1 0.98]; % Upper bounds for          %
x1,y1,x2,y2

Y  = lhsdesign(P,N,'criterion','correlation');
M0 = bsxfun(@plus,lb,bsxfun(@times,Y,(ub-lb)));
XSYN = [0.023,0.027,0.043,0.047];% predermined values of %
crack location [X1 Y1 X2 Y2]
deFac = 0.3; % depth of crack/thickness

deltaSyn =[22895.9059109555 146094.423694625 189708.704735365
     286910.008300141 303291.384436828 293620.527092000]
% Synthetic data generated using ASYN and deFac

deltaScale=[13104.9504536692     173337.074126823
     173337.074126823 455531.973975404 278677.448767910
     278677.448767910];
% Data used for scaling purpose

XSOL = zeros(P,N);
options = optimoptions('fmincon','Display','iter',...
      'Algorithm','interior-point','PlotFcn',...
    'optimplotfvalconstr', 'OutputFcn',@outfun);

  options = optimoptions(options,'StepTolerance',1e-40);
 options = optimoptions(options,'ConstraintTolerance',…
1e-10);

%   edit optimplotfval
%   set(gca, 'YScale', 'log');
%   options = optimset(options,'PlotFcns',  {
@optimplotlogfval });
fval = zeros(1,P); exitflag = zeros(1,P); output = {};
```

```
display = {};
for i = 1:P
T0 = M0(i,:);
A = [];
b = [];
Aeq = [];
beq = [];
nonlcon = [];
lb = [0.0   0.0   0.0    0.0   0.2];
ub = [0.1   0.1   0.1    0.1   0.98];

% Set up shared variables with outfun
global history searchdir
history.x = [];
history.fval = [];
searchdir = [];
[Xsol,fval(i),exitflag(i),output{i}] = fmincon(@(X)
inversequations(X,...
    deltaSyn,deltaScale), T0,
A,b,Aeq,beq,lb,ub,nonlcon,options);
XSOL(i,:) = Xsol;

xhist{i} = history.x;
fvalhist{i} = history.fval;
searchdirhist{i} = searchdir;
end
 figure()
 for ii=1:P
 semilogy(1:length(fvalhist{ii}), fvalhist{ii}); hold on
 end
 xlabel(['Itteration for ',num2str(P), ' sample ponits']);
ylabel({'log(favl)'});
title('fval vs Itterations')
 hold off
figure()
 for jj=1:N
  subplot(2,3,jj)
for ii=1:P
 plot(1:length(fvalhist{ii}), searchdirhist{ii}(:,jj));
 hold on
  xlabel('Itteration')
ylabel({'Gradient w.r.t. varriable',num2str(jj)});
title('Gradient vs Itterations')
end
hold off
 end
figure()
 for ii=1:P
     subplot(2,5,ii)
```

```
     for jj = 1:length(fvalhist{ii})
        plot(xhist{ii}(jj,1:2:3), xhist{ii}(jj,2:2:4),...
           'Color', [0 0 1 0.5]);

        hold on
     % scatter1 =
scatter(xhist{ii}(jj,1:2:3),xhist{ii}(jj,2:2:4),'MarkerFaceCol
or','r','MarkerEdgeColor','k');
 %scatter1.MarkerFaceAlpha = .05;
        hold on
 end
     plot(mean(xhist{ii}(:,1:2:3),2),
mean(xhist{ii}(:,2:2:4),2),'.-r')
     plot(XSYN(1:2:3),XSYN(2:2:4),'-g','LineWidth',3)

     hold off
     alpha(0.1)
     xlabel({'l(a = 0.1m)'});
     ylabel({'b(b = 0.1m)'});
     xt = [0.035];
     yt = [0.035];
str = {'\leftarrow Target'};

text(xt,yt,str)
title('Target vs convergence set = ',num2str(ii))
 xlim([0 .1]);  ylim([0 .1])
 end
%  figure()
%  for ii=1:P
% xvec = repmat(0.5,length(xhist{ii}(:,5)),1)
%    subplot(2,5,ii)
% yline(xhist{ii}(:,5)); hold on
% plot(xvec,xhist{ii}(:,5),'.-r')
%  yline(deFac,'-g','LineWidth',3)
%  end
%  hold off
%   xlim([0 1])
%  ylim([0 1]
%%
colScale = -log10(fval./(max(fval)+1e-2));
colScale = colScale./max(colScale);
figure()
hold on
for ii=[1:P]
    plot(XSOL(ii,1:2:4),XSOL(ii,2:2:4),'-','Color',...
        [0 0 1 ],'LineWidth',3*colScale(ii))
     xt = [0.002+sum(XSOL(ii,1:2:4))/2];
     yt = [sum(XSOL(ii,2:2:4))/2];
str = {ii};
```

```
text(xt,yt,str)
    end
hold on
plot(XSYN(1:2:end),XSYN(2:2:end),'--
r','LineWidth',1.5*colScale(1));
xlabel({'length(a = 0.1m)'});
ylabel({'breadth(b = 0.1m)'});
hold off
axis equal
xlim([0, 0.1])
ylim([0, 0.1])
% figure()
% yline(deFac,'--r','LineWidth',1); hold on
% for JJ = 1:P
% Y = yline(XSOL(JJ,size(N)),'-','Color',...
%  [0 0 1],'LineWidth',3*colScale(ii))
% end
% hold off
% xlim([0, 1])
% ylim([0, 1])
% %
LR = linspace(0.1,0.9,5);
figure()
 for ii=1:P
      subplot(2,5,ii)
      for jj =5
        plot(xhist{ii}(:,jj),'Color', [0 0 1 LR(jj)]);   hold
on

     % scatter1 =
scatter(xhist{ii}(jj,1:2:3),xhist{ii}(jj,2:2:4),'MarkerFaceCol
or','r','MarkerEdgeColor','k');
 %scatter1.MarkerFaceAlpha = .05;
%         hold on
   end
%      plot(mean(xhist{ii}(:,1:2:3),2),
mean(xhist{ii}(:,2:2:4),2),'.-r')
%      plot(XSYN(1:2:3),XSYN(2:2:4),'-g','LineWidth',3)
     yline(deFac,'--r','LineWidth',4); hold on
     hold off
     alpha(0.1)
     xlabel({'iterations'});
     ylabel({'d/h'});
     xt = [0.5];
     yt = [0.22];
str = {' Target crack'};
text(xt,yt,str)
% title('depth ratio  vs convergence set =',num2str(ii))
 colScale = -log10(fval./(max(fval)+1e-2));
```

```
colScale = colScale./max(colScale);

figure()
htmlGray = [128 128 128]/255;
%  for ii=1:P
%       subplot(2,5,ii)
%       for jj =5
jj=5;
        plot(xhist{1}(:,jj),'-','Color',...
   [0 0 1],'LineWidth',2.5*colScale(1));
         hold on
        plot(xhist{2}(:,jj),'-','Color',...
      [0 1 0],'LineWidth',2.5*colScale(2));
         hold on
          plot(xhist{3}(:,jj),'-','Color',...
      [0 0 1],'LineWidth',2.5*colScale(3));
         hold on
          plot(xhist{4}(:,jj),'-','Color',...
       [0 0.4470 0.7410],'LineWidth',2.5*colScale(4));
         hold on
          plot(xhist{5}(:,jj),'-','Color',...
 [0 0 1],'LineWidth',2.5*colScale(5));
         hold on
          plot(xhist{6}(:,jj),'-','Color',...
  [0.8500 0.3250 0.0980],'LineWidth',2.5*colScale(6));
         hold on
          plot(xhist{7}(:,jj),'-','Color',...
htmlGray,'LineWidth',2.5*colScale(7));
         hold on
          plot(xhist{8}(:,jj),'-','Color',...
     [0.4940 0.1848 0.5560],'LineWidth',2.5*colScale(8));
         hold on
          plot(xhist{9}(:,jj),'-','Color',...
   [0.4660 0.6740 0.1880],'LineWidth',2.5*colScale(9));
         hold on
          plot(xhist{10}(:,jj),'-','Color',...
    htmlGray,'LineWidth',2.5*colScale(10));

        hold on
 yline(deFac,'--r','LineWidth',2.5);
     hold off
     alpha(0.1)
     xlabel({'iterations'});
     ylabel({'d/h'});
     xt = [0.5];
     yt = [0.22];
str = {' Target crack'};
text(xt,yt,str)
title('depth ratio  vs convergence set =',num2str(ii))
```

```
%     end
```

References

[1] A. Zolfaghari, A. Zolfaghari, and F. Kolahan, “Reliability and sensitivity of magnetic particle nondestructive testing in detecting the surface cracks of welded components,” *Nondestructive Testing and Evaluation*, vol. 33, no. 3, pp. 290–300, 2018.

[2] H. Sohn, H. J. Lim, M. P. Desimio, K. Brown, and M. Derriso, “Nonlinear ultrasonic wave modulation for online fatigue crack detection,” *J Sound Vib*, vol. 333, no. 5, pp. 1473–1484, Feb. 2014.

[3] Q. Shuai and J. Tang, “Enhanced modelling of magnetic impedance sensing system for damage detection,” *Smart Mater Struct*, vol. 23, no. 2, p. 025008, 2013.

[4] Y. J. Yan and L. H. Yam, “Online detection of crack damage in composite plates using embedded piezoelectric actuators/sensors and wavelet analysis,” *Compos Struct*, vol. 58, no. 1, pp. 29–38, 2002.

[5] C. A. Paget, S. Grondel, K. Levin, and C. Delebarre, “Damage assessment in composites by Lamb waves and wavelet coefficients,” *Smart Mater Struct*, vol. 12, no. 3, p. 393, 2003.

[6] M. Krawczuk, “Natural vibrations of rectangular plates with a through crack,” *Archive of Applied Mechanics* , vol. 63, no. 7, pp. 491–504, 1993.

[7] C.-C. Chang and L.-W. Chen, “Damage detection of a rectangular plate by spatial wavelet based approach,” *Applied Acoustics*, vol. 65, no. 8, pp. 819–832, 2004.

[8] M. Rucka and K. Wilde, “Application of continuous wavelet transform in vibration based damage detection method for beams and plates,” *J Sound Vib*, vol. 297, no. 3–5, pp. 536–550, 2006.

[9] W. S. McCulloch and W. Pitts, “A logical calculus of the ideas immanent in nervous activity,” *Bull Math Biophys*, vol. 5, pp. 115–133, 1943.

[10] J. E. Stephens and R. D. VanLuchene, “Integrated assessment of seismic damage in structures,” *Computer-Aided Civil and Infrastructure Engineering*, vol. 9, no. 2, pp. 119–128, 1994.

[11] P. Tsou and M.-H. H. Shen, “Structural damage detection and identification using neural networks,” *AIAA journal*, vol. 32, no. 1, pp. 176–183, 1994.

[12] P. Cornwell, S. W. Doebling, and C. R. Farrar, “Application of the strain energy damage detection method to plate-like structures,” *J Sound Vib*, vol. 224, no. 2, pp. 359–374, 1999.

[13] H. Hu, B.-T. Wang, C.-H. Lee, and J.-S. Su, “Damage detection of surface cracks in composite laminates using modal analysis and strain energy method,” *Compos Struct*, vol. 74, no. 4, pp. 399–405, 2006.

[14] R. Loendersloot, T. H. Ooijevaar, L. Warnet, A. de Boer, and R. Akkerman, “Vibration based structural health monitoring of a composite plate with stiffeners,” in *24th*

International Conference on Noise and Vibration Engineering, ISMA 2010, Katholieke Universiteit Leuven, 2010, pp. 909–924.

[15] X. T. Hu, Z. Y. Qin, and F. L. Chu, "Damage detection in plate structures based on space-time autoregressive moving average processes," in *Journal of Physics: Conference Series*, IOP Publishing, 2011, p. 012119.

[16] S. W. Doebling, C. R. Farrar, and M. B. Prime, "A summary review of vibration-based damage identification methods," *Shock and vibration digest*, vol. 30, no. 2, pp. 91–105, 1998.

[17] F. Wang and T. Chan, "Review of vibration-based damage detection and condition assessment of bridge structures using structural health monitoring," in *Proceedings of the Second Infrastructure Theme Postgraduate Conference: Rethinking Sustainable Development-Planning, Infrastructure Engineering, Design and Managing Urban Infrastructure*, Queensland University of Technology, 2009, pp. 35–47.

[18] W. Fan and P. Qiao, "Vibration-based damage identification methods: a review and comparative study," *Struct Health Monit*, vol. 10, no. 1, pp. 83–111, 2011.

[19] P. Cawley and R. D. Adams, "The location of defects in structures from measurements of natural frequencies," *J Strain Anal Eng Des*, vol. 14, no. 2, pp. 49–57, 1979.

[20] Y. Luo, C. A. Featherston, and D. Kennedy, "A hybrid model for modelling arbitrary cracks in isotropic plate structures," *Thin-Walled Structures*, vol. 183, p. 110345, 2023.

[21] A. S. U. Manual, "Abaqus 6.11," *http://130.149*, vol. 89, no. 2080, p. v6, 2012.

[22] S. Christides and A. D. S. Barr, "One-dimensional theory of cracked Bernoulli-Euler beams," *Int J Mech Sci*, vol. 26, no. 11–12, pp. 639–648, 1984.

[23] W. M. Ostachowicz and M. Krawczuk, "Analysis of the effect of cracks on the natural frequencies of a cantilever beam," *J Sound Vib*, vol. 150, no. 2, pp. 191–201, 1991.

[24] J. Hu and R. Y. Liang, "An integrated approach to detection of cracks using vibration characteristics," *J Franklin Inst*, vol. 330, no. 5, pp. 841–853, 1993.

[25] G. Hearn and R. B. Testa, "Modal analysis for damage detection in structures," *Journal of structural engineering*, vol. 117, no. 10, pp. 3042–3063, 1991.

[26] A. Teughels, J. Maeck, and G. De Roeck, "Damage assessment by FE model updating using damage functions," *Comput Struct*, vol. 80, no. 25, pp. 1869–1879, 2002.

[27] M. Ge and E. M. Lui, "Structural damage identification using system dynamic properties," *Comput Struct*, vol. 83, no. 27, pp. 2185–2196, 2005.

[28] E. N. Chatzi, B. Hiriyur, H. Waisman, and A. W. Smyth, "Experimental application and enhancement of the XFEM–GA algorithm for the detection of flaws in structures," *Comput Struct*, vol. 89, no. 7–8, pp. 556–570, 2011.

[29] J. A. Escobar, J. J. Sosa, and R. Gomez, "Structural damage detection using the transformation matrix," *Comput Struct*, vol. 83, no. 4–5, pp. 357–368, Jan. 2005.

[30] P. F. Rizos, N. Aspragathos, and A. D. Dimarogonas, “Identification of crack location and magnitude in a cantilever beam from the vibration modes,” *J Sound Vib*, vol. 138, no. 3, pp. 381–388, 1990.

[31] W. Wittrick and F. Williams, “A general algorithm for computing natural frequencies of elastic structures,” *Q J Mech Appl Math*, vol. 24, no. 3, pp. 263–284, 1971.

[32] S. Caddemi and I. Calio, “Exact closed-form solution for the vibration modes of the Euler-Bernoulli beam with multiple open cracks,” *J Sound Vib*, vol. 327, no. 3–5, pp. 473–489, Nov. 2009.

[33] S. Caddemi and I. Calio, “Exact solution of the multi-cracked Euler–Bernoulli column,” *Int J Solids Struct*, vol. 45, no. 5, pp. 1332–1351, 2008.

[34] S. Caddemi and I. Calio, “The exact explicit dynamic stiffness matrix of multi-cracked Euler-Bernoulli beam and applications to damaged frame structures,” *J Sound Vib*, vol. 332, no. 12, pp. 3049–3063, Jun. 2013.

[35] A. Labib, D. Kennedy, and C. Featherston, “Free vibration analysis of beams and frames with multiple cracks for damage detection,” *J Sound Vib*, vol. 333, no. 20, pp. 4991–5003, Sep. 2014.

[36] N. T. Khiem and H. T. Tran, “A procedure for multiple crack identification in beam-like structures from natural vibration mode,” *Journal of Vibration and Control*, vol. 20, no. 9, pp. 1417–1427, 2014.

[37] N. T. Khiem and L. K. Toan, “A novel method for crack detection in beam-like structures by measurements of natural frequencies,” *J Sound Vib*, vol. 333, no. 18, pp. 4084–4103, 2014.

[38] S. H. Jazi, M. Hadian, and K. Torabi, “An exact closed-form explicit solution of free transverse vibration for non-uniform multi-cracked beam,” *J Sound Vib*, vol. 570, p. 117986, 2024.

[39] M. Chati, R. Rand, and S. Mukherjee, “Modal analysis of a cracked beam,” *J Sound Vib*, vol. 207, no. 2, pp. 249–270, 1997.

[40] T. G. Chondros, A. D. Dimarogonas, and J. Yao, “A continuous cracked beam vibration theory,” *J Sound Vib*, vol. 215, no. 1, pp. 17–34, 1998.

[41] A. Morassi, “Identification of a crack in a rod based on changes in a pair of natural frequencies,” *J Sound Vib*, vol. 242, no. 4, pp. 577–596, Sep. 2001.

[42] S. Caddemi and I. Caliò, “Exact reconstruction of multiple concentrated damages on beams,” *Acta Mech*, vol. 225, pp. 3137–3156, 2014.

[43] D. P. Patil and S. K. Maiti, “Detection of multiple cracks using frequency measurements,” *Eng Fract Mech*, vol. 70, no. 12, pp. 1553–1572, 2003.

[44] B. P. Nandwana and S. K. Maiti, “Detection of the location and size of a crack in stepped cantilever beams based on measurements of natural frequencies,” *J Sound Vib*, vol. 203, no. 3, pp. 435–446, 1997.

[45] T. D. Chaudhari and S. K. Maiti, “A study of vibration of geometrically segmented beams with and without crack,” *Int J Solids Struct*, vol. 37, no. 5, pp. 761–779, 2000.

[46] S. Chinchalkar, “Determination of crack location in beams using natural frequencies,” *J Sound Vib*, vol. 247, no. 3, pp. 417–429, 2001.

[47] J. Lee, “Identification of multiple cracks in a beam using natural frequencies,” *J Sound Vib*, vol. 320, no. 3, pp. 482–490, 2009.

[48] A. Ghadami, A. Maghsoodi, and H. R. Mirdamadi, “A new adaptable multiple-crack detection algorithm in beam-like structures,” *Archives of Mechanics*, vol. 65, no. 6, pp. 469–483, 2013.

[49] A. Maghsoodi, A. Ghadami, and H. R. Mirdamadi, “Multiple-crack damage detection in multi-step beams by a novel local flexibility-based damage index,” *J Sound Vib*, vol. 332, no. 2, pp. 294–305, 2013.

[50] P. Nandakumar and K. Shankar, “Multiple crack damage detection of structures using the two crack transfer matrix,” *Struct Health Monit*, vol. 13, no. 5, pp. 548–561, 2014.

[51] L. Rubio, J. Fernández-Sáez, and A. Morassi, “Identification of two cracks with different severity in beams and rods from minimal frequency data,” *Journal of Vibration and Control*, vol. 22, no. 13, pp. 3102–3117, 2016.

[52] T. Y. Kam and T. Y. Lee, “Detection of cracks in structures using modal test data,” *Eng Fract Mech*, vol. 42, no. 2, pp. 381–387, 1992.

[53] S. Hassiotis and G. D. Jeong, “Identification of stiffness reductions using natural frequencies,” *J Eng Mech*, vol. 121, no. 10, pp. 1106–1113, 1995.

[54] N. Bicanic and H. Chen, “Damage identification in framed structures using natural frequencies,” *Int J Numer Methods Eng*, vol. 40, no. 23, pp. 4451–4468, 1997.

[55] P. G. Nikolakopoulos, D. E. Katsareas, and C. A. Papadopoulos, “Crack identification in frame structures,” *Comput Struct*, vol. 64, no. 1–4, pp. 389–406, 1997.

[56] A. Pau, A. Greco, and F. Vestroni, “Numerical and experimental detection of concentrated damage in a parabolic arch by measured frequency variations,” *Journal of Vibration and Control*, vol. 17, no. 4, pp. 605–614, 2011.

[57] Y. Lee and M. Chung, “A study on crack detection using eigenfrequency test data,” *Comput Struct*, vol. 77, no. 3, pp. 327–342, 2000.

[58] A. Greco and A. Pau, “Damage identification in Euler frames,” *Comput Struct*, vol. 92, pp. 328–336, 2012.

[59] A. Labib, D. Kennedy, and C. A. Featherston, “Crack localisation in frames using natural frequency degradations,” *Comput Struct*, vol. 157, pp. 51–59, May 2015.

[60] M. I. Friswell, J. E. T. Penny, and S. D. Garvey, “A combined genetic and eigensensitivity algorithm for the location of damage in structures,” *Comput Struct*, vol. 69, no. 5, pp. 547–556, 1998.

[61] P. G. Bakir, E. Reynders, and G. De Roeck, “An improved finite element model updating method by the global optimization technique ‘Coupled Local Minimizers,’” *Comput Struct*, vol. 86, no. 11–12, pp. 1339–1352, 2008.

[62] X. Liu, N. A. J. Lieven, and P. J. Escamilla-Ambrosio, “Frequency response function shape-based methods for structural damage localisation,” *Mech Syst Signal Process*, vol. 23, no. 4, pp. 1243–1259, 2009.

[63] R. P. C. Sampaio, N. M. M. Maia, and J. M. M. Silva, “Damage detection using the frequency-response-function curvature method,” *J Sound Vib*, vol. 226, no. 5, pp. 1029–1042, 1999.

[64] M. P. Limongelli, “The interpolation damage detection method for frames under seismic excitation,” *J Sound Vib*, vol. 330, no. 22, pp. 5474–5489, 2011.

[65] Y. Zhang, S. T. Lie, and Z. Xiang, “Damage detection method based on operating deflection shape curvature extracted from dynamic response of a passing vehicle,” *Mech Syst Signal Process*, vol. 35, no. 1–2, pp. 238–254, 2013.

[66] N. M. M. Maia, R. A. B. Almeida, A. P. V Urgueira, and R. P. C. Sampaio, “Damage detection and quantification using transmissibility,” *Mech Syst Signal Process*, vol. 25, no. 7, pp. 2475–2483, 2011.

[67] Y. Xia, H. Hao, J. M. W. Brownjohn, and P. Xia, “Damage identification of structures with uncertain frequency and mode shape data,” *Earthq Eng Struct Dyn*, vol. 31, no. 5, pp. 1053–1066, 2002.

[68] Y. Xia and H. Hao, “Statistical damage identification of structures with frequency changes,” *J Sound Vib*, vol. 263, no. 4, pp. 853–870, 2003.

[69] E. Simoen, G. De Roeck, and G. Lombaert, “Dealing with uncertainty in model updating for damage assessment: A review,” *Mech Syst Signal Process*, vol. 56, pp. 123–149, 2015.

[70] L. S. Katafygiotis and J. L. Beck, “Updating models and their uncertainties. II: Model identifiability,” *J Eng Mech*, vol. 124, no. 4, pp. 463–467, 1998.

[71] J. L. Beck and L. S. Katafygiotis, “Updating models and their uncertainties. I: Bayesian statistical framework,” *J Eng Mech*, vol. 124, no. 4, pp. 455–461, 1998.

[72] E. Figueiredo, L. Radu, K. Worden, and C. R. Farrar, “A Bayesian approach based on a Markov-chain Monte Carlo method for damage detection under unknown sources of variability,” *Eng Struct*, vol. 80, pp. 1–10, 2014.

[73] S. Arangio and F. Bontempi, “Structural health monitoring of a cable-stayed bridge with Bayesian neural networks,” in *Design, Assessment, Monitoring and Maintenance of Bridges and Infrastructure Networks*, Routledge, 2020, pp. 163–175.

[74] M. T. Vakil-Baghmisheh, M. Peimani, M. H. Sadeghi, and M. M. Ettefagh, “Crack detection in beam-like structures using genetic algorithms,” *Appl Soft Comput*, vol. 8, no. 2, pp. 1150–1160, 2008.

[75] C. B. Yun and E. Y. Bahng, “Substructural identification using neural networks,” *Comput Struct*, vol. 77, no. 1, pp. 41–52, 2000.

[76] C. Y. Kao and S.-L. Hung, “Detection of structural damage via free vibration responses generated by approximating artificial neural networks,” *Comput Struct*, vol. 81, no. 28–29, pp. 2631–2644, 2003.

[77] S. Moradi, P. Razi, and L. Fatahi, “On the application of bees algorithm to the problem of crack detection of beam-type structures,” *Comput Struct*, vol. 89, no. 23–24, pp. 2169–2175, 2011.

[78] P. P. Lynn and N. Kumbasar, “Free vibration of thin rectangular plates having narrow cracks with simply supported edges,” *Development in Mechanics*, vol. 4, pp. 911–928, 1967.

[79] R. Solecki, “Bending vibration of simply supported rectangular plates with internal rigid support,” *Int J Eng Sci*, vol. 18, no. 11, pp. 1309–1318, 1980, doi: https://doi.org/10.1016/0020-7225(80)90122-6.

[80] B. Stahl and L. M. Keer, “Vibration and stability of cracked rectangular plates,” *Int J Solids Struct*, vol. 8, no. 1, pp. 69–91, 1972.

[81] H. Yoshitaro and O. Katsutoshi, “Vibrataion of Cracked Rectangular Plates,” *The Japan Society of Mechanical Engineers*, vol. 23, no. 1980, pp. 732–740, 1980.

[82] R. Solecki, “Bending vibration of a simply supported rectangular plate with a crack parallel to one edge,” *Eng Fract Mech*, vol. 18, no. 6, pp. 1111–1118, 1983.

[83] Q. Guan-Liang, G. Song-Nian, and J. Jie-Sheng, “A finite element model of cracked plates and application to vibration problems,” *Comput Struct*, vol. 39, no. 5, pp. 483–487, 1991.

[84] T. Fujimoto, K. Wakata, F. Y. Cao, and H. Nisitani, “Vibration analysis of a cracked plate subjected to tension using a hybrid method of FEM and BFM,” in *Materials Science Forum*, Trans Tech Publ, 2003, pp. 407–414.

[85] A. Saito, M. P. Castanier, and C. Pierre, “Estimation and veering analysis of nonlinear resonant frequencies of cracked plates,” *J Sound Vib*, vol. 326, no. 3–5, pp. 725–739, 2009.

[86] M. Bachene, R. Tiberkak, and S. Rechak, “Vibration analysis of cracked plates using the extended finite element method,” *Archive of Applied Mechanics*, vol. 79, pp. 249–262, 2009.

[87] L. M. Keer and C. Sve, “On the bending of cracked plates,” *Int J Solids Struct*, vol. 6, no. 12, pp. 1545–1559, 1970, doi: https://doi.org/10.1016/0020-7683(70)90063-6.

[88] H. P. Lee, “Fundamental frequencies of annular plates with internal cracks,” *Comput Struct*, vol. 43,no.6, pp.1085–1089, 1992, doi:https://doi.org/10.1016/0045-7949(92)90009-O.

[89] H. P. Lee and S. P. Lim, “Free vibration of isotropic and orthotropic rectangular plates with partially clamped edges,” *Applied Acoustics*, vol. 35, no. 2, pp. 91–104, 1992, doi: https://doi.org/10.1016/0003-682X(92)90025-N.

[90] K. M. Liew, K. C. Hung, and M. K. Lim, “A solution method for analysis of cracked plates under vibration,” *Eng Fract Mech*, vol. 48, no. 3, pp. 393–404, 1994.

[91] S. E. Khadem and M. Rezaee, “Introduction of Modified Comparison Function For Vibration Analysis of A Rectangular Cracked Plate, ” *J Sound Vib*,vol.236,no.2,pp.245–258, 2000, doi: https://doi.org/10.1006/jsvi.2000.2986.

[92] G. Y. Wu and Y. S. Shih, “Dynamic instability of rectangular plate with an edge crack,” *Comput Struct*, vol.84,no.1,pp.1–10,2005,doi: https://doi.org/10.1016/ j.compstruc.2005.09.003.

[93] M. H. Shen and C. Pierre, “Natural modes of Bernoulli-Euler beams with symmetric cracks,” *J Sound Vib*, vol. 138, no. 1, pp. 115–134, 1990.

[94] Y. G. Xiao, Y. M. Fu, and X.-D. Zha, “Bifurcation and chaos of rectangular moderately thick cracked plates on an elastic foundation subjected to periodic load,” *Chaos Solitons Fractals*, vol. 35, no. 3, pp. 460–465, 2008.

[95] A. Israr, M. P. Cartmell, E. Manoach, and I. Trendafilova, “Analytical modeling and vibration analysis of partially cracked rectangular plates with different boundary conditions and loading,” *Journal of Applied Mechanics, Transactions ASME*, vol. 76, no. 1, pp. 1–9, 2009.

[96] C. S. Huang and A. W. Leissa, “Vibration analysis of rectangular plates with side cracks via the Ritz method,” *J Sound Vib*, vol. 323, no. 3–5, pp. 974–988, Jun. 2009, doi: 10.1016/j.jsv.2009.01.018.

[97] K. Maruyama and O. Ichinomiya, “Experimental study of free vibration of clamped rectangular plates with straight narrow slits,” *JSME international journal. Ser. 3, Vibration, control engineering, engineering for industry*, vol. 32, no. 2, pp. 187–193, 1989.

[98] D. Wu and S. S. Law, “Anisotropic damage model for an inclined crack in thick plate and sensitivity study for its detection,” *Int J Solids Struct*, vol. 41, no. 16–17, pp. 4321–4336, 2004.

[99] D. Wu and S. S. Law, “Damage-detection-oriented model for a cracked rectangular plate,” in *Smart Structures and Materials 2004: Sensors and Smart Structures Technologies for Civil, Mechanical, and Aerospace Systems*, SPIE, 2004, pp. 470–481.

[100] D. Wu and S. S. Law, “Damage localization in plate structures from uniform load surface curvature,” *J Sound Vib*, vol. 276, no. 1–2, pp. 227–244, 2004.

[101] J. R. Rice and N. Levy, “The part-through surface crack in an elastic plate,” *J Appl Mech*, pp. 185–172, 1972.

[102] F. Delale and F. Erdogan, “Line-spring model for surface cracks in a Reissner plate,” *Int J Eng Sci*, vol. 19, no. 10, pp. 1331–1340, 1981.

[103] R. B. King, “Elastic-plastic analysis of surface flaws using a simplified line-spring model,” *Eng Fract Mech*, vol. 18, no. 1, pp. 217–231, 1983.

[104] C. Y. Yang, “Line spring method of stress-intensity factor determination for surface cracks in plates under arbitrary in-plane stresses,” in *Fracture Mechanics: Nineteenth Symposium*, ASTM International, 1988.

[105] N. Miyazaki, “An application of a line-spring model to a transient analysis of the dynamic stress intensity factor,” *Int J Fract*, vol. 39, pp. R77–R80, 1989.

[106] P. F. Joseph and F. Erdogan, “Surface crack in a plate under antisymmetric loading conditions,” *Int J Solids Struct*, vol. 27, no. 6, pp. 725–750, 1991, doi: https://doi.org/10.1016/0020-7683(91)90031-A.

[107] P. V. Joshi, N. K. Jain, and G. D. Ramtekkar, “Analytical modeling and vibration analysis of internally cracked rectangular plates,” *J Sound Vib*, vol. 333, no. 22, pp. 5851–5864, Oct. 2014.

[108] T. Bose and A. R. Mohanty, “Vibration analysis of a rectangular thin isotropic plate with a part-through surface crack of arbitrary orientation and position,” *J Sound Vib*, vol. 332, no. 26, pp. 7123–7141, Dec. 2013.

[109] A. Gupta, N. K. Jain, R. Salhotra, and P. V. Joshi, “Effect of crack location on vibration analysis of partially cracked isotropic and FGM micro-plate with non-uniform thickness: An analytical approach,” *Int J Mech Sci*, vol. 145, pp. 410–429, Sep. 2018, doi: 10.1016/j.ijmecsci.2018.07.015.

[110] M. Ranjbaran and R. Seifi, “Analysis of free vibration of an isotropic plate with surface or internal long crack using generalized differential quadrature method,” *J Strain Anal Eng Des*, vol. 55, no. 1–2, pp. 42–52, 2020, doi: 10.1177/0309324719886976.

[111] J. Heo, Y. Zhenghao, X. Wenxuan, O. Selda, and E. and Oterkus, “Free vibration analysis of cracked plates using peridynamics,” *Ships and Offshore Structures*, vol. 15, no. sup1, pp. S220–S229, Dec. 2020, doi: 10.1080/17445302.2020.1834266.

[112] Y. Ma, S. Zhang, J. Fan, Y. Wang, and Z. Deng, “Analytical solution of forced vibration of rectangular plates with part through surface crack based on wave propagation method,”*Comput Struct*, vol.299,p.107402,2024,doi: https://doi.org/10.1016/ j.compstruc.2024.107402.

[113] C. Bilello, “Theoretical and experimental investigation on damaged beams under moving systems,” *University of Palermo: PhD Thesis*, 2001.

[114] P. H. Kirkegaard and A. Rytter, “Vibration based damage assessment of a civil engineering structures using a neural network,” Dept. of Building Technology and Structural Engineering, Aalborg University, 1994.

[115] M. A. Pérez and R. Serra-López, “A frequency domain-based correlation approach for structural assessment and damage identification,” *Mech Syst Signal Process*, vol. 119, pp. 432–456, 2019.

[116] N. Stubbs, C. Farrar, J.-T. Kim, and C. R. Farrar, “Field verification of a non-destructive damage localization and severity estimation algorithm,” 1995.

[117] Y. Zhang, L. Wang, S. T. Lie, and Z. Xiang, “Damage detection in plates structures based on frequency shift surface curvature,” *J Sound Vib*, vol. 332, no. 25, pp. 6665–6684, 2013, doi: https://doi.org/10.1016/j.jsv.2013.07.028.

[118] K. Dems and Z. Mróz, “Identification of damage in beam and plate structures using parameter-dependent frequency changes,” *Engineering Computations* , vol. 18, pp. 96–120, 2001.

[119] Y. Y. Li, L. Cheng, L. H. Yam, and W. O. Wong, “Identification of damage locations for plate-like structures using damage sensitive indices: strain modal approach,” *Comput Struct*, vol. 80, no. 25, pp. 1881–1894, 2002.

[120] L. H. Yam, Y. Y. Li, and W. O. Wong, “Sensitivity studies of parameters for damage detection of plate-like structures using static and dynamic approaches,” *Eng Struct*, vol. 24, no. 11, pp. 1465–1475, 2002.

[121] U. Lee and J. Shin, “A structural damage identification method for plate structures,” *Eng Struct*, vol. 24, no. 9, pp. 1177–1188, 2002.

[122] Y. Lu, L. Ye, Z. Su, L. Zhou, and L. Cheng, “Artificial neural network (ANN)-based crack identification in aluminum plates with Lamb wave signals,” *J Intell Mater Syst Struct*, vol. 20, no. 1, pp. 39–49, 2009.

[123] S. Khatir and M. A. Wahab, “Fast simulations for solving fracture mechanics inverse problems using POD-RBF XIGA and Jaya algorithm,” *Eng Fract Mech*, vol. 205, pp. 285–300, 2019.

[124] E. J. Williams, A. Messina, and B. S. Payne, “A frequency-change correlation approach to damage detection,” in *Proceedings of the 15th International Modal Analysis Conference*, 1997, p. 652.

[125] S. Hosseini-Hashemi, M. Fadaee, and S. R. Atashipour, “A new exact analytical approach for free vibration of Reissner–Mindlin functionally graded rectangular plates,” *Int J Mech Sci*, vol. 53, no. 1, pp. 11–22, 2011.

[126] Z. Yang, X. Chen, J. Yu, R. Liu, Z. Liu, and Z. He, “A damage identification approach for plate structures based on frequency measurements,” *Nondestructive Testing and Evaluation*, vol. 28, no. 4, pp. 321–341, 2013.

[127] Y. Jiang, J. Xiang, B. Li, X. Chen, and L. Lin, “A hybrid multiple damages detection method for plate structures,” *Sci China Technol Sci*, vol. 60, no. 5, pp. 726–736, 2017.

[128] J. Pan, Z. Zhang, J. Wu, K. R. Ramakrishnan, and H. K. Singh, “A novel method of vibration modes selection for improving accuracy of frequency-based damage detection,” *Compos B Eng*, vol. 159, pp. 437–446, 2019.

[129] M. Krawczuk, M. Palacz, and W. Ostachowicz, “Wave propagation in plate structures for crack detection,” *Finite elements in analysis and design*, vol. 40, no. 9–10, pp. 991–1004, 2004.

[130] B. Titurus, M. I. Friswell, and L. Starek, “Damage detection using generic elements: Part I. Model updating,” *Comput Struct*, vol. 81, no. 24–25, pp. 2273–2286, 2003.

[131] B. Titurus, M. I. Friswell, and L. Starek, “Damage detection using generic elements: Part II. Damage detection,” *Comput Struct*, vol. 81, no. 24–25, pp. 2287–2299, 2003.

[132] C. T. Horibe and F. W. Williams, “Crack identification in plates using genetic algorithm,” *Journal of Structural Mechanics*, pp. 1312–1319, 2011.

[133] T. Yin, H. Lam, and H. Chow, “A Bayesian probabilistic approach for crack characterization in plate structures,” *Computer-Aided Civil and Infrastructure Engineering*, vol. 25, no. 5, pp. 375–386, 2010.

[134] E. Z. Moore, K. D. Murphy, and J. M. Nichols, “Crack identification in a freely vibrating plate using Bayesian parameter estimation,” *Mech Syst Signal Process*, vol. 25, no. 6, pp. 2125–2134, 2011.

[135] R. Solecki, “Bending vibration of a rectangular plate with arbitrarily located rectilinear crack,” *Eng Fract Mech*, vol. 22, no. 4, pp. 687–695, 1985.

[136] D. Singh, M. Castaings, and C. Bacon, “Sizing strip-like defects in plates using guided waves,” *NDT & E International*, vol. 44, no. 5, pp. 394–404, 2011.

[137] E. N. Chatzi, B. Hiriyur, H. Waisman, and A. W. Smyth, “Experimental application and enhancement of the XFEM-GA algorithm for the detection of flaws in structures,” *Comput Struct*,vol.89,no.7–8,pp.556–570,Apr.2011,doi: 10.1016/ j.compstruc.2010.12.014.

[138] J. Xiang and M. Liang, “A two-step approach to multi-damage detection for plate structures,” *Eng Fract Mech*, vol. 91, pp. 73–86, 2012.

[139] S. C. Mohan, D. K. Maiti, and D. Maity, “Structural damage assessment using FRF employing particle swarm optimization,” *Appl Math Comput*, vol. 219, no. 20, pp. 10387–10400, 2013.

[140] D. Dinh-Cong, T. Vo-Duy, V. Ho-Huu, H. Dang-Trung, and T. Nguyen-Thoi, “An efficient multi-stage optimization approach for damage detection in plate structures,” *Advances in Engineering Software*, vol. 112, pp. 76–87, 2017.

[141] L. B. Freund and G. Herrmann, “Dynamic fracture of a beam or plate in plane bending,” 1976.

[142] R. E. Moore, *Methods and applications of interval analysis*. Society for Industrial and Applied Mathematics, 1979.

[143] S. S. Rao, *Vibration of continuous systems*. John Wiley & Sons, 2019.